UNIVERSITA' DEGLI STUDI DI NAPOLI "FEDERICO II"

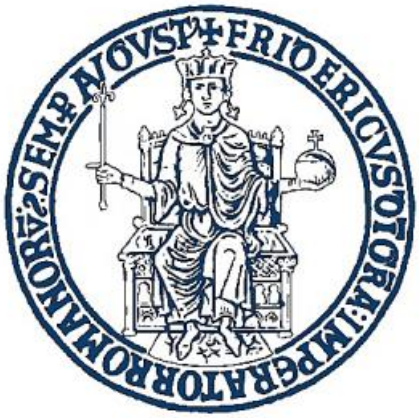

PhD thesis in Industrial Products and Process Engineering

(XXXV cycle)

# *"PLATFORM FOR MULTIFUNCTIONAL PARTICLES IN BIOSENSING APPLICATIONS"*


**Nicoletta Martone**

**Supervisor:**
Prof. Dr. Paolo Antonio Netti
Prof. Dr. Filippo Causa
**Advisor:**
Dr. Edmondo Battista

**Coordinator:**
Prof. Dr. Andrea D'Anna


2019-2022

# TABLE OF CONTENTS

# ABSTRACT

Microgels are versatile materials due to their hydrophilic, bio-friendly, and highly tunable nature, making them applicable in various biomolecule detection. The microgels-based platform is composed of multifunctional particles which possess multiple components and properties tunable to fulfil the requirements of the applications. The chemical flexibility of hydrogel microparticles and microgels allows the embedding of several building blocks into their structure during the synthesis. Anchoring groups on particles are used to immobilize probes of diverse natures such as antibodies, enzymes, or oligonucleotide strands. Particles active for the detection of a target or more than one biomarker can be obtained. The high biocompatibility and antifouling properties of hydrogel make possible the employing of the microgels-based platform in biosensing and inspired the development of several sophisticated applications, such as biosensors.

My PhD project aims to widen the applications of the microgels-based platform towards new goals in the biosensing field to have innovative bioassays. Microgels can be produced with multiple functions thanks to their chemical flexibility. During their synthesis, different building blocks can be introduced into the reactor allowing their co-polymerization with the cross-linking agent. Core microgels with different physical and chemical properties are produced according to the desired properties to confer. The microgels are used to develop an ultrasensitive and innovative immunoassay for the detection of new biomarkers such as proteins and antibodies. Nowadays, immunoassays are the most spread analytical procedures used to measure proteins in biological samples. Analytes and disease biomarkers are usually present in fluid and serum at subfemtomolar concentrations. For this reason, methods and devices featured by both sensitive target detection and broad analytical ranges are required. As the first application in the immunoassay field, core microgels with Rhodamine dye as an optical barcode are adopted as the carrier of both anti-Fab antibodies and the HRP enzyme. Magnetic particles functionalized with anti-Fc antibodies are involved as capture particles. When the target antigen IgG is present, the two antibodies used can form a sandwich structure capturing the target. Microgels bound to beads can be separated magnetically from the sample. Particle clusters are formed and visible by a confocal laser scanning microscope (CLSM). The cluster area increases as the target concentration increase too. After

the interaction, unbound microgels are separated from the solution and used to produce a colourimetric signal for target detection. Increasing the target concentration in samples, the number of free microgels in the solution decreases. The colourimetric signal produced by HRP-microgels free in solution decreases too. Single-entity detection approaches and miniaturized structures are increasingly spreading to overcome the limits linked to sensitivity. The flexibility of the particle-based platform allows for decreasing the number of particles involved in the assay. The application of the single-entity method and the use of microfluidic devices can lead to the development of bioassays characterized by ultrahigh sensitivity.

# CHAPTER 1

## 1. INTRODUCTION

Microgels are polymeric particles characterized by colloidal stability and swelling capacity in water. They consist of a three-dimensional polymeric network whose diameter varies between 10 nm and 1 μm, capable of absorbing a large amount of water.[1,2] Microgels are synthesized with different chemical strategies and opportunely functionalized with probes to detect circulating biomarkers in human serum.[3] In the biosensor field, hydrogel-based technologies have attracted considerable attention during the last years, as confirmed by the number of studies published. This huge interest is due to the hydrophilic, bio-friendly and highly tunable nature of these materials, which make them very suitable in diagnostics[4,5] and many other biomedical fields such as drug delivery[6], tissue engineering[7] and pharmaceutical applications[8]. The high biocompatibility and antifouling properties[9] of hydrogel make possible the employing of the microgels-based platform in biosensing and inspired the development of several sophisticated applications, such as biosensors.[10,11]

The work presented in this thesis aims to expand the potential of the microgels-based platform in the biosensing field to overcome the limitations associated with techniques already in use. In order to lay out a framework for the topics covered in the thesis, this chapter outlines: (1) the potential of the microgels-based platform, (2) methods used for microgels synthesis and (3) Immunoassays for protein detection.

### 1.1 THE MICROGEL-BASED PLATFORM

The microgel-based platform is composed of multifunctional particles which have extensive applications owing to bearing various functions in an integral whole and possessing multiple components and properties. Their structures and functions can be modified to fulfil the requirements of the applications. Multifunctional particles possess multiple components and properties such as core-shell particles in which the core and the shell act distinct roles, as well as particles incorporated or conjugated with other functional species. Thus, microgels and hydrogel microparticles can be produced with multiple functions thanks to their chemical flexibility. During their synthesis, different building blocks can be introduced into the reactor allowing their co-polymerization with the cross-linking agent such as

PEGDMA. In this way, separated batches of particles can be decorated with anchoring groups of different natures such as carboxyl group, amine group, or epoxy group. Another possibility is to mix building blocks during the synthesis: particles with different functional groups on the same surface are generated. The anchoring groups are then exploited for the covalent immobilization of probes. Ensembles of microgels can be coated with antibodies, enzymes, proteins, or oligonucleotide strands individually, or various probes can be mixed resulting in particles active against diverse targets. This makes possible the employing of the microgels-based platform in biosensing and diagnostic fields for the detection of more biomarkers. Battista et al.[12] obtained core double-shells PEG microgels through a multistep procedure in which alternating fluorescent and non-fluorescent concentric hydrogel shells are synthesized around a core particle. The first fluorescent acrylate dye is embedded in the core and followed by a non-fluorescent shell. The last outermost shell is synthesized by using a second fluorescent acrylate dye and an anchoring group, such as the carboxyl group. The subsequent bioconjugation with oligonucleotide strands was useful to detect DNA biomarkers. The developed assay was based on the optical fluorescence readout. The flexibility of microgels allows having spectrally encoded microgels created with a different number of dyes: The dyes ratio was modulated between their fluorescence emission (Fluo/Rhod) obtaining a robust and reproducible spectral encoding.[13] The outermost shell of these particles containing acrylic acid was used to bind dye-modified nucleic acids probes. Multiplex assays have been performed by using microgels synthesized with different spectrally encoding and then functionalized with double-strand probes specific for different microRNAs. When they have been spiked into the serum sample under test, the presence of miRNA targets has been highlighted by the probe fluorescence emission and the identity of the miRNA is revealed by reading the ratio of Fluo/Rhod of microgels.[14] This characteristic was important for the creation of a multiplex assay to detect more than one biomolecule in the same sample at the same time. By changing the fluorophores ratio in the core and the shell, microgels with different optical barcodes have been obtained. Oligonucleotide assays with a microgels-based platform had higher sensitivity and lower limit of the detection (LOD) than assays with the same probes not conjugated to microgels. The increase in sensitivity is due to the confinement of probes onto the surface of nanometric particles producing an enhancement of fluorescent signal. Upon the detection event, femtomolar (fM)

concentrations were recovered lowering the limit of detection to 5 orders of magnitude if compared with the probes alone. This represents a modular platform that can be generalized for any direct detection applied to a wide spectrum of biomedical applications. Beyond the possibility of multiplexing assay and flexibility of functionalization, another advantage linked with the use of microgels is the possibility to test complex biological fluids. In general, the presence of biomolecules could interfere during the assay. Differently, microgels were not affected by the complexity of the sample thanks to their antifouling properties, allowing direct and specific detection without any surface treatment.[15]

### 1.1.1 MICROGELS SYNTHESIS

The methods of preparation for microgel are microfluidics and batch synthesis. Microfluidic techniques can be divided into droplet generation-based methods and flow lithography.

- Droplet generation

The aqueous dispersed phase meets the continuous phase at a cross-junction where droplets are pinched off.[16],[17] In this case, synthetic polymer networks are obtained by cross-linking acrylate and methacrylate monomers which are formed by shining UV/Vis light. Different variables such as flow rates, the viscosity of the fluid, dimensions of the geometry, and capillary number (Ca) in the following equation

$$Ca = \mu U/\gamma$$

μ = viscosity of the continuous phase;
U = speed of the continuous phase;
γ = interfacial tension between the continuous and dispersed phases.

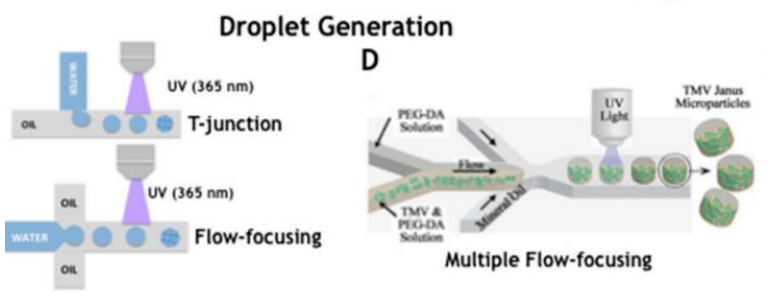


**Figure 1**: droplet generation.

Doyle et al.[18] reported an innovative method for the continuous production of hydrogel particles under flow in a PDMS microfluidic device with high throughput. With this

technique, they were able to obtain a high number of codes by combining graphical and spectral encoding.[19] This approach has been defined as continuous flow lithography and it relies on a rectangular microfluidic channel where multiple co-flowing streams pass over a pulsing UV light, that is projected through a mask from the objective, to give complex shapes.

- Flow lithography

This technique involves the production of hydrogel particles under flow conditions in a PDMS microfluidic device. The method is carried out in a rectangular microfluidic channel with multiple co-flowing streams that pass under a pulsating UV light to obtain the rapid and continuous formation of about 18,000 particles per second. An innovative technology based on this method is represented by "stop-flowing lithography", according to which the flow stops for a few milliseconds to allow polymerization through the mask. Pregibon et al.[20] generated a new method based on continuous-flow lithography to produce PEG particles in a single step with distinct regions. These multifunctional particles are equipped with a fluorescent, graphically encoded region for optical determination and a probe-loaded region for analyte encoding and target capture.

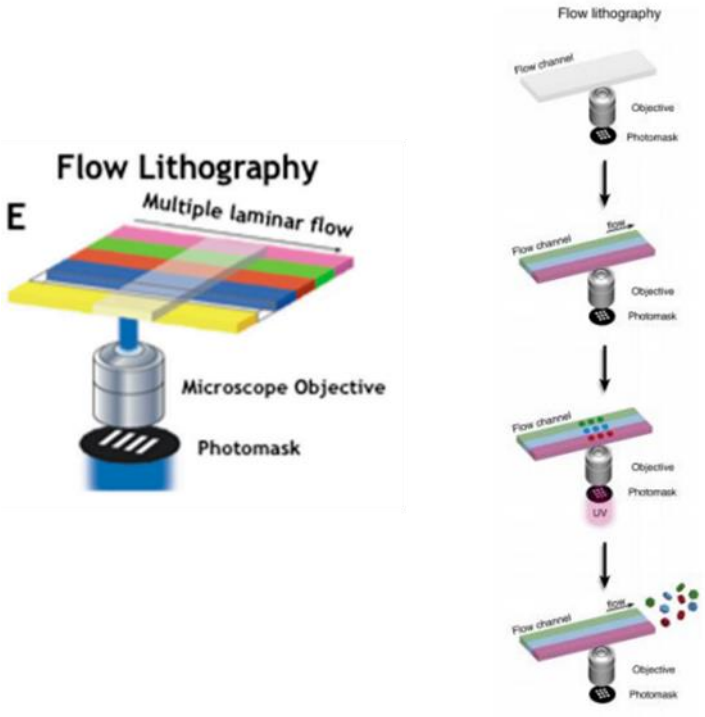


**Figure 2**: Flow lithography

- Batch synthesis[21]

This type of synthesis typically consists of a nucleation, aggregation and growth mechanism and allows to control of the size distribution, colloidal stability and the presence of functional groups at specific positions.

The approach is characterized by the co-polymerization of vinyl monomers with a crosslinking agent. There are three types of particle formation: homogeneous nucleation, deriving from the emulsion and obtained from complexation.

Homogeneous nucleation is the mechanism by which microgels are obtained from initially homogeneous (or almost homogeneous) solutions. The particles derived from the emulsion are aqueous droplets of a pre-gel solution formed starting from an oily or saline phase and, subsequently, polymerization takes place in microgels. Finally, the particles are obtained through the mixture of two diluted and water-soluble polymers which lead to the formation of complexes.

The most used mechanism is homogeneous nucleation, where a solution of soluble monomer is fed into the reactor and microgels are formed through polymerization. The basic requirement is that the polymer is insoluble during the process leading to the formation of precursor particles. Then they aggregate and the surface charge density increases until it reaches stability to particles of similar or larger size. The particles that form first are called primary and must be synthesized at the low conversion of the monomer to obtain a monodisperse product. Next particles are deposited on the already existing stable microgels contributing to the growth of the particles.

## 1.2 IMMUNOLOGICAL ASSAY

Biological assays are analytical procedures in which a probe is used as a recognition element for the qualitative identification or quantitative measurement of a target entity. The probe can bind the target, and after the binding event, an optical, electrical, or fluorescence signal is produced and quantified by a detection method. Biological assays can be classified on the base of the nature of the probe and the method involved to read the signal.

The immunological assay is one of the most spread classes of bioassay applied in pharmaceutical, veterinary, environmental, and biosensing fields for the identification of target biomolecules such as drugs, antibodies, oligonucleotide strands, proteins, steroids, and pollutants.[22]

The antibody-antigen interaction is the most important reaction in all immunoassays in which antibodies are used as a probe to recognize the specific antigen target.

The reaction at the base of the antigen-antibody interaction is:

$$Ag + Ab = Ag\text{-}Ab$$

where Ag is the antigen, Ab is the antibody and Ag-Ab is the formed immune complex.

Antibodies are very selective biomolecules which only bind to their specific targets, even in the presence of a huge range of other materials in the sample. The antibody-antigen binding reaction is characterized by two important parameters: affinity and avidity.[23]

The measure of the strength of the binding is called affinity expressed as the concentration of an antibody-antigen complex at equilibrium.[24] The affinity constant ranges from micro ($10^{-6}$) to pico ($10^{-12}$) molar. So, the higher the antibody affinity is, the highest the target amount is bound in a short period. Hence, high-affinity antibodies are usually preferred in immunochemical techniques.

Antibodies and antigens are multivalent, so they possess more than one binding site. The measure of the total binding strength of an antibody at every binding site is termed avidity. It depends on the antibody's affinity for the epitope and the number of binding sites per antibody and antigen molecule.

After the capture of the target, the generation of a signal is necessary for the identification of the target. It will be recovered by using a detection method and then, quantification will be possible. Usually, for the generation of a signal, labels as enzymes, radioisotopes, fluorophores, or dyes are used.[25] In general, the immunoassay is characterized by two important parameters: sensitivity and specificity. Sensitivity is the analyte concentration below which the imprecision becomes unacceptable meaning that high sensitivity immunoassay can respond to a low amount of analyte.[26] This parameter is defined by the antigen-antibody binding constant because the greater the values of the binding constant are, the greater the sensitivity of immunoassay will be. The detection method can limit the sensitivity of the assay avoiding observing a lower amount of target.

Specificity is the capacity to discriminate between closely related molecular structures in the assay. The analyte unequivocally has to be detected in biological matrices, preferentially without prior sample extraction. It depends on the type of antibody used to detect the target: polyclonal antibodies can bind different binding

sites on the same antigen showing less specificity, instead, a more specific monoclonal one can bind only one antigen site. The evaluation of specificity can be performed by conducting the assay in presence of species with a structure similar to the target.[27]

As a first classification, immunoassays can be divided into homogeneous and heterogeneous ones.

In the heterogeneous format, a solid surface such as a microwell plate is used for the immobilization of the probe. It can be carried out in an antigen-capture or antibody-capture format, depending on whether the solid phase is coated with an antibody or antigen (analyte), respectively. After the target is added, interaction and binding between antigen and antibodies occur. Before the recovery of the signal, a separation or washing step is needed to eliminate the unreacted sample in wells that could interfere with the detection signal. In this case, the immobilization of probes reduces the rate of the binding event between the probe and the target. Contrarily, free probes in the sample characterized the homogeneous format and, in this way, the distance that the analyte molecule has to move to interact with the antibody is reduced, decreasing the rate of the reaction. In this case, no washing step or separation is needed.

In both heterogeneous and homogeneous assays, the fundamental elements always are antibodies-antigen pair and a tracer, a biomolecule able to generate a signal to quantify the target. Beyond these common elements, different formats are possible by varying the detection method, the nature of the tracer and the type of its generated signal. The most common formats used in different fields are competitive and non-competitive formats.

### 1.2.1 COMPETITIVE IMMUNOASSAY

The competitive immunoassay is characterized by a competition between the target and a tracer acting as a competitor,[28] for a limited number of antibodies that can be free in solution or bound to a surface.

Usually, the tracer can be either a molecule with a similar structure to the target or the target molecule itself that has been labelled: in both cases, their affinity for the antibody involved is weaker than target-antibody affinity. The decrease in affinity, due to the difference in structures of the biomolecule used, allows the competition between the target and tracer for the antibody. For this purpose, antibodies, tracers, and samples under test are spiked to allow competition.[29]

When the target analyte is not present, the competitor will be bound to the antibody and the recovered signal will be high. When the analyte in the sample is significantly higher than the concentration of the competitor, the antibody binding sites will be preferentially occupied by the analyte[30] and most of the tracer will be free in the solution. The signal produced by the tracer will be inversely proportional to the target analyte.

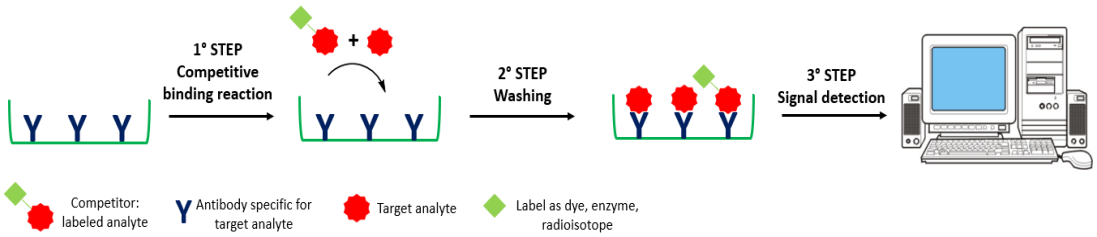


**Figure 3:** Schematic example of the heterogeneous competitive format.

This format is possible also by performing two sequential steps. In the first one, the sample containing target molecules and antibodies is mixed to allow the binding event between them. In the next step, the tracer is added to allow the quantification of the antibodies unoccupied by the target. In this case, there is no real competition and the tracer is added directly to quantify how much the target is not bound to the antibodies. The detected signal will be inversely proportional to the target.

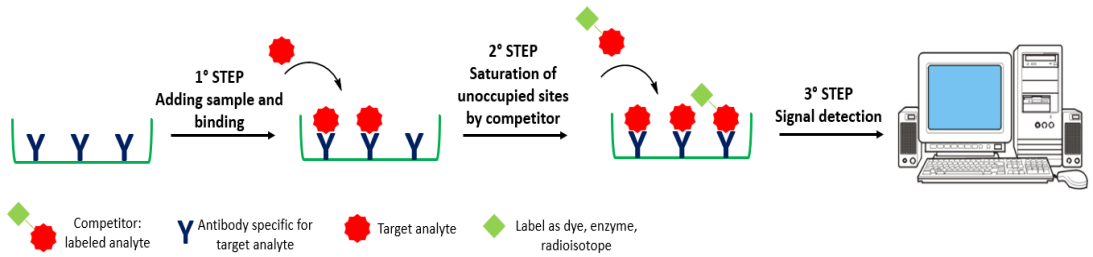


**Figure 4:** Competitive assay in two steps format.

The sensitivity of a competitive assay can be increased by the modulation of dissociation constant $K_D$, the concentration of antibodies and antigens. An evaluation of the sensitivity of the competitive assay can be obtained by deriving the equation of IC50 that represents the concentration of analyte producing a 50% inhibition of the maximum signal S. The response of the competitor S can be

obtained by measuring the signal in absence of the analyte, the situation in which all the antibodies are bound to the competitor.
The immunoassay is governed by two equilibria, the first one involving the antigen-antibody interaction and the second one involving the labelled competitor-antibody interaction:

$$K_D = [Ab][Ag]/[Ag\text{-}Ab]$$

$$K_D^* = [Ab][Ag^*]/[Ab\text{-}Ag^*]$$

where $K_D$ and $K_D^*$ are the dissociation constants for the two reactions given by the concentration of free antibody [Ab], the antigen target [Ag] and the competitor [Ag*] and the immune complexes [Ab-Ag] and [Ab-Ag*].
Starting from these equations, the IC50 expression is derived:

$$IC50 > [Ag_0^*] + K_D$$

IC50 is always higher than the dissociation constant. When the competitor concentration is far below the $K_D$, the IC50 approaches its theoretical limit ($K_D$).[31] Thus, the IC50 value of a competitive assay has a theoretical limit that cannot be further reduced for a given detection antibody. The sensitivity of a competitive assay can be improved by reducing the competitor concentration, using a detection antibody with high affinity, or reducing the detection of antibody concentration.

### 1.2.2 DISPLACEMENT ASSAY

The displacement assay is another possible competitive format in which the difference in affinity between the tracer and the target is fundamental. There is a competition between labelled antigens and unlabeled antigens for the same binding site of an antibody.[32] First, antibodies are saturated by the competitor and then, the unlabeled antigen is added. The antibody-competitor complexes will dissociate in the presence of free, unlabeled antigens that can displace the tracer and bind the binding site. This is possible because the reaction between an antibody with its antigen is very specific and some modifications in antigen structure lead to a lower affinity between them. The unlabeled antigen-antibody complex is more stable than the labelled antigen-antibody complex. The difference in affinity of the two antigens is necessary to have the detection and quantification of the target, thus sometimes is useful to choose a competitor with a similar structure to the target and not the antigen itself linked to a label. In this way, the difference in affinity for the antibodies will be higher and the displacement will be simpler.[33]

The displacement format is composed of a first step in which antibodies undergo contact only with the labelled competitor to have the saturation of all the binding sites. As in the previous case, the target and the competitor have different affinities for the binding sites due to the difference in structure between them. Thus, the sample containing the target molecule is added and displaces the tracer to bind antibodies forming a more stable complex. Consequently, the signal produced by the competitor as a tracer is recovered by a detection method: it decreases proportionally to the target amount present in the sample.[34]

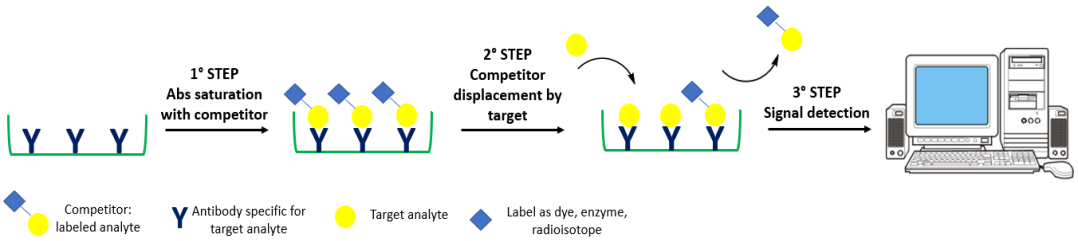


**Figure 5:** Schematic representation of displacement assay.

### 1.2.3 NON-COMPETITIVE ASSAY

The non-competitive design usually called sandwich assay is a format very spread and used for large analytes possessing more than one recognition site on their structure.[35] The principal characteristic is the use of two antibodies able to bind non-overlapping sites on the same antigen. Usually, the sandwich assay is performed in a heterogeneous form using a microwell plate and in each well, antibodies are immobilized. The first type of antibody is a “capture antibody” fixed onto the support that comes first in contact with the antigen. It should have high specificity for the target molecule and discriminate from other biomolecules. After washing, the solid support containing the antigen-antibody structure is incubated with a secondary antibody of detection that binds the free side of the target and forms the “sandwich structure”. The detection antibody usually is labelled with a probe to produce a signal proportionally to the target amount.

In the sandwich format, different types of probes can be used to label the detection antibody and to report the target event through fluorescent, chemiluminescent, colourimetric or radiation signalling. One of the most spread immunoassays in the sandwich format is called Enzyme-linked immunosorbent assay, ELISA,[36] considered a gold standard technique. It is used to detect a wide range of targets and in particular, it is the central method for protein quantification. In general, in the ELISA

system, an enzyme is linked to the secondary antibody as a label and the signal recovered is produced when the specific substrate for the enzyme is introduced. The reaction between them gives a colour formation in which intensity will be proportional to the target amount.

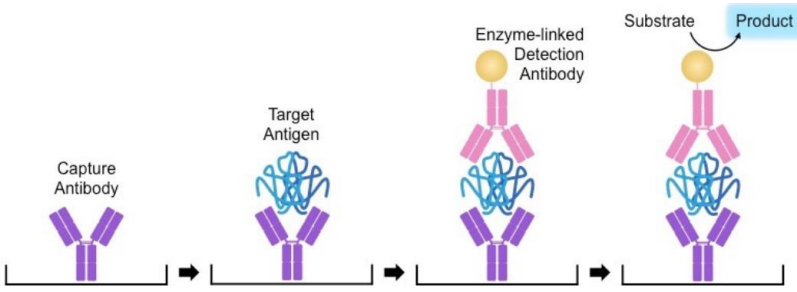


**Figure 6:** ELISA assay representation in the "sandwich" format.

The standard ELISA format allows the detection of a single target per well by coating each well with a different type of antibody specific for the different target analyte. In this way, the sample is introduced in each well where different targets are assayed at the same time.[37] The production of a signal in separated wells will show the presence of a target of different nature. ELISA assay is an example of a planar array performed by using a microtiter plate or a planar array with a precise location.

### 1.2.4 IMMUNOASSAY BASED ON PARTICLES

Nowadays, to measure protein panels in a single assay, planar arrays[38] are widely used for disease diagnosis, and prognosis, as well as, for biochemical analysis.[39]

A planar array or microarray is based on flat solid support onto which probe molecules (such as an antibody) are deposited. It is used for the detection of proteins by performing competitive and non-competitive format assays (Figure 5). The probe in each location is specific for a known target molecule and by using probes of different natures attached to the same grid, a multiplex assay can be performed. The term multiplex refers to multiple assays performed on the same sample useful to assay more than one target at the same time. The identity of each probe molecule is known from its location in the grid by positional encoding.[40]

Even if microarray allows for massively multiplexed measurement, they consume large quantities of reagents and time. Probe molecules must be attached to the array under the same conditions using the same surface chemistry, which may not be suitable for all probes. The rates of binding between probe and biomolecule on planar arrays are limited by diffusion to the surface.[41]

Because of microarray disadvantages, there has been an interest in developing suspension arrays or beads-based assays as an alternative approach for protein detection. Micrometre-sized solid particles (beads) are used for attaching probe biomolecules, such as antigens or antibodies for immunoassays. As functionalized beads are free in solution, the antibody-antigen match is favourited, and their binding displays faster reaction kinetics. Contrary to microarrays in which a limited number of probes can be attached to the grid, probes can be conjugated to millions of microspheres at the same time. Separate batches of microspheres can be functionalized by a variety of proven chemistries in solution under conditions that are optimum for each probe. When microspheres are used, the panel can easily be changed by adding or subtracting microspheres with different probes and they facilitate the separation and washing steps.

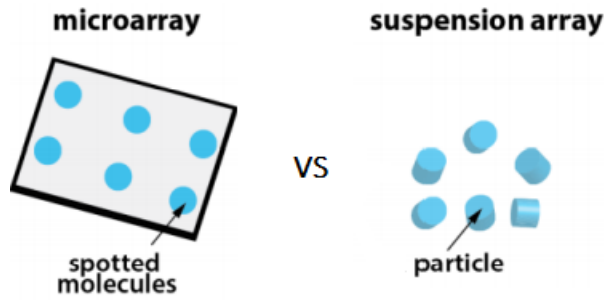


**Figure 7**: Microarray is formed by antibodies spotted onto membranes, glass slides, or other solid supports. The suspension array is based on the use of micro or nanoparticles of different natures functionalized with antibodies.

The use of beads is widely diffused in the immunoassay field. Particles of different natures can be employed in the application of each format assay, competitive or non-competitive for the detection of a wide range of analytes.

Walt et al.[9] designed a very sensitive competitive immunoassay for the detection of cortisol protein employing a fluorescence method of detection. The assay involved the competition between the analyte coated onto magnetic beads and the analyte target in the sample under test. The first step of the immunoassay is the mixing of biotinylated antibodies specific for the detection, the sample and magnetic beads. When the target is absent in the sample, antibodies bind the protein onto the surface of the bead. After the magnetic separation, a streptavidin enzyme is added and the beads are labelled with the enzyme, thanks to the biotin-streptavidin interaction. In the end, fluorescence detection is possible when the substrate for the enzyme is added, and their reaction will give a product able to

emit fluorescence. Otherwise, when the target is present, antibodies prefer to bind the cortisol-free solution rather than the antigen immobilized on the beads. When the enzyme is added, a decrease in the signal occurs. With the increase in cortisol concentration, the signal decreased proportionally because of competition. At the moment of the signal detection, the sample is loaded onto an array of microwells in which each bead was placed in only one well. The confinement of the fluorescent product generated by the enzymatic reaction within the well assures high fluorescence intensity that can be easily detected. This allows having an assay more sensitive than the standard ELISA which is not appropriate for the detection of low amounts of protein.

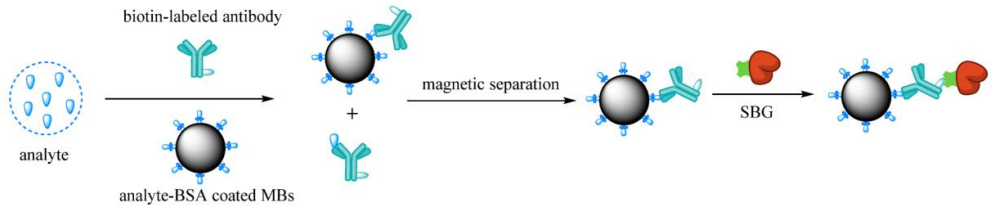


**Figure 8:** Representation of competitive immunoassay based on magnetic beads.

The sensitivity of beads-based immunoassay can be improved, and a lower amount of target can be detected than the classical planar array. Li et al.[42] designed an ELISA-like detection method combining gold nanoparticles AuNPs and magnetic beads MBs for the capture of Procalcitonin protein PCT. Gold nanoparticles were functionalized with primary antibody Ab1 and horse peroxidase enzyme HRP, while the detection antibody Ab2 was immobilized onto the surface of the magnetic particles. When the target protein was present, the two antibodies Ab1 and Ab2 bind the target leading to a sandwich structure. Then, beads were isolated from the solution, magnetically. When the enzyme substrate (TMB) was introduced, it reacted with the enzyme onto AuNPs producing a colourimetric signal. As the PCT quantity increased, the signal increased, consequently. Because of the multiple HRPs coupled onto gold nanoparticles rather than one antibody linked to one enzyme in the conventional ELISA, the produced signal was amplified. When the substrate is introduced, also in presence of a low amount of protein, a quantifiable signal is produced, and a substantial improvement of the detection sensitivity was achieved. The limit of detection was 5-fold lower than classical ELISA.

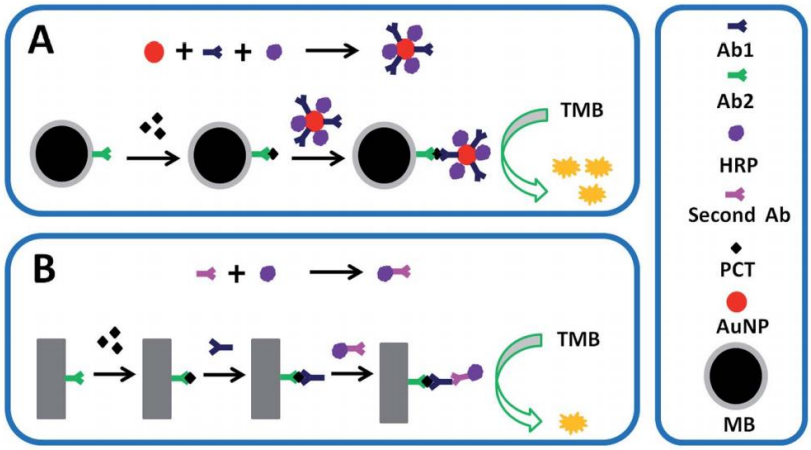


**Figure 9**: Principle of detection. (a) Magnetic bead and enzyme-antibody labelled AuNP-based ELISA and (b) conventional colourimetric ELISA

A suspension array gives the possibility to widen the number of target analytes that can be detected in the same assay. This is possible by performing a multiplex assay allowing the simultaneous measurement of multiple clinical parameters from the same sample, decreasing the time and cost.[43]

Because beads do not have a well-defined position, some forms of codes can be involved so that each bead can be identified in the solution. After the probe-antigen binding has taken place, the target on their surface can be detected.

The most well-established encoding technique is based on spectral or optical encoding. Microspheres are doped with fluorescent dye or fluorophores obtaining a different set of beads characterized by a unique code. The code is determined from the fluorescence intensity of each particle, read using a flow-cytometer, spectrofluorometer or laser microscopy. An increase in encoding capacity can be obtained by using multiple dyes in different concentration ratios: The number of unique codes available is equal to $X^{N-1}$ ($X^N$ if a zero level of all dyes is included), where X is the number of dyes used and N the number of available concentration levels of each dye.[44] The unique emission spectrum produced by a particular ratio of the two dyes serves as the identification method. The standard ELISA and other classical format assays were not sufficient for the detection of an ultralow amount of proteins in the sample. The limited sensitivity of ELISA allows for the detection target until the picomolar (pM) quantity of proteins. Differently, analytes and disease biomarkers are present in fluid and serum at subfemtomolar concentrations. To reach these concentrations, approaches based on single-entity

detection and miniaturized structures are increasingly investigated in recent times.[45] The volume of the sample is restricted to a single entity to generate a high local concentration easily to detect thanks to the signal amplification in the confined volume.

Single-Molecule Array (SiMoA) is an approach born from the work of Walt et al.[46,47,48] that makes use of arrays of femtoliter-sized reaction wells that can isolate and detect single molecules. SiMoA allows the detection of single protein molecules in serum simultaneously at subfemtomolar concentrations. Rissin et al.[49] developed the digital ELISA assay employing SiMoA. A classical sandwich structure was formed with free secondary detection antibodies and capture antibodies onto magnetic beads. A fluorescent signal was produced by the enzyme and quantified.[50]

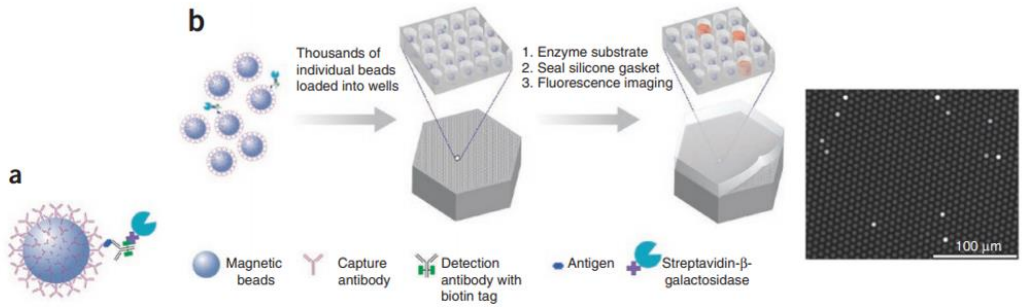


**Figure 10:** a) a sandwich structure formed onto magnetic bead; b) representation of miniaturized assay in femtoliter-sized reaction wells and fluorescent image of the bead confinement in wells.

By using the array of femtoliter-sized wells, the fluorescent signal generated by the enzymes was confined to a small volume producing a high local concentration of fluorescent molecules.

Transportation and confinement of single entities into these small containers have been facilitated through microfluidic techniques.

The displacement assay is another possible competitive format in which there is competition between labelled and unlabeled antigens for antibodies.[51] First, antibodies are saturated by the competitor and then, the unlabeled antigen is added. The free unlabeled antigens can displace the competitor due to their higher specificity.[52] Consequently, the signal produced by the competitor as the tracer is recovered by a detection method: it decreases proportionally to the target amount present in the sample.[53]

## 1.3 OPTICAL BARCODING

Suspension array gives the possibility to perform multiplex assay allowing the simultaneous measurement of target analytes from the same sample, decreasing the time and cost.[54]

The microsphere barcode is the key to the suspension array. The most well-established encoding technique is based on spectral or optical encoding. Microspheres are doped with fluorescent dye obtaining a different set of beads characterized by a unique code. The code is determined from the fluorescence intensity of each particle, read using a flow-cytometer, spectrofluorometer or laser microscopy. An increase in encoding capacity can be obtained by using multiple dyes in different concentration ratios.[55] The barcode confers a higher capacity for multiplex analysis.

Luminex Corporation invented xMAP technology[56] in which coloured polystyrene beads with a diameter of 5 µm are used to carry out biological assays. Beads were synthesized with internal dyes as an optical barcode that identifies each microsphere. Bead sets with a unique code were coated with an antibody specific to a particular biological target, allowing the simultaneous capture of multiple analytes in a single sample. Reading the code, rather than determining the position, the identity of the probe molecules attached to the microspheres was revealed. The number of codes increased by increasing the number of dyes. In Figure 11, three dyes have been incorporated into beads in different ratios. By using a single excitation wavelength, the three dyes could be excited emitting their characteristic fluorescent signals: a huge number of different codes were possible.

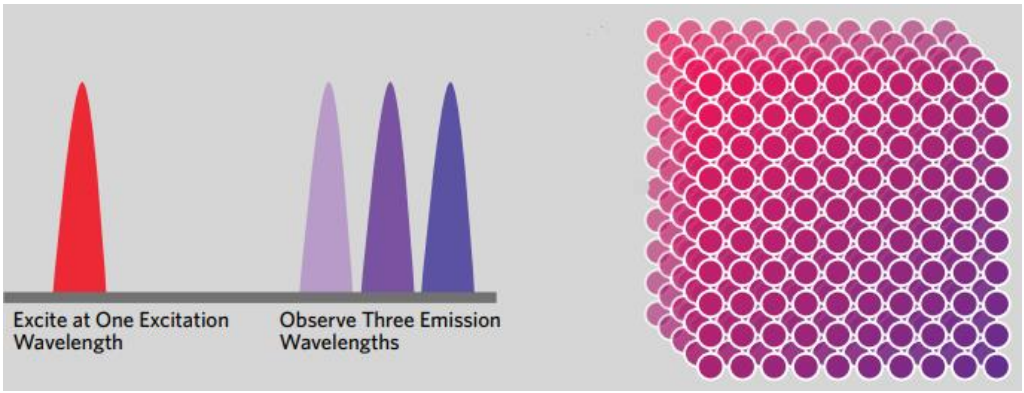


**Figure 11:** Luminex beads doped with three-dye products yielding 500 unique microsphere sets.

Luminex polystyrene beads were used to perform the assay in a competitive or sandwich format. Thus, a second dye was useful in both cases and it excited with a second excitation wavelength to allow the observation and detection of a biological assay on the microsphere surface (Figure 12). Using this process, xMAP Technology allowed multiplexing of up to 500 unique bioassays within a single sample.

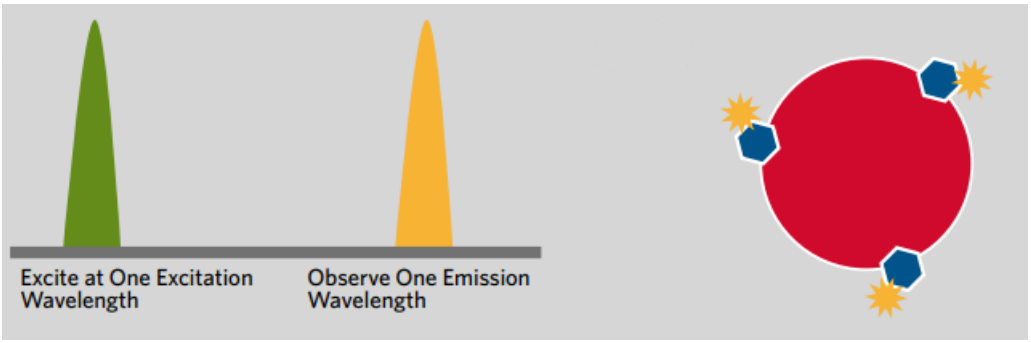


**Figure 12**: Binding event of analyte target showed by a dye report on beads surface.

The encoding capacity depends on the number of dyes used and their possible amount ratios.

A similar approach used semiconductor quantum dots rather than organic fluorophores to encode the microparticles. The quantum dots typically consist of a core of cadmium selenide (CdSe) or cadmium telluride (CdTe) characterized by a very broad excitation spectrum and fluorescence emission generally narrower than organic dyes.[57] QDs are also brighter and more resistant to photobleaching than fluorescent dyes. These properties made QDs ideal for encoding because quantum dots of different sizes can be excited with a single wavelength and the emission can be tuned by varying their radius. Potentially, many individual emission wavelengths for encoding were provided. The quantum dots were incorporated into polymer microbeads during the synthesis or entrapped by solvent swelling methods, or the quantum dots themselves can be functionalized with molecules attached directly to their surface. By mixing QDs with different emission wavelengths at different concentrations, significantly larger combinations can be interrogated with a single excitation wavelength.[58]

Han et al.[59] synthesized different sets of polystyrene beads doped with QDs by the swelling method. QDs of a single colour was entrapped by swelling the beads in a solvent mixture of appropriate solvents containing quantum dots. When solvents were eliminated, QDs were encapsulated into particle pores obtaining a physical

encapsulation. QDs embedded in single-colour-coded beads showed excitation spectra very similar to those of free QDs, and the emission maxima remained unchanged. This was due to the bead's porous structure acting as a matrix to spatially separate the embedded QDs and avoided the formation of aggregates in a heterogeneous population.

Following these single-colour studies, multicolour QD-tagged beads have been prepared by incorporating QDs at precisely controlled ratios in polymer beads. By changing the ratio of embedded QDs, different barcodes were obtained (Figure 10).

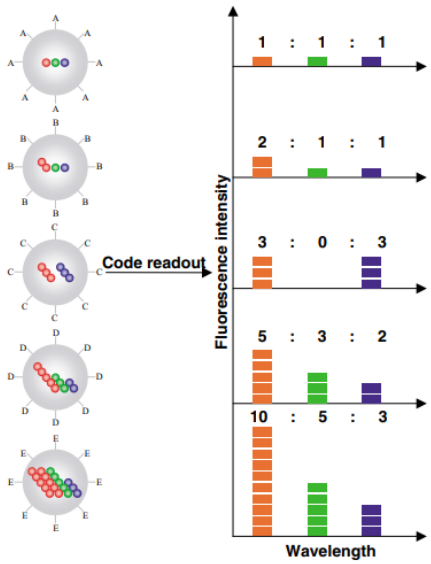


**Figure 13**: optical coding based on controlled ratios in beads.

However, beads as well as any other solid surface suffer from some limitations, such as non-specific interactions and low kinetics of reactions. The hydrogel particle-based platform is a more versatile tool for biomolecule analysis than existing particle systems because of many advantages linked to its use. Hydrogels, by definition, are three-dimensional cross-linked networks that can retain a huge amount of water to the mass of the polymer.[60] Many polymers are available to synthesize hydrogels as collagen, gelatin, chitosan, hyaluronic acid, alginate, poly(vinyl alcohol) (PVA), however, polyethylene glycols (PEGs) are the most used for diagnostic applications. PEG derivatives are extensively adopted for their good solubility in an aqueous buffer required for biomolecule manipulation,[61] low-cost production at different molecular weights and chemical functionalities. Particularly,

polyethylene glycols (PEG) are very adapted for particle synthesis employed in beads-based assays thanks to their biocompatibility and low-biofouling properties.[62] Hydrogel microparticles can be easily functionalized with probes of different natures (proteins, molecular beacons, aptamers, and double-strand probes) to capture and quantify clinically relevant biomarkers.

## 1.4 ENZYME IN BIOSENSING

Enzymes are biocatalysts with high selectivity, specificity, and activity under mild conditions. Enzymes are proteins with molecular weights ranging from 10.000 to 2.000.000, endowed with an active site in which the biological function is performed. The enzyme increases the rate of a particular reaction through the binding of the substrate in its active site. The enzyme returns to its original state after the reaction. Enzymes have very high specificity for the substrates and catalyse only specific chemical reactions.[63] Thus, they are categorized based on the catalytic reaction they can perform (e.g., hydrolase, peroxidase, polymerase, etc.). Due to their abilities as specialized catalysts combined with the reduced process time, low cost-effective, nontoxicity and eco-friendly characteristics, they have found a vast variety of applications in the food, agriculture, chemicals,[64] and pharmaceutical industry.[65,66] Presently, proteins and enzymes are used routinely in the medical field and diagnosis[67] of various diseases and biosensors development. A striking example is the sensors for glucose determination which market probably is the biggest in the diagnostic field.[68]

Enzyme-based biosensors hold the largest market share of commercial biosensors due to significant benefits, such as miniaturization, real-time diagnosis capability, bedside clinical testing and portability. A miniaturized enzyme biosensor for lactase and glucose determination has been developed.[69] Glucose oxidase and lactate oxidase are immobilized on ultramicroelectrodes composed of platinum and then used to determine the glucose concentration in the culture cell system of human breast epithelial cells.

The use of the enzyme allows for obtaining biosensors with high sensitivity and specificity. Specificity is the capacity to discriminate between closely related molecular structures in the sample and it depends on the biosensor type, the complexity of the sample and surface modification.

Several developed enzyme biosensors have been already commercialized and used in health care management (i.e., home blood glucose monitoring, portable clinical analyzers, etc.).

An enzyme biosensor combines an enzyme with a transducer to produce a signal proportional to the target analyte concentration. This signal can result from the reaction catalysed by the enzyme as a change in proton concentration,[70] release or uptake of oxygen,[71] light emission or absorption. Based on the type of transducer used to convert the signal to a measurable response, different types of biosensors are distinguished. Recently, an amperometric biosensor for the preliminary screening of cancer was developed.[72] The detection of the prostate cancer marker, L-fucose, was attempted by using gold nanoparticle (AuNP)-modified electrodes onto which dehydrogenase enzyme (CcPDH) was immobilized. The application of a low potential provided the oxidation of the L-fucose generating a measurable catalytic current. The biosensor exhibited high sensitivity and a low detection limit and it can be utilized in point-of-care testing for the first screening of cancer.

Biosensors involving transducers that generate an optical change are classified as optical biosensors.[73] Among the optical methods, absorptiometry, fluorescence[74] and surface plasmon resonance (SPR)[75] have had the biggest success. An enzyme-based optic fibre biosensor was developed for the estimation of inorganic phosphate in urine samples.[76] Zhang et al designed a novel platform for glucose detection using a miniaturized optical fibre SPR biosensor.[77] An enzymatic reaction through the device allowed obtaining an SPR differential signal corresponding specifically to glucose concentration. The colourimetric biosensor works by detecting a particular analyte through colour changes easily by the naked eye. In the case of enzyme-based biosensors, the colour change is produced by a specific reaction between the enzyme and its substrate. A multicolorimetric ELISA assay was developed for the determination of HCV based on multiple colour variants through the etching of AuNRs and the oxidation of 3,3′,5,5′-tetramethylbenzidine (TMB). The ELISA assay was integrated into a microfluidic device resulting in a portable and low-cost biosensor for rapid POC detection of HCV.[78] Colourimetric sensors are easy to prepare, allow fast detection, and have pretty good sensitivity.

However, the most challenging disadvantage of the enzyme-based biosensor for in vivo analysis is a reduced signal response and selectivity, due to the presence of fouling agents and interference caused by chemicals present in the sample matrix. Among the efforts to address the problems, enzyme engineering and hybrid

biomaterial incorporation have been used to promote enzyme stability and minimize endogenous interference. The present developments trends of enzymatic biosensors are directed toward device miniaturization, multiplexed detection, and applicable expansion to bedside patient and home testing devices such as paper-based test kits, lab-on-a-chip and biochip sensing devices, which require minimum sample pretreatment, and low reagent and power requirements.

### 1.4.1 ENZYME IMMOBILIZATION

For almost all applications, enzymes needed immobilization on support before their use. This produces enzyme stabilization, the handling easier and enhancing their separation from a reaction mixture.[79] The usual supports for enzyme immobilization are polymer or magnetic beads, polymer layers, microgels and hydrogels. In particular, nanoparticles are considered the ideal support due to the minimized diffusional limitations, maximum surface area per unit mass, and high enzyme loading capability. Several model enzymes, including lysozyme, horseradish peroxidase, catalase, and trypsin, adsorb strongly to both inorganic and organic nanoparticles.

Enzymes can attach to support either through physical bonding (such as hydrophobic interactions) or covalent bonding.

Physical bonding is easy and fast, and it occurs through the adsorption of the enzyme on the supports by forming hydrophobic interactions such as van der Waals and hydrogen bonds. The possibility of lacking the immobilized enzyme can reduce the potential use of the functionalized support. Most of the studies on enzyme immobilization focus on the covalent bonding between enzymes and functional carriers.[80] The enzyme immobilization on support provides a more stable system that reduces denaturation and conformational changes in the enzyme structure.[81] This results in less responsiveness to environmental changes such as pH value and temperatures. Different chemistries of immobilization are possible based on the type of functional groups present on the supports. When the solid supports are nanoparticles with a surface decorated with carboxyl groups, an activation step is needed against the amine ones to form strong covalent peptide bonds with the lysine groups protein. The most common way to activate carboxyl groups consists in preparing a succinimidyl ester by reacting with N-hydroxysuccinimide (NHS) and N-ethyl-N'-(3-(dimethylamino)propyl)carbodiimide (EDC) used as activation reagents.[82]

Usually, gold nanostructures and nanoparticles are decorated with thiol groups that can be involved in a chemical modification of the surface. Gold surfaces can bind Cysteine (Cys) amino acid strongly via the thiol group acting as the linker for enzyme immobilization. Vorster et al.[83] used cysteine-modified gold nanostars AuNSs (AuNSs–Cys) for the covalent coupling of NHS-terminated GOx for glucose detection. Li et al.[84] developed a catalytic nanodevice using glucose oxide as the enzyme. Gold nanoparticles decorated with linkers modified with a carboxyl group at the end. The glucose oxidase enzyme GO immobilized on the surface of carboxyl-terminated alkanethiol-modified AuNPs through the EDC/NHS coupling reaction. Otherwise, particles functionalized with epoxy groups can react without previous activation. The epoxy groups react with amino groups of biomolecules by a ring-opening reaction of the epoxy group. Peng et al.[85] immobilized the Thrombin enzyme on dynabeads®M-270 epoxy magnetic beads by a direct covalent binding method. Enzyme-functionalized particles were used to develop a screening method for the detection of thrombin inhibitors in a Danshen medicinal herb with cardiovascular action.

### 1.4.2 ENZYME ACTIVITY

The applicability and potential of enzyme biosensors and enzyme-based techniques depend on the catalytic activity of the enzyme used as a recognition element. After the immobilization onto particles or supports, the catalytic activity of the enzyme should be determined as the capacity to react with its specific substrate. The substrate used is the 3,3',5,5'-tetramethylbenzidine (TMB, Sigma-Aldrich) that HRP converts from its colourless form to its oxidized green product. The absorbance of the solution presented two peaks at 370 nm and 562 nm. The TMB colour development process was stopped by the addition of an acidic stopping solution to quench the redox activity. The blue-green reaction product is converted into a yellow species producing a shift of the absorbance maximum to 450 nm. The catalytic activity of free HRP was determined and compared to that of bound enzyme on microgels following the experimental protocol published by Yan et al. [86] The HRP activity was evaluated by studying its ability to oxidize peroxidase colourimetric substrate TMB and determining kinetics parameters. The activity unit (U) is defined as the amount of enzyme that catalyses 1 µmol of product per minute. The specific activity (SA, U $mg^{-1}$) is defined as activity units per milligram of the enzyme. First, solutions of known HRP concentration (5 ng/ml, 10 ng/ml, 20 ng/ml,

30 ng/ml) are prepared in the MES buffer used for the coupling reaction. A 96-well plate is used for the absorbance reading filling the wells with up to 200 µL of HRP solutions. 50 uL of TMB working reagents are introduced in each well and absorbance values are measured at the plate reader at 562 nm every 20 seconds. So, for each solution, a kinetics curve of Abs against time was obtained. In the first part of the curve, absorbance variations were approximately linear to the reaction times. The value of the slope in the initial rate period ($\Delta A/\Delta t$) of the enzyme reaction is constant and represents the substrate µmol processed per minute (U).

## 1.5 AIM OF THE WORK

This PhD work aims to expand the potential of the microgels-based platform in the biosensing field to overcome the limitations associated with techniques already in use. In the first chapter, the synthesis of multifunctional particles is presented. Core microgels with different structural properties are obtained by keeping constant the synthesis process, varying the building blocks involved and the moment in which they participate in the reaction. Core microgels with different physical and chemical properties are produced according to the desired properties to confer

In the second chapter, a novel bioassay based on magnetic beads and PEG microgels for antibody detection is presented. Microgels are adopted as the carrier of anti-Fab antibody and HRP enzyme, while magnetic particles are functionalized with anti-Fc antibodies acting as capture particles. Anti-Fab and anti-Fc antibodies are used for recognition of the target antigen human IgG forming a sandwich structure. Particle clusters are formed and visible by the confocal laser scanning microscope (CLSM). The cluster area increases as the target concentration increase too. After the interaction, unbound microgels are separated from the solution and used to produce a colourimetric signal for target detection. Increasing the target concentration in samples, the number of free microgels in the solution decreases. The colourimetric signal produced by HRP-microgels free in solution decreases too.

# CHAPTER 2


## ABSTRACT

The microgel-based platform is composed of PEG multifunctional particles possessing multiple components and properties. Microgels are polymeric particles characterized by colloidal stability, biocompatibility and antifouling properties. Due to their chemical flexibility, their structures and features are modifiable to fulfil the requirements of the applications. We wonder if it is possible to synthesize microgels by using the same mechanism with different chemistry in an easy way and obtain a controllable size and unidimensional.

In this work, PEG core microgels with different physical and chemical properties are produced by suspension polymerization. Different particles are obtained by keeping the synthesis process constant, adding chemicals at different moments and varying their nature. Two cores R1-COOH, defined bulk and surface, respectively are produced by using the acrylic acid monomer to create carboxyl groups on their surface for further conjugation. The difference is that the acrylic acid is introduced at different moments during the reaction synthesis and different products are obtained. Furthermore, two cores R1-AMPS are synthesized with an additional monomer (AMPS) to confer a higher negative surface charge. Core R1-AMPS 0.1 and core R1-AMPS 1 differ in the AMPS amount: the first one has a molar quantity of AMPS 10 folds smaller than AAc (1:10) and the second one has a molar amount of AMPS equal to AAc (1:1). Core R1-COOH bulk presents a diameter higher than the Core R1-COOH surface whose surface charge is more negative, due to the confinement of Aac on the outer shell of microgels. The core R1-AMPS shows a smaller size than the core R1-COOH particles. The surface charge of the R1-AMPS 1 microgels is more negative than the other microgels. The presence of the AMPS allows for maintaining a more negative charge at pH 3 compared to cores R1-COOH, where a charge close to 0 is displayed. At high pH values, the deprotonation of the carboxylic groups results in a repulsive force among them causing the swelling particles. This effect is greater for the core R1-COOH bulk in which COOH groups are present both on the surface and in the bulk of particles. In conclusion, the presented process can be modified according to the properties of microgels to confer, avoiding more complex structures such as core/shell particles.

# 1. INTRODUCTION

Microgels are polymeric particles characterized by colloidal stability and swelling capacity in water. They consist of a three-dimensional polymeric network whose diameter varies between 10 nm and 1 μm, capable of absorbing a large amount of water. Hydrogel microparticles and microgels are synthesized with different chemical strategies and opportunely functionalized with probes to detect circulating biomarkers in human serum.[87] The high biocompatibility and antifouling properties[88] of hydrogel make possible the use of the microgels-based platform in biosensing and inspired the development of several sophisticated applications, such as biosensors.[89,90] Pelton et al.[91] introduced a novel type of microgel-based biosensors for the detection of different pathogens. In their work, PNIPAM microgels were initially functionalized with either an antibody (IgG) or DNA aptamer and then, used as ink on filter paper deposited through ink-jet printing to produce inexpensive test paper. The microgel-based platform is composed of multifunctional particles[92] which have extensive applications owing to bearing various functions in an integral whole and possessing multiple components and properties. Their structures and functions can be modified to fulfil the requirements of the applications.[93]

The most used synthesis method is constituted by the radical polymerization of vinyl monomers with a cross-linker. Other reagents can be introduced with different functional groups in the reactor for further chemical derivations. Their synthesis is essentially summarized in three categories based on the particle formation mechanism: homogeneous nucleation, emulsification, and complexation. In the first case, microgel particles are formed throughout the polymerization in a solution of soluble monomer, including a cross-linking agent. To obtain good control over the particle formation, the polymer obtained during the polymerization must be insoluble in the solution. The homogeneous nucleation includes emulsion polymerization in which the monomer is present as a suspension mixed with a surfactant and a free radical initiator. Emulsion polymerization is a robust method to obtain core-shell microgels. The core particles are firstly prepared by conventional emulsion polymerization and then are used as seeds for the second-stage shell polymerization. Battista et al.[94] obtained core double-shells PEG microgels through a multistep procedure in which alternating fluorescent and non-fluorescent concentric hydrogel shells are synthesized around a core particle. The first fluorescent acrylate dye is embedded in the core and followed by a non-

fluorescent shell. The last outermost shell is synthesized by using a second fluorescent acrylate dye and an anchoring group, such as the carboxyl group. The second method is emulsification. In this case, an aqueous pre gel solution (a monomer or a polymer) is suspended in an oil phase to give a water-in-oil emulsion. In the second step gelation, the emulsion droplets undergo a chemical reaction to crosslink each emulsion droplet. The last method involves diluting solutions of oppositely charged polyelectrolytes to form colloidally dispersed, polyelectrolyte complexes. Microfluidics methods are arising to achieve major control over the size and shape of microgels, to use milder chemistry and reduce the time and cost of the synthesis. Pregibon et al.[95] generated a new method based on "continuous-flow" lithography to produce PEG particles in a single step with distinct regions. These multifunctional particles are equipped with a fluorescent, graphically encoded region for optical determination and a probe-loaded region for analyte detection and target capture.

Thus, microgels and hydrogel microparticles can be produced with multiple functions thanks to their chemical flexibility.[96] During their synthesis, different building blocks can be introduced into the reactor allowing their co-polymerization with the cross-linking agent. NIPAM and HMABP multifunctional core-shell microgels were prepared by Hellweg and coworkers[97] via seeded precipitation polymerization. In this case, for example, catalytic activity was conferred to the microgels through palladium nanoparticle incorporation.

Separated batches of particles can be decorated with anchoring groups of different natures such as carboxyl group, amine group, or epoxy group. Another possibility is to mix building blocks during the synthesis: particles with different functional groups on the same surface are generated. The anchoring groups are then exploited for the covalent immobilization of probes. Microgels can be coated with antibodies,[98] enzymes,[99,100] or oligonucleotide strands[101] individually, or various probes can be mixed resulting in particles active against diverse targets.[102] This makes possible the use of the microgels-based platform in biosensing and diagnostic fields for the detection of more biomarkers. The subsequent bioconjugation with oligonucleotide strands was useful to detect DNA biomarkers. The developed assay was based on the optical fluorescence readout. The flexibility of microgels allows having spectrally encoded microgels created with a different number of dyes. The dyes ratio was modulated between their fluorescence emission (Fluo/Rhod) obtaining a robust and reproducible spectral encoding.[103] The

outermost shell of these particles containing acrylic acid was used to bind dye-modified nucleic acids probes.

Multiplex assays have been performed by using microgels synthesized with different spectrally encoding and then functionalized with double-strand probes specific for different microRNAs. When they have been spiked into the serum sample under test, the presence of miRNA targets has been highlighted by the probe fluorescence emission and the identity of the miRNA is revealed by reading the ratio of Fluo/Rhod of microgels.[104] This characteristic was important for the creation of a multiplex assay to detect more than one biomolecule in the same sample at the same time. By changing the fluorophores ratio in the core and the shell, microgels with different optical barcodes have been obtained. Oligonucleotide assays with microgels-based platforms had higher sensitivity and lower limit of the detection (LOD) than assays with the same probes not conjugated to microgels. The low limit of detection is due to the confinement of probes onto the surface of nanometric particles producing an enhancement of fluorescent signal.[14] Upon the detection event, femtomolar (fM) concentrations were recovered lowering the limit of detection to 5 orders of magnitude if compared with the probes alone. This represents a modular platform that can be generalized for any direct detection applied to a wide spectrum of biomedical applications.

Recently, a very sensitive colourimetric multiplex immunoassay has been developed involving hydrogel particles functionalized post-synthesis.[105,106] The remnant double bonds in the hydrogel were exploited to conjugate thiolated antibodies via thiol–ene click reaction.[107]

Beyond the possibility of multiplexing assay and flexibility of functionalization, another advantage linked with the use of microgels is the possibility to test complex biological fluids. In general, the presence of biomolecules could interfere during the assay. Differently, PEG microgels were not affected by the complexity of the sample. Many polymers are available to synthesize hydrogels as collagen, gelatin, chitosan, hyaluronic acid, alginate, poly(vinyl alcohol) (PVA), however, polyethylene glycols (PEGs) are the most used for diagnostic applications. PEG derivatives are extensively adopted for their good solubility in an aqueous buffer required for biomolecule manipulation,[108] low-cost production at different molecular weights and chemical functionalities. Particularly, polyethylene glycols (PEG) are very adapted for particle synthesis employed in bioassays thanks to their biocompatibility and low-biofouling properties.[109] The hydrogel-based platform

gives the possibility to change the number of particles involved and at the same time, the number of probes on their surface. The tunability of such parameters is fundamental to improving the sensitivity and the limit of detection of the assay. Caputo et al.[110] developed a microgel-based bioassay making use of core/shell microgels functionalized with double-strand probes specific for the biomarker. In the presence of the oligonucleotide target, fluorescence emission by probes is recovered with a proportional intensity to the target amount. The sensitivity of the assay has been improved substantially by scaling and decreasing the number of microgels used and acting as a target concentrator. At a fixed amount of the target, a lower number of microgels showed high sensitivity: each microgel approached its saturation point in which the highest probe levels bound to the target are reached, showing enhancement in signal emission per single particle. In this way, lower and lower biomolecule targets can be revealed, improving sensitivity, and reaching a femtomolar limit of detection. The use of engineered hydrogels allows their integration in miniaturized devices[111] for optical readout directing towards the more and more sensitive assay[112,113] and pushing these technologies as a point of care device.[114]

We wonder if it is possible to synthesize microgels with different chemistry in an easy way and obtain a controllable size, unidimensional and by using the same mechanism.

In this work, core microgels with different physical and chemical properties are produced. The synthesis of multifunctional particles is carried out by keeping constant the synthesis process, varying the building blocks involved and the moment in which they participate in the reaction. In this way, different microgels are obtained according to the desired properties to confer, avoiding more complex structures such as core/shell particles.

# 1. MATERIALS AND METHODS

## 2.1 MATERIALS

Poly (ethylene glycol) Dimethacrylate Mn 550 (PEGDMA), Alcohol Polyvinyl 40-88 (PVA), Rhodamine B Methacryloxy-Tricarbonyl, Dimethyl sulfoxide (DMSO), Acrylic Acid (Aac), Potassium Persulfate (KPS), 2-Acrylamide-2-Methyl-1- Acid Propanesulfonate (AMPS), 1-Ethyl-3- (3-dimethyl aminopropyl) carbodiimide (EDC), N Hydroxyisuccinimide (NHS), Acid 2- (N-Morpholino) Ethane sulfonic (MES), Tris

(Hydroxymethyl) Aminomethane (TRIS), Phosphate Buffer Saline (PBS), Immunoglobulin G Atto647N (IgGAtto647N) were purchased from Sigma-Aldrich.

## 2.2 CORE SYNTHESIS

PEG microgels with different monomers were prepared according to a previously reported work.[18]

Microgels are obtained by free-radical precipitation polymerization carried out in a three-neck, 100 mL round-bottom flask to which a filtered, aqueous solution of 1% (w/v) PVA, 1% (w/v) PEGDMA were added and heated to 65 ° C. The reaction was initiated by adding KPS aqueous solution (to make a final KPS concentration of 2mM). The solution turned turbid, indicating successful initiation. After 10 minutes, Rhodamine B dye (0.1 mM) was added to the stirred mixture.

Different core microgels are produced by varying monomers during the reaction. Acrylic acid and AMPS are used and added at different times referring to the KPS addition, as reported in the following table:

| **Core microgels** | **Acrylic acid** | | **AMPS** | |
|---|---|---|---|---|
| | Quantity (mg) | Time (min) | Quantity (mg) | Time (min) |
| R1-COOH bulk | 125 mg | 0 | / | / |
| R1-COOH surface | 125 mg | 10 | / | / |
| R1-AMPS 0.1 | 125 mg | 10 | 35.8 mg | 20 |
| R1-AMPS 1 | 125 mg | 10 | 358 mg | 20 |

The solution was allowed to heat and stir for an additional 5 h while being purged with N2 gas. The course of the reaction was monitored by the dynamic light scattering DLS (Malvern Zetasizer Nano ZS instrument, 633 nm laser, 173° scattering angle) determining the increase of particle size. After 5 hours, the reaction was stopped by cooling to 0°C in an ice bath. The microgels were dialyzed for 15 days against distilled water, purified several times by centrifuging for 15 minutes at 12000 rpm and resuspending in deionized water to remove unreacted monomers, oligomers and surfactants and stored at 4 °C until further use.

## 2.3 CHEMICAL-PHYSICAL CHARACTERIZATION

### 2.3.1 PARTICLE SIZE AND SIZE DISTRIBUTION

Measurements were conducted using Dynamic light scattering (Malvern Zetasizer Nano ZS instrument, 633 nm laser, 173° scattering angle) which allowed calculation of the intensity-average diameter of the particles via the Stokes-Einstein equation. The hydrodynamic diameter (Dh) was determined in the presence of water. A total of 3 runs (each comprised of 3 cycles) were conducted; the experimental uncertainties represent the standard error of the mean of 3 replicate runs.

### 2.3.2 ZETA POTENTIAL AND ELECTROPHORETIC MOBILITY

Measurements were conducted using a Malvern Zetasizer Nano ZS instrument (Malvern Instruments Ltd, Worcestershire, UK). Polystyrene cuvettes were used as sample holders and were rinsed twice with the sample solution before use. The zeta potential, ξ, and electrophoretic mobility were determined in the presence of $10^{-3}$M KCl as the background electrolyte at 0.1% w/v microgel concentration. The experimental uncertainties represent the standard error of the mean of 3 runs (each comprised of 3 cycles).

### 2.3.3 COOH CONTENT

Potentiometric titrations were performed using Compact Titrator G20 (Mettler Toledo AG, Analytical Schwerzenbach, CH) to determine the COOH content of microgels. Samples were prepared by suspending 0.050 g of the microgel in 50 mL of $10^{-3}$M KCl solution. Titrations were run in a thoroughly cleaned, 100 mL beaker fitted with a pH electrode and NaOH (0.1 M, freshly prepared from Standard volumetric concentrates) was used as the titrant. During the titration, pH was measured as the function of the volume of the delivered standard NaOH solution. After each 25 µL of titrant was delivered into the microgel dispersions, followed by magnetic stirring until the pH value was stable and recorded. The total volume of standard NaOH solution delivered at the equivalence point was used to calculate the carboxyl content of microgels.

### 2.3.4 VISCOMETRY AND PARTICLE MASS DETERMINATION

Ubbelohde viscometer was used for determining the intrinsic viscosity of different microgel preparation as already described by Romeo et al.[115]

Capillary viscometry is conceptually simple: the time it takes a volume of polymer solution to flow through a thin capillary is compared to the time for a solvent flow. The flow time (t) for either is proportional to the viscosity (η) and inversely proportional to the density (ρ).

$$t\ solvent = \frac{\eta\ solvent}{\rho\ solvent}$$

$$t\ solution = \frac{\eta solution}{\rho\ solution}$$

The relative viscosity is defined as:

$$\eta rel = \frac{t\ solution}{t\ solvent}$$

In this work, the flowing time of diluted microgel solution at different concentrations was measured. Each time is an average of 5 run measurements. For the particle mass determination, the Bachelor-Einstein fitting was performed by using Origin software.

### 2.3.5 SPECTROFLUORYMETRY

2300 EnSpire multilabel reader (PerkinElmer, Waltham, MA) was used to measure the fluorescence emission intensity and to record the fluorescence emission spectra. To quantify the fluorescence emission of the encoded microgel, all microgel sets were excited at a specific wavelength ($\lambda_{ex}$Fluoresceine= 488 nm, $\lambda_{ex}$Rhodamine= 540 nm, $\lambda_{ex}$ATTO532= 532 nm, $\lambda_{ex}$ATTO488= 488 nm).

### 2.3.6 CLSM IMAGING FOR FLUORESCENCE QUANTIFICATION

Confocal laser scanning microscope Leica SP5 using Helium-neon laser 543 nm and 633 nm, Argon laser 488 nm was used to collect fluorescence images of microgels. 20 µl of microgels diluted solutions were loaded onto µ-slide channels (Ibidi, Martinsried, DE). The objective used was HCX PL APO CS 63.0x1.40 oil, section thickness about 1µm, scan speed 8000 Hz, image size 77.5x77.5 $\mu m^2$. For microgel experiments, 200 microparticles were selected for each sample (i.e. different target concentrations) to be analyzed and their fluorescence quantified. All captured images were analysed with a public domain image-processing Image J (version1,43i, NIH, Bethesda, MD) to calculate the fluorescence mean and standard deviation of each sample.

## 2.4 MICROGELS FUNCTIONALIZATION

The microgel surface is functionalized with IgG-Atto647N through a coupling reaction. The activation of the carboxy groups is performed by using 1-Ethyl-3-(3-dimethyl aminopropyl) carbodiimide (EDC) and N-Hydroxy succinimide (NHS).[116]
250 µg of microgels are suspended in 1 mL of 2-(N-Morpholino) Ethane Sulfonic acid (MES) buffer solution (50 mM, pH 6) and centrifuged (10.000 rpm, 10 minutes, 4°C). After removing the supernatant, the pellet is suspended in 500 µL of MES and 19 mg of EDC and 23 mg of NHS (0.1 M and 0.2 M, 1:2) are added dropwise.

After 3 hours, 10 µg of anti-IgG atto647N antibodies (10 µg/mL) are added. The reaction is allowed to run overnight at room temperature. Then, the reaction solution is centrifuged for 10 minutes (10.000 rpm, 4°C) and, after removing the supernatant, a solution of 450 µL of MES and 50 µL of TRIS (pH 8) is added.
After removing all the supernatant, PBS (pH 8) is added to the functionalized microgels to a final concentration of 250 µg/ml. The solution is stored at 4°C until further use.

## 2. RESULTS AND DISCUSSION

The microgel-based platform is composed of multifunctional particles with multiple properties and functions which can be modified to fulfil the requirements of the applications. Thanks to their chemical flexibility, microgels are synthesized by the polymerization of different building blocks with the cross-linking agent obtaining different functional groups on the same surface. We wonder if it was possible to synthesize microgels with different chemistry in an easy way and obtain a controllable size, one-dimensional and always with the same mechanism.
In this work, core microgels with different physical and chemical properties are produced by keeping constant the synthesis process. Two cores R1-COOH, defined bulk and surface, respectively are produced by using the acrylic acid monomer to create carboxyl groups on their surface. The difference is that the acrylic acid is introduced at different moments during the reaction synthesis and different products are obtained. Furthermore, two cores R1-AMPS are produced by introducing an additional monomer (AMPS) resulting in microgels with different properties. Core R1-AMPS 0.1 and core R1-AMPS 1 differ in the number of AMPS: the first one has a molar quantity of AMPS 10 folds smaller than AAc (1:10) and the second one has a molar amount of AMPS equal to AAc (1:1).

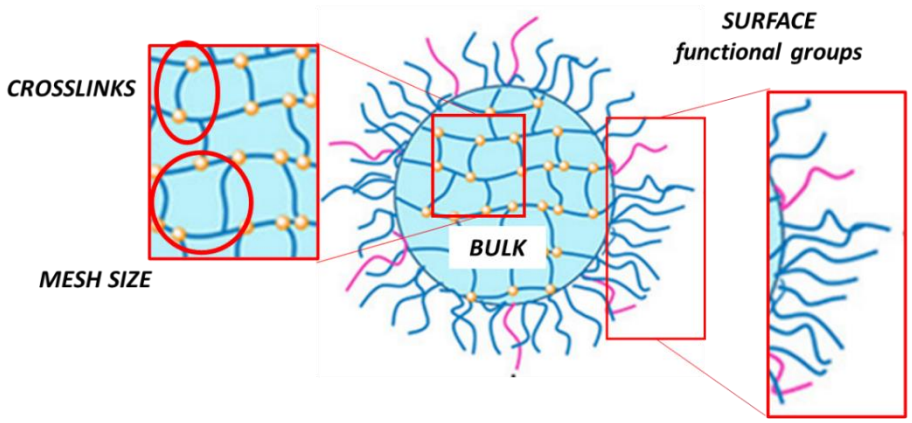


**Figure 1:** Microgels structure.

## 3.1 CORE SYNTHESIS

The reaction used for the core synthesis is suspension precipitation free-radical polymerization.[117] The cross-linking agent PEGDMA reacts with two co-monomers: acrylic acid and rhodamine as a fluorescent dye. The reaction starts with potassium persulfate (KPS) as an initiator that at 65°C, creates free radicals. Growing chains are formed by acting as nucleation sites on which the polymer aggregates.

Under polymerization conditions, the resulting oligomeric network is insoluble by producing their precipitation and forming precursor particles. Their surface charge density increases until the colloidal stability is reached so that primary particles are formed. Polyvinyl alcohol (PVA) is used as a surfactant to stabilize the growing nuclei to aggregation during the reaction. Acrylic acid is used to obtain microgels with carboxylic groups (-COOH) on their surface. These groups are useful for microgel functionalization with biomolecules.

Rhodamine is polymerized inside the microgels to create an optical barcode for particle detection.

Four different types of microgels are produced and defined: Core R1 COOH bulk, Core R1 COOH surface and two Cores R1 AMPS surface.

## 3.2 CORE R1 COOH BULK

For the Core R1-COOH bulk synthesis, PEGDMA and acrylic acid are introduced into the reactor at the beginning of the reaction. After 1h, the KPS initiator is added, and co-monomers polymerize. Rhodamine is added after 10 minutes. Resultant microgels are characterized by the -COOH functional groups both in the bulk and on the surface with the same probability. The quantities of the reagents are shown in the following table:

| Chemicals | Quantity |
|---|---|
| PVA 1% | 50 mL |
| PEGDMA | 500 mg |
| KPS | 27 mg |
| Rhodamine | 333 $\mu$L |
| Aac | 125 mg |

**Table 1:** Quantity of chemicals used in Core R1 COOH bulk synthesis.

The polymerization reaction is analyzed by taking aliquots of mixture solution at a distance of 10 minutes and analyzed at the DLS to evaluate the growth of microgels.

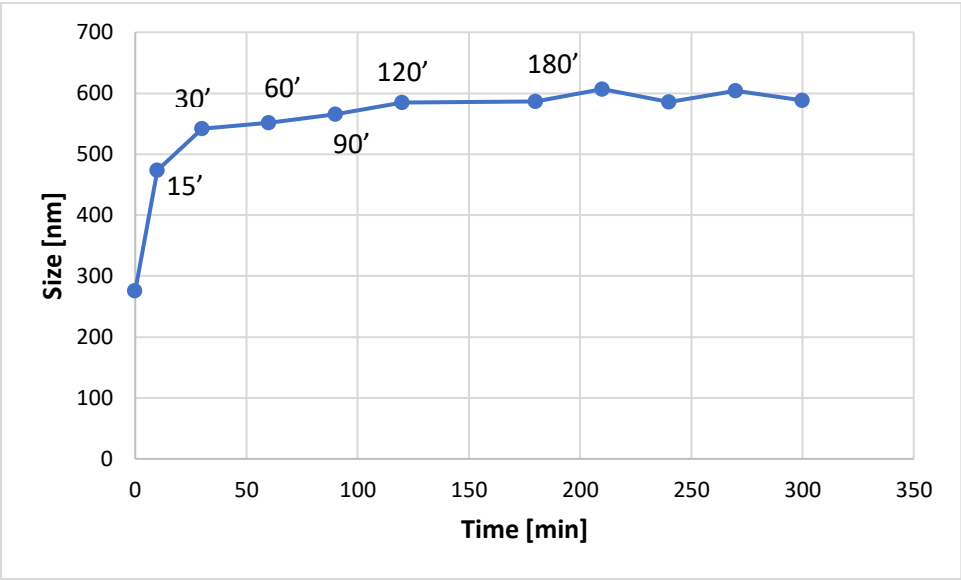


**Figure 2:** Hydrodynamic diameter variation during the reaction.

The minute 0 corresponds to the KPS addition resulting in particles of 275.9±8.5 nm. A significant size enhancement is noted after 10 minutes, then the diameter value reaches a plateau after two hours. The final microgel size is about 604.2±7.9 nm.

After the synthesis, microgels are purified by centrifugation and characterized to determine their physical, chemical, and optical properties. Microgels size determination is conducted using Dynamic light scattering. Core microgels result in uniform size with a hydrodynamic diameter of 760.2±16.1 nm. The polydispersity index (PDI) recorded is very low 0.076 highlighting that the microgel solution was monodisperse. The microgels show a negative zeta potential of around -20.1±0.5 mV due to the presence of acrylic acid on the surface. This negative charge confers colloidal stability allowing them to stay suspended and not aggregated. These functional groups are fundamental for the subsequent functionalization of microgel surfaces with antibodies or other biomolecules.

Size and zeta potential were evaluated at different pH values. Solutions of 40$\mu$g/mL microgels were prepared in water with three different pH values: pH 3, pH 7 and pH 10. To obtain the solution at pH 3, 0.1 M HCl was added, while for those at pH 7 and pH 10, NaOH 0.1 M was added. Measurements are made with Compact Titrator G20 (Mettler Toledo AG, Analytical Schwerzenbach, CH). In the following chart, I have reported size and zeta potential values:

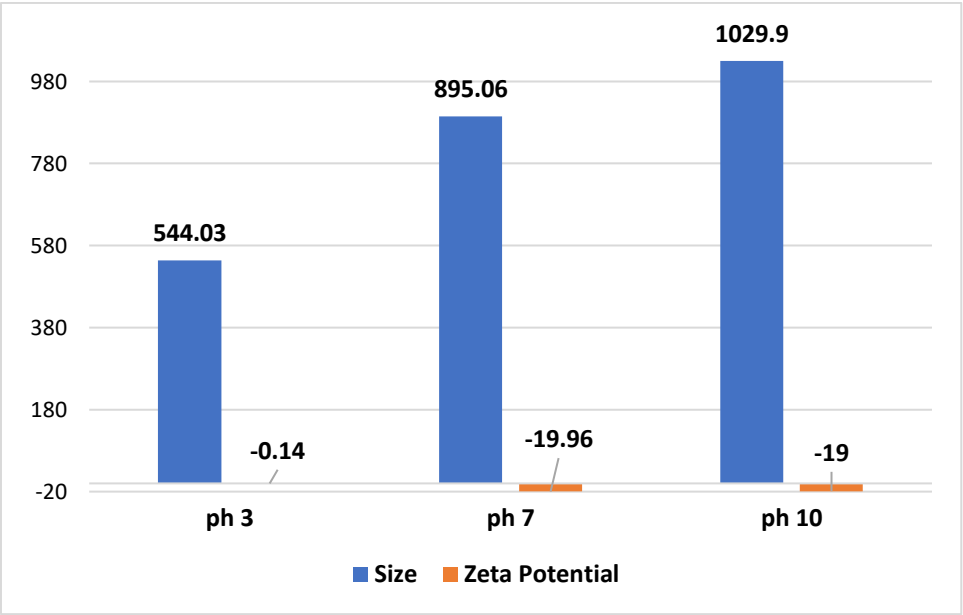


**Figure 3**: Size and Zeta Potential at different pH values.

Both size and zeta potential change as a function of the pH values. As result, microgels size tends to increase as the pH value increases due to the deprotonation of the -COOH groups producing negative charges onto the surface.

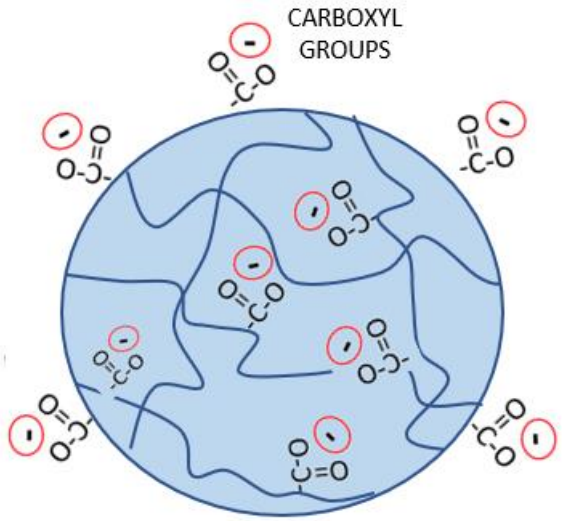


**Figure 4**: Core R1-COOH bulk with COOH groups both in bulk and on the surface.

The repulsive force produces a visible swelling for each pH value thus, the microgel size passed from 544.1±9.3 nm to 1029.9±17.1 nm.

The zeta potential decreases from pH 3 to pH 7 due to the deprotonation of carboxyl groups onto the surface. At pH 3, the zeta potential value is 0.14±0.04 mV.

At pH 7, COOH groups are completely deprotonated, and the negative charge is -19.96±0.66 mV, thus the surface charge is constant until pH 10 (-19.1±0.7 mV).
The optical characterization was performed by recording the spectra with fluorescence spectrophotometry. For all samples, an integration time of 0.2 s and varying the slit values, input and output, were used to have a value of S1 less than $2x10^6$. The spectra shown in the figure are S1/R1 which is the signal of the sample corrected to a reference reflector. The samples were excited at 548 nm and emission was collected from 568 to 715 nm. Spectra of microgels were recorded at a concentration of 40 µg/mL by varying pH values.

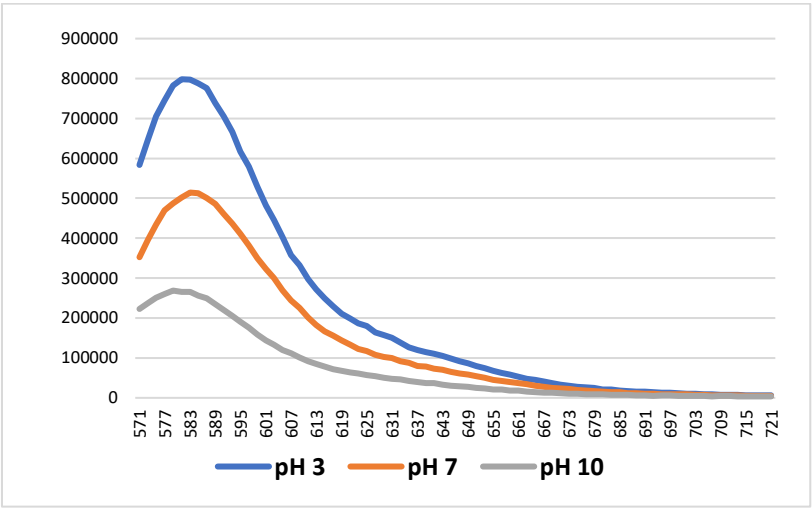


**Figure 5:** Emission spectra of Core R1-COOH bulk at different pH values.

The spectra show that microgels present a higher intensity of emission at pH 3 decreasing at basic pH. The microgel fluorescence emission is compared to that of rhodamine B acrylate in solution at diverse pH.

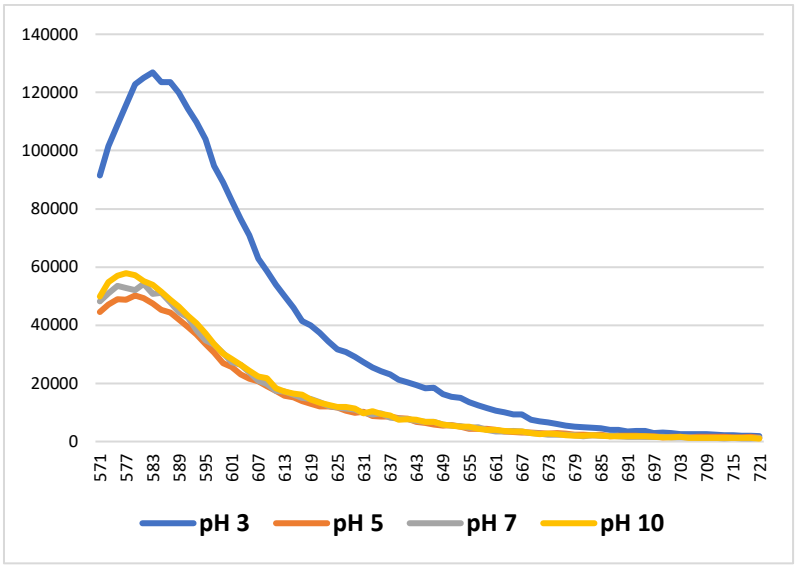


**Figure 6:** emission spectra of Rhodamine B at different pH values.

Spectra of Rhodamine emission show a behaviour similar to that of rhodamine in microgels. At pH 3, Rhodamine B has a structure featured by a lactone ring that when opened, tends to rotate and emits a strong fluorescence; while at basic pH, this ring is closed and the fluorescence intensity is lower.

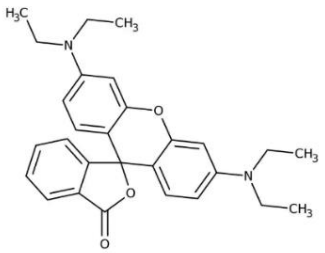


**Figure 7:** Rhodamine B structure.

Microgels with a concentration of 40 µg/ml in water are characterized using the confocal laser scanning microscope. The acquired images are analyzed by using the ImageJ software. The following graphs show the size and fluorescence distributions of the core R1-COOH bulk obtained by mediating the data of 5 images.

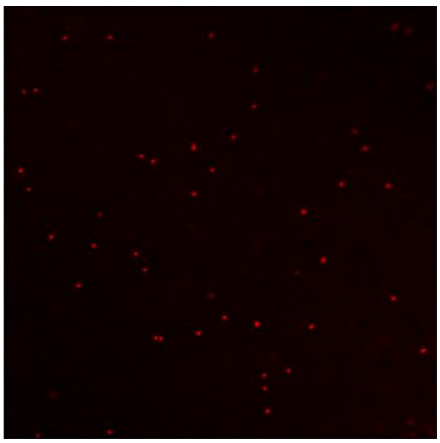

**Figure 8:** Core R1-COOH bulk.

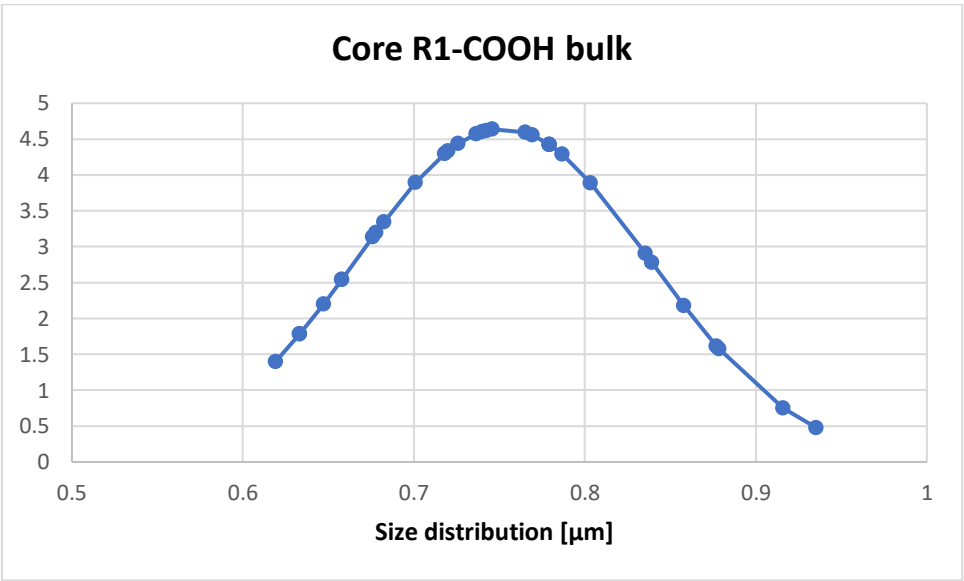


**Figure 9:** Size distribution of core R1-COOH bulk.

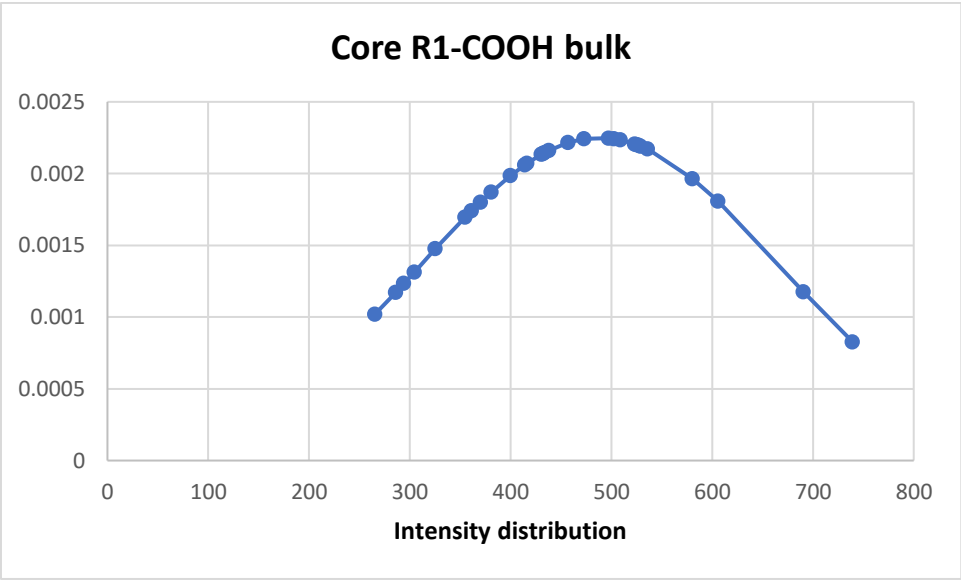


**Figure 10:** Fluorescence intensity distribution of core R1-COOH bulk.

The size distribution of R1-COOH bulk microgels is uniform at 752.2±16.1 nm and the microgels solution is monodisperse. The distribution of fluorescence emission is uniform at a value of 463.5±14.18.
The mass of the particles and the number of particles per mg of solution are determined by using the Ubbelohde viscometer.

| **Diameter [nm]** | **k [$cm^3/g$]** | **$m_p$ [mg]** | **$n_p/mg$** |
|---|---|---|---|
| 760 | 17,7 | $1{,}3 \cdot 10^{-11}$ | $3{,}26 \cdot 10^{13}$ |

**Table 2:** Mass particle determination.

The particle mass is $1{,}3 \cdot 10^{-11}$ mg and the number of particles/mg is $3{,}26 \cdot 10^{13}$.
For the chemical characterization, potentiometric titration was carried out to determine the number of -COOH groups in microgels.
The COOH moles per particle are determined.

| **Mol COOH/mg** | **N° COOH/mg** | **N° Particles/mg** | **N° COOH/particles** | **Mol COOH/particles** |
|---|---|---|---|---|
| $1{,}73 \cdot 10^{-6}$ | $1{,}04 \cdot 10^{18}$ | $3{,}05 \cdot 10^{13}$ | $3{,}41 \cdot 10^{4}$ | $5{,}7 \cdot 10^{-20}$ |

**Table 3:** COOH number determination.

Microgels are decorated with carboxyl groups on the surface allowing further functionalization with biological probes. It has been chosen the anti-IgG antibody

linked to a fluorescent dye, Atto-647N fluorophore. In this way, after the coupling reaction, it is possible to have a direct signal of the trend and yield of the reaction. The immobilization of antibodies started with the activation of carboxylic groups on the microgel surface (250 µg/ml) towards amine groups of antibodies to create a covalent amine bond. This latter has been performed by using Ethyl-N'-(3-(dimethylamino)propyl)carbodiimide hydrochloride (EDC) and N-hydroxy succinimide (NHS) in MES buffer (50 mM, pH=6) for 1 hour. The optimized EDC/NHS concentrations ratio was 0.1 M/0.2 M. After the activation, 10 µg of anti-IgG Atto-647N was added and the reaction was performed overnight. Then, the microgels were purified by centrifugation to remove the unreacted antibodies in the solution. At the end of the reaction, a Dynamic Light Scattering analysis of the 10 µg/mL sample in PBS was carried out both before and after functionalization.

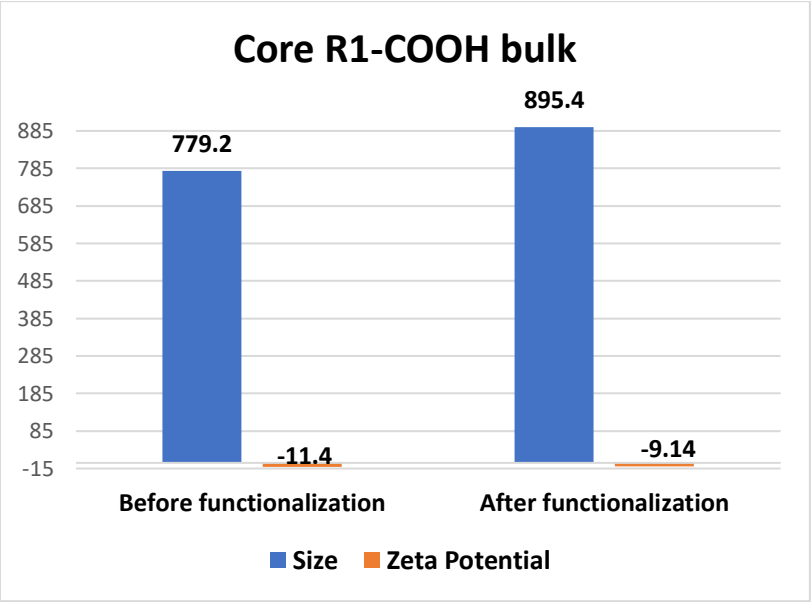


**Figure 11:** Size and zeta potential values before and after functionalization.

After microgel activation with EDC/NHS, the microgel diameter is 779.2±31.5nm. After conjugation, the diameter of microgels increases from 779.2±43.7 nm to 895.4±51.8 nm due to the presence of antibodies. The negative charge on the surface decreases from -11.4±0.8 mV to -9.14±0.7 mV. These results show that microgels functionalization occurs.

In addition, a confocal laser scanning microscope was used to acquire images of the microgel sample (10 µg/ml) showing a fluorescent signal due to the Atto-647N dye of the antibodies.

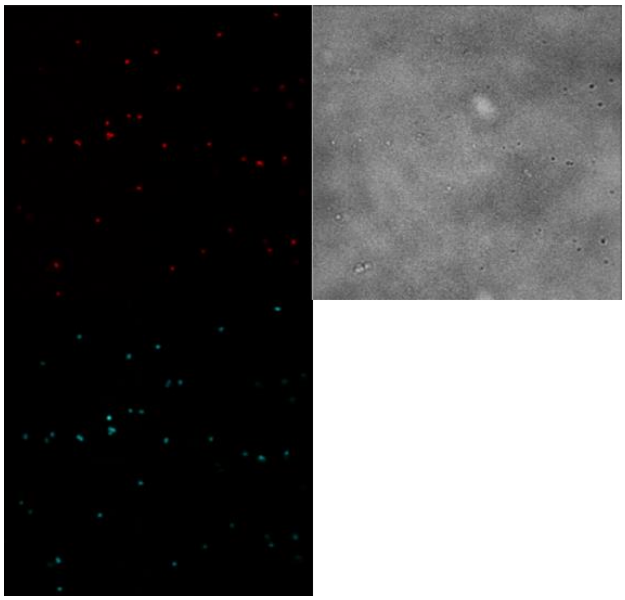

**Figure 12:** images of Core R1-COOH bulk functionalized with anti-IgG Atto647N.

These results highlighted that covalent immobilization occurred and thus, the microgels were functionalized. The acquired images were analyzed by using ImageJ software to determine the size of particles and fluorescence intensity of Rhodamine and Atto647N. Data obtained from the average of 7 images are shown in the following graphs.

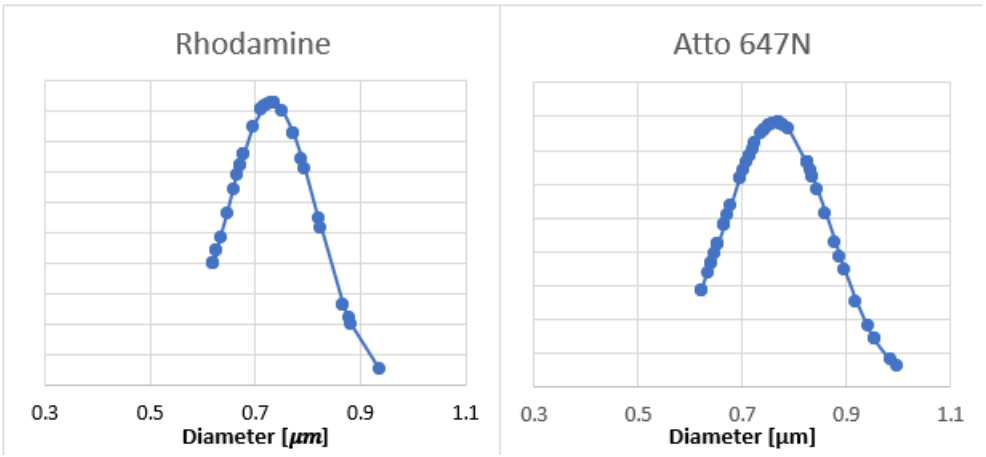


**Figure 13:** Size distribution of Core R1-COOH bulk.

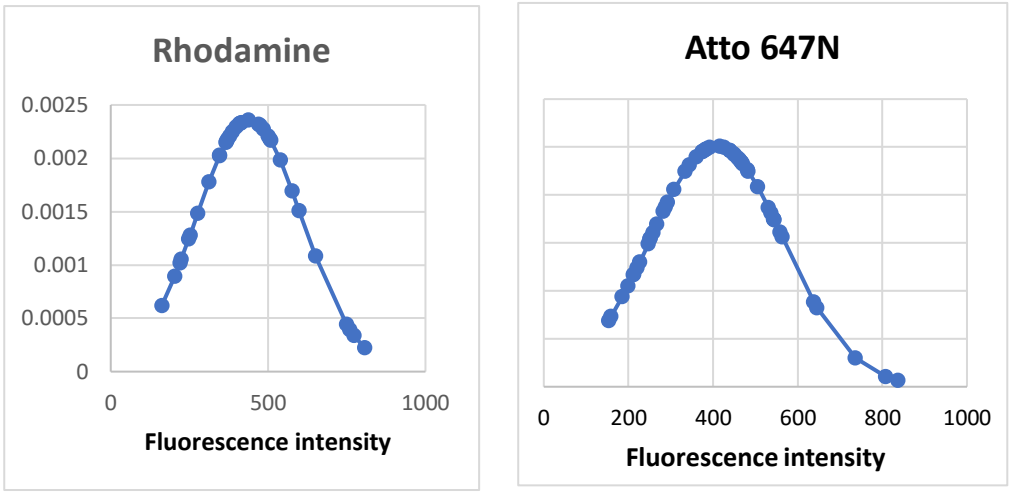


**Figure 14:** intensity distribution of Core R1-COOH bulk.

The sample appears monodispersed after conjugation and the fluorescence intensity is uniform for both fluorophores.

The emission spectra of functionalized microgels with a concentration of 10 µg/mL in water are evaluated by using the spectrophotometer:

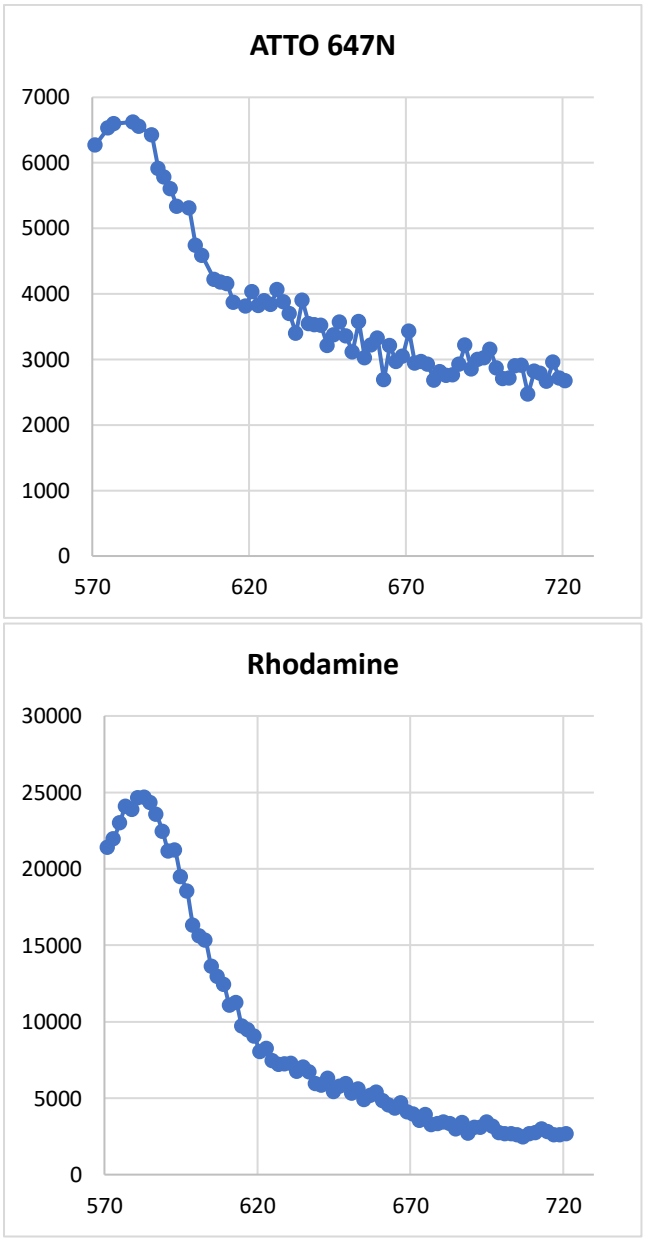


**Figure 15:** Emission spectra of R1-COOH bulk with anti-IgG Atto647N.

The maximum peak for the Rhodamine dye of microgels is at 580 nm and for the Atto647N dye at 655 nm. The fluorescence intensity of Rhodamine is about 10 folds greater than that of Atto647N.

## 3.3 CORE R1-COOH SURFACE

The Core R1-COOH surface is prepared through the same procedure used for CoreR1-COOH bulk with the difference that the Aac is introduced into the reactor after the formation of nuclei. To trigger the reaction, the KPS initiator is introduced into the reactor in which only PEGDMA was present.

After 10 minutes, precursor particles are formed, and acrylic acid is introduced. In this way, it polymerizes in the outer shell and not in the bulk.

The chemicals quantities used are as follows:

| Chemical | Quantity |
|---|---|
| PVA 1% | 50 mL |
| PEGDMA | 500 mg |
| KPS | 27 mg |
| Rhodamine | 333 $\mu$L |
| Aac | 125 mg |

**Table 4:** Quantity of chemicals used in Core R1 COOH surface synthesis.

The particle growth is followed by taking aliquots of mixture solution at a distance of 10 minutes, starting from KPS addition. Aliquots are analyzed at the DLS to evaluate the growth of microgels.

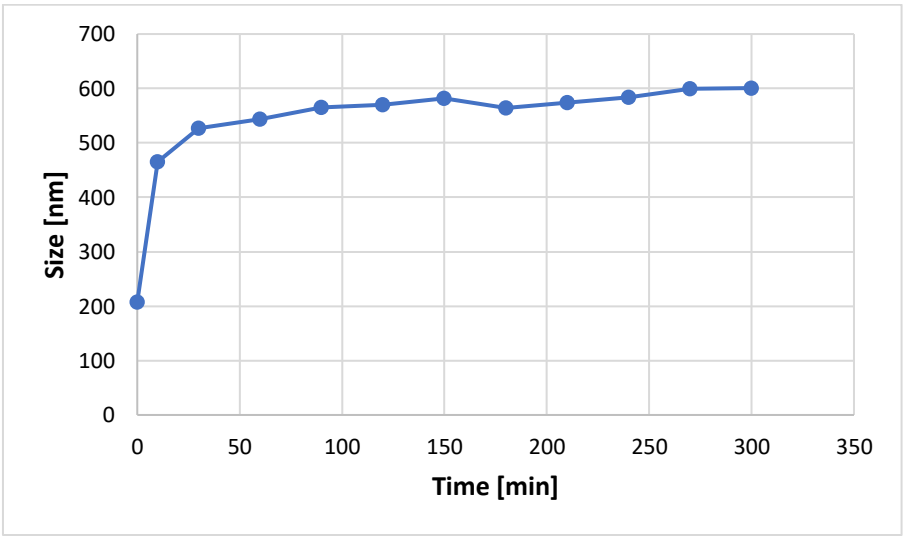


**Figure 16:** Hydrodynamic diameter variation during the reaction.

After 10 minutes later KPS addition, the diameter of the PEGDMA nuclei is 464.9±4.0 nm while the diameter of microgels after purification is 749.4±11.9 nm with PDI equal to 0.052. The Zeta Potential value is -23.3 ± 0.8 mV, showing a slightly more negative charge than the Core R1-COOH bulk. To monitor the swelling behaviour, microgel solutions (40 µg/ml) in water at pH 3, pH 7 and pH 10 are prepared and analyzed by dynamic light scattering. Zeta potential and size values are reported in the following chart:

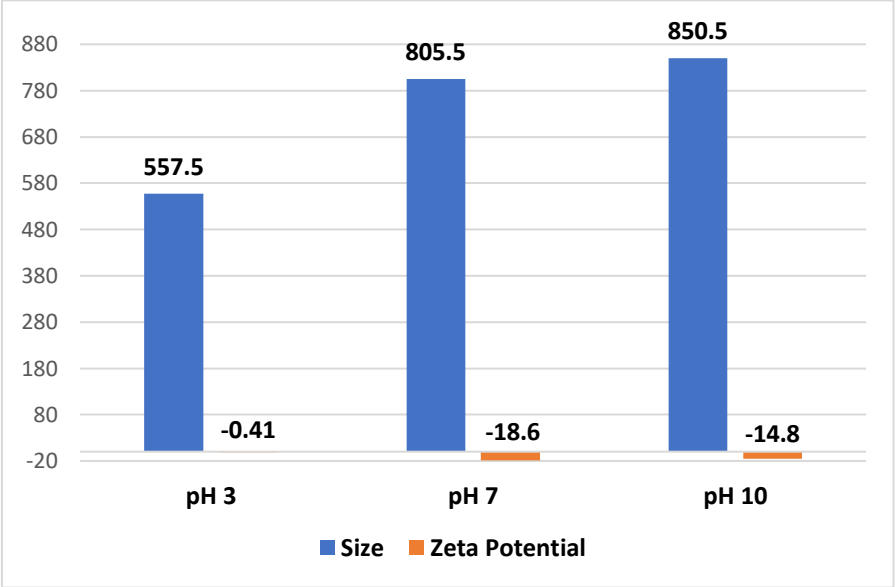


**Figure 17:** Size and Zeta Potential determination at different pH values.

From pH 3 to pH 10, the microgel size increases from 557.5±17.14 nm to 805.5±27.4 nm due to the deprotonation of the carboxyl groups. At pH 10, the diameter is 850.5±0.4 nm. The trend displayed for the size is not confirmed for the Zeta Potential. From pH 3 to pH 7, it decreases from -0.41± 0.1 mV to -18.57± 0.8 mV for the deprotonation of -COOH groups present on the surface; from pH 7 to pH 10, it decreases from -18.57± 0.8 mV to -14.77±0.4 mV.

The optical characterization was performed by recording the spectra with fluorescence spectrophotometry. For all samples, an integration time of 0.2 s and varying the slit values, input and output, were used to have a value of S1 less than 2x106. The spectra shown in the figure are S1/R1 which is the signal of the sample corrected to a reference reflector. The samples were excited at 548 nm and emission was collected from 568 to 715 nm. Spectra of microgels were recorded at a concentration of 40 µg/mL by varying pH values.

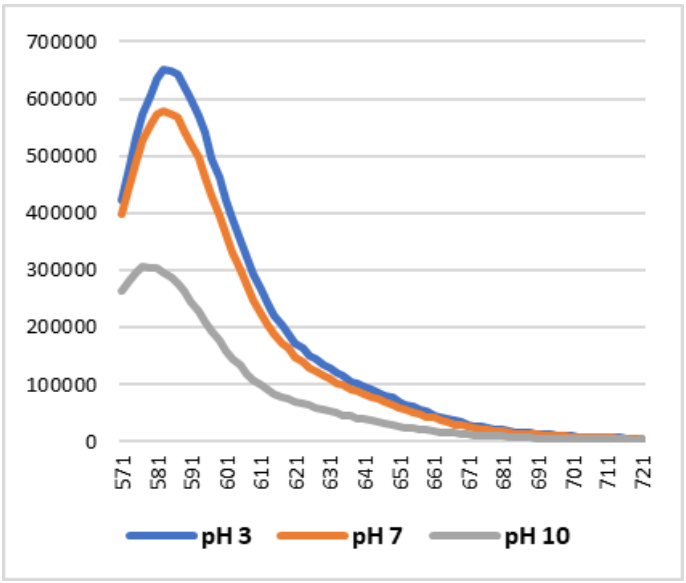


**Figure 18:** emission spectra of Core R1-COOH surface at different pH values.

The spectra show that microgels present a higher intensity of emission at pH 3 decreasing at basic pH. As in the previous case, the microgel fluorescence emission is compared to that of rhodamine B acrylate at diverse pH. Rhodamine in microgels follows the same trend as rhodamine in solution. Microgels with a concentration of 40µg/ml in water were characterized using the confocal laser scanning microscope. The acquired images were analyzed using the ImageJ software. The following graphs show the size and fluorescence distributions of the core R1-COOH surface obtained by mediating the data of 5 images.

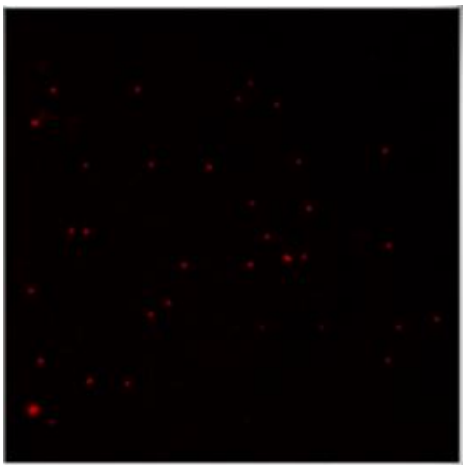

**Figure 19:** Core R1-COOH surface.

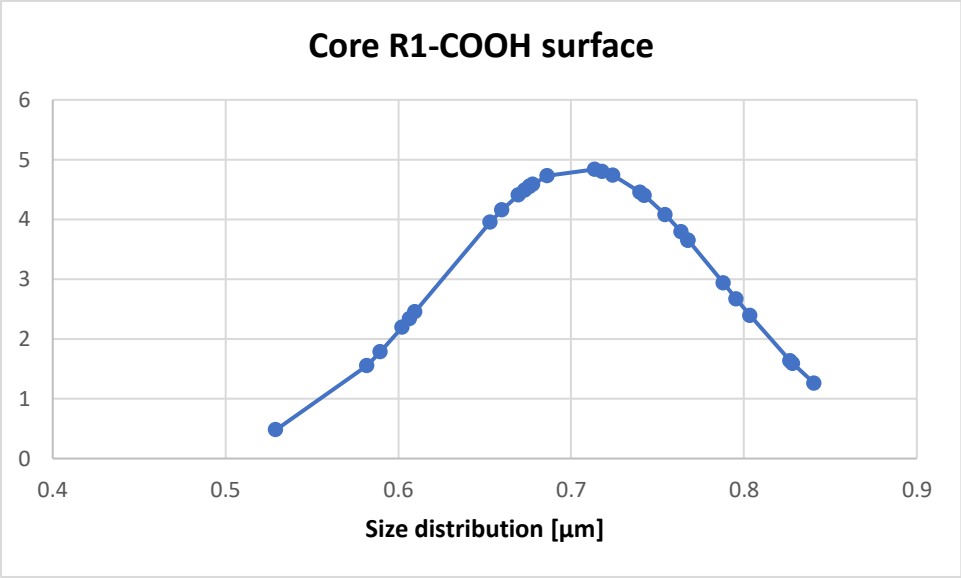


**Figure 20:** Size distribution of core R1-COOH surface.

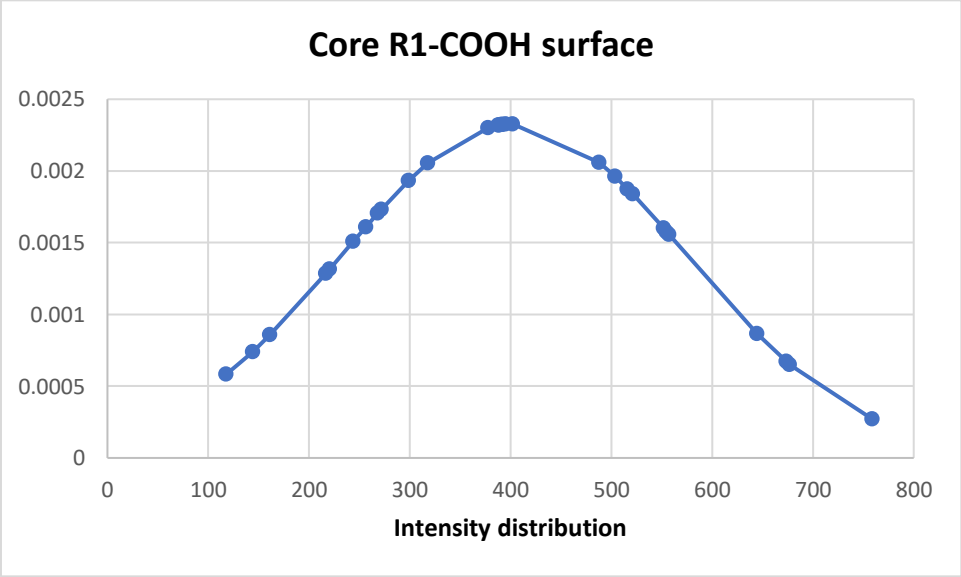


**Figure 21:** Fluorescence intensity distribution of core R1-COOH.

As shown, the size distribution of R1-COOH bulk microgels is uniform at 705.7±18.8 nm and the microgels solution is monodisperse. The distribution of fluorescence emission is uniform at a value of 403.5±17.1.

The mass of the particles and the number of particles per milligram of solution are determined by using the Ubbelohde viscometer.

| Diameter [nm] | k [$cm^3/g$] | $m_p$ [mg] | $n_p/mg$ |
|---|---|---|---|
| 749,4 | 18,2 | $1{,}21 \cdot 10^{-11}$ | $2{,}28 \cdot 10^{13}$ |

**Table 5:** mass particle determination.

The particle mass is $1{,}21 \cdot 10^{-11}$ mg with $2{,}28 \cdot 10^{13}$ particles/mg.
For the chemical characterization, potentiometric titration is carried out to determine the presence of -COOH groups within the microgels.
The COOH moles number per particle is determined.

| Mol COOH/mg | N° COOH/mg | N° Particles /mg | N° COOH/particles | Mol COOH/particles |
|---|---|---|---|---|
| $9{,}75 \cdot 10^{-7}$ | $5{,}87 \cdot 10^{17}$ | $2 \cdot 10^{13}$ | $2{,}94 \cdot 10^{4}$ | $4{,}9 \cdot 10^{-20}$ |

**Table 6:** COOH number determination.

Microgels are decorated with carboxyl groups on the surface allowing further functionalization with biological probes. It has been chosen the anti-IgG antibody linked to a fluorescent dye, Atto-647N fluorophore. In this way, after the coupling reaction, it has been possible to have a direct signal of the trend and yield of the reaction. The immobilization of antibodies started with the activation of carboxylic groups on the microgel surface (250 µg/ml) towards amine groups of antibodies to create a covalent amine bond. This latter has been performed by using Ethyl-N'-(3-(dimethylamino)propyl)carbodiimide hydrochloride (EDC) and N-hydroxy succinimide (NHS) in MES buffer (50 mM, pH=6) for 1 hour. The optimized EDC/NHS concentrations ratio was 0.1 M/0.2 M. After the activation, 10 µg of anti-IgG Atto-647N was added and the reaction was performed overnight. Then, the microgels were purified by centrifugation to remove the unreacted antibodies in the solution. At the end of the reaction, a Dynamic Light Scattering analysis of the 10 µg/mL sample in PBS was carried out both before and after functionalization.

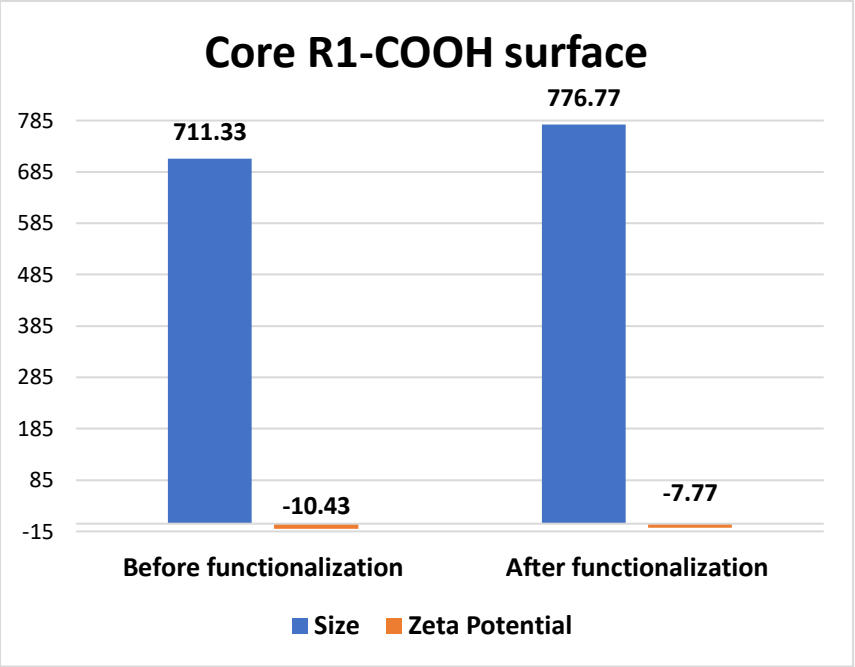


**Figure 22:** Size and zeta potential values before and after functionalization.

After microgel activation with EDC/NHS, the microgel diameter is 711.3±17.0 nm. After conjugation, the diameter of microgels increases from 711.3±17.0 nm to 776.8±50.0 nm due to the presence of antibodies. The negative charge on the surface decreases from -10.4±0.8 mV to -7.77±0.5 mV. These results show that microgels functionalization occurs. In addition, confocal laser scanning microscopy is used to acquire images of the microgel sample (10 µg/ml) showing a fluorescent signal due to the Atto-647N dye of the antibodies.

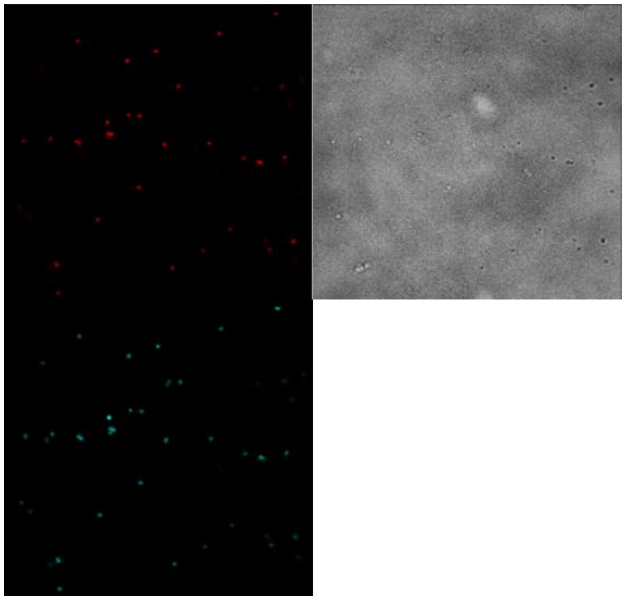

**Figure 23:** images of Core R1-COOH surface microgels functionalized with anti-IgG Atto647N.

These results highlighted that the covalent immobilization occurred and thus, the microgels are functionalized. The acquired images were analyzed by using ImageJ software to determine the size of particles and fluorescence intensity of Rhodamine and Atto647N. Data obtained from the average of 7 images are shown in the following graphs.

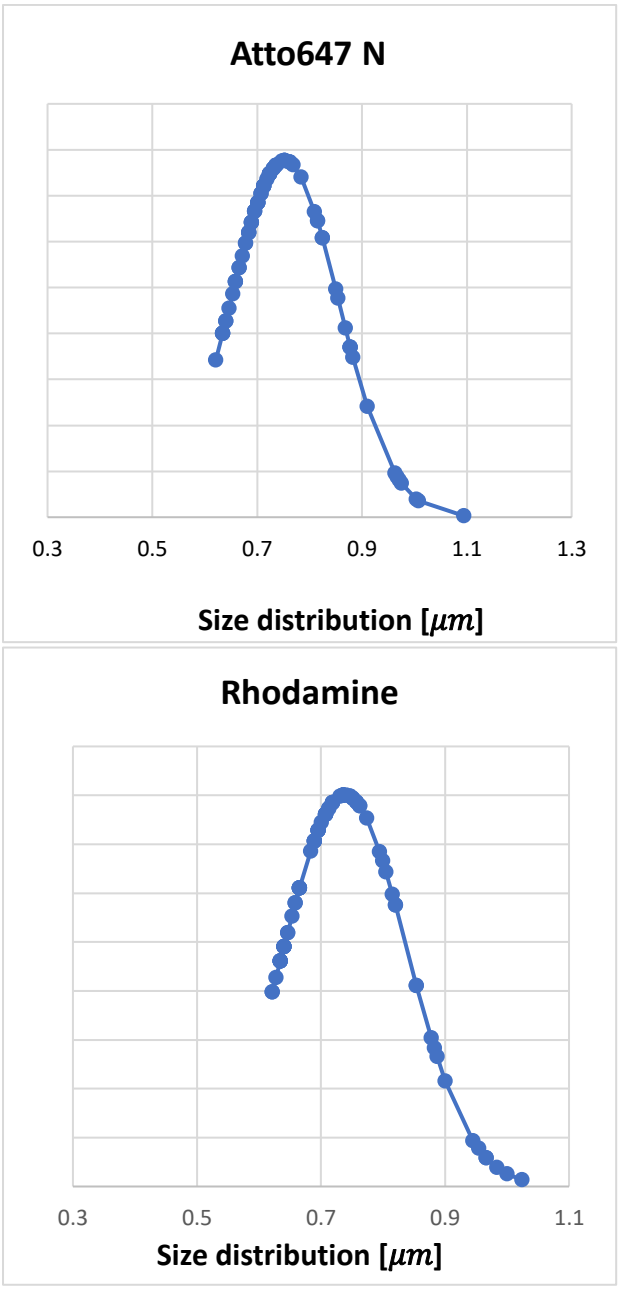


**Figure 24:** size distribution of Core R1-COOH surface.

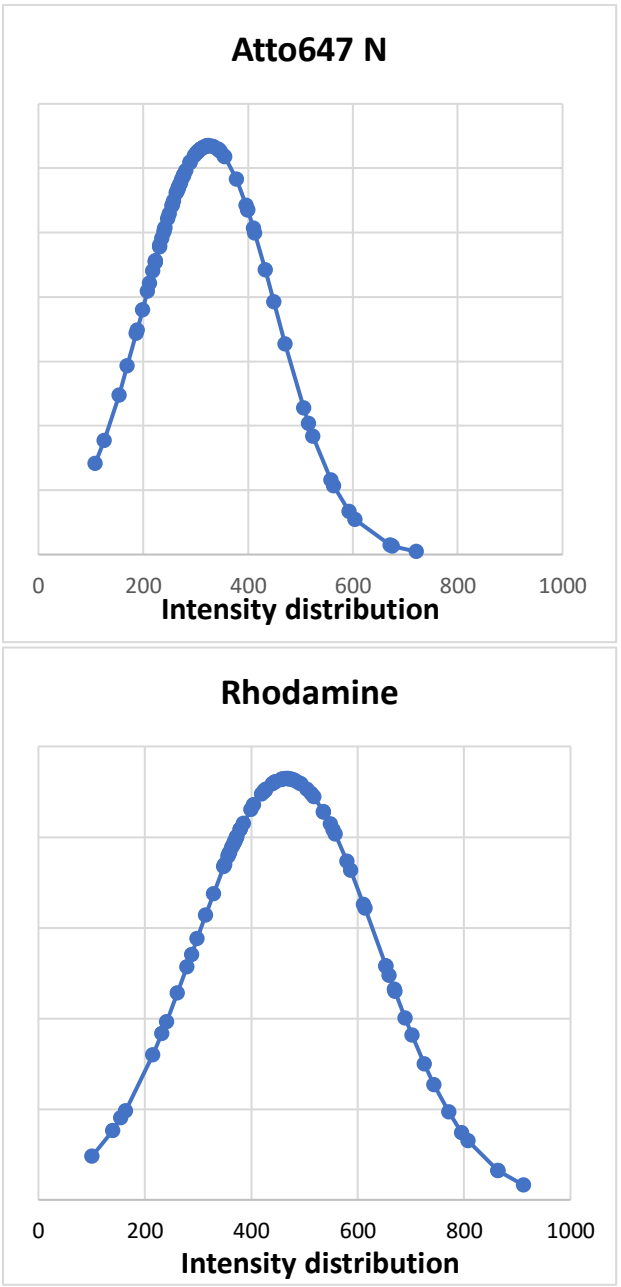


**Figure 25:** Emission intensity distribution of Core R1-COOH surface.

The sample appeared monodispersed after conjugation with the probe and the fluorescence intensity was uniform for both fluorophores.

The emission spectra of functionalized microgels with a concentration of 10 µg / mL in water are evaluated:

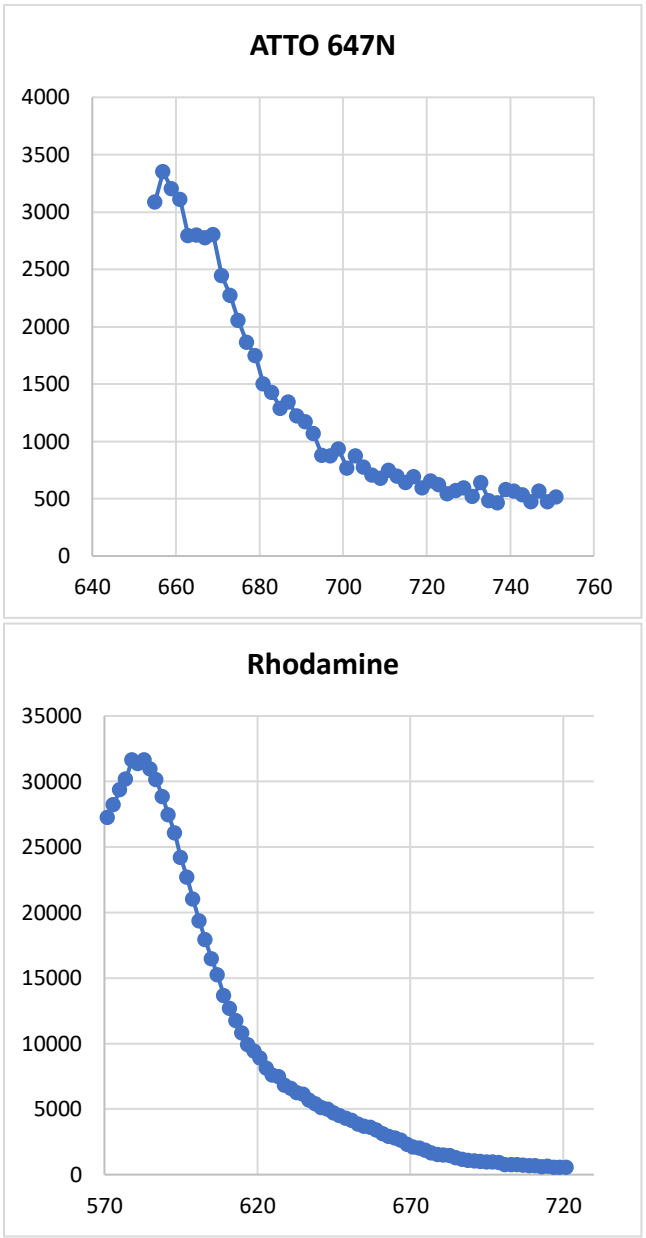


**Figure 26:** Emission spectra of R1-COOH surface with anti-IgG Atto647N.

The maximum peak for the Rhodamine dye was at 580 nm and for the Atto647N dye at 655 nm. The fluorescence intensity of Rhodamine is about 10 folds greater than that of Atto647N.

## 3.4 CORE R1-AMPS SURFACE

The third type of core is prepared by using a novel monomer Acid 2-Acrylamide-2-Methyl-1-Propanesulfonate (AMPS).

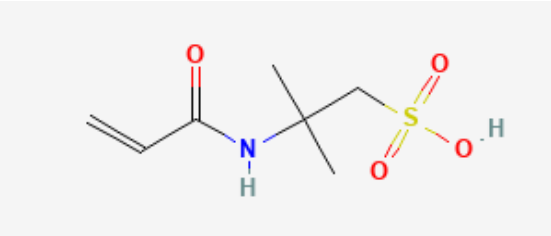


**Figure 27:** Structure of Acid 2-Acrylamide-2-Methyl-1-Propanesulfonate (AMPS).

AMPS is an acrylic monomer of sulphonic acid, very reactive and hydrophilic and has been added to the reaction to give the microgels a more negative charge.

The synthesis procedure is the same as the previous reactions. The difference is the presence of the new co-monomer AMPS. Two attempts are performed: in the first case Core R1-AMPS 0.1, AMPS is used in a molar ratio of 1:10 with Aac (3.46 mM), and in the second case Core R1-AMPS 1, it is used in a molar ratio of 1:1 with Aac (34.6 mM).

The PVA and PEGDMA are degassed with $N_2$ gas for 1 hour and then the KPS initiator is added. After 10 minutes, both Rhodamine and Aac are added to the flask. After a further 10 minutes (20 minutes after the introduction of the KPS), the 2-Acrylamide-2-Methyl-1-Propanesulfonate (AMPS) acid is introduced into the reactor. Subsequently, the reaction proceeds similarly to the previous ones.

The chemicals quantities used are as follows:

| Chemical | R1-AMPS 0,1 | R1-AMPS 1 |
|---|---|---|
| PVA 1% | 50 mL | 50 mL |
| PEGDMA | 500 mg | 500 mg |
| KPS | 27 mg | 27 mg |
| Rhodamine | 333 $\mu$L | 333 $\mu$L |
| Aac | 125 mg | 125 mg |
| AMPS | 35.8 mg | 358 mg |

**Table 7:** Quantity of chemicals used in Core R1 AMPS surface synthesis.

Aliquots of the two mixture solutions are taken at a distance of 10 minutes, starting from KPS addition. Aliquots are analyzed at the DLS to evaluate the growth of microgels.

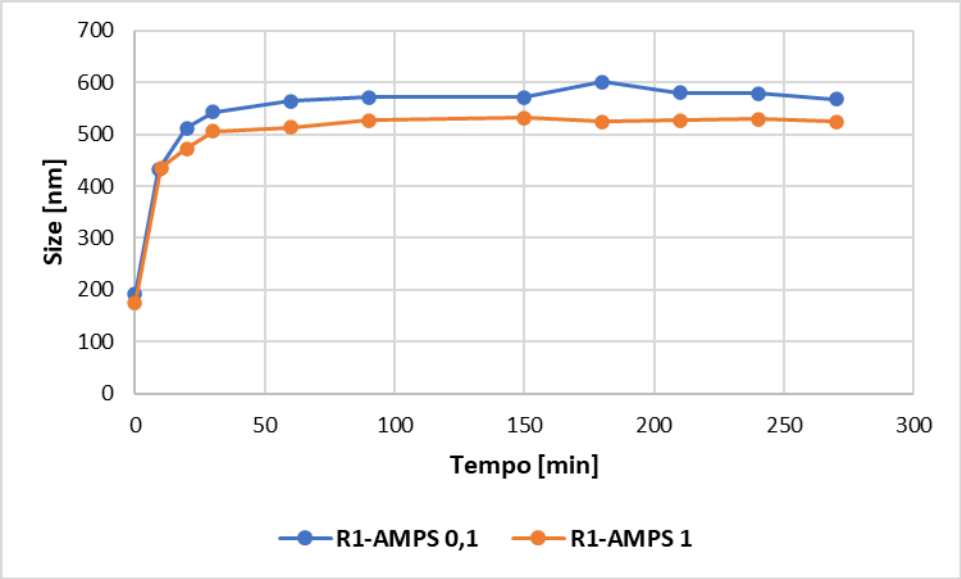


**Figure 28:** Hydrodynamic diameter variation during the reaction.

After 10 minutes later KPS addition, the diameter for both syntheses is very similar (431.5±7.3 nm for Core R1 AMPS 0,1 and 435.5±6.9 nm for Core R1 AMPS 1). At the end of the reaction, the diameter of core R1-AMPS 0.1 is 567.7±11.3 nm and that of core R1-AMPS 1 is 524.6±8.4 nm.
After purification, samples are analyzed at the DLS:

| Core microgel | Size (nm) | Zeta Potential (mV) | PDI |
|---|---|---|---|
| R1-AMPS 0,1 | 665.6±17.5 | -21.1±0.9 | 0.02 |
| R1-AMPS 1 | 641.3±10.3 | -25.5±0.8 | 0.02 |

**Table 8:** size and zeta potential determination of Core R1-AMPS.

The size of both types of particles is smaller than the Core R1-COOH (760.2±16.1 nm for Core R1-COOH bulk and 749.4±11.9 nm Core R1-COOH surface) and the PDI value showed the solutions are monodispersed. The size was 665.6±17.5 nm and 641.3±10.3 nm respectively for the core R1-AMPS 0,1 and core R1-AMPS 1.
For the core R1-AMPS 0.1, microgels show a zeta potential value of -21.1±0.9 mV, similar to core R1-COOH (-20.1±0.5 mV V for Core R1-COOH bulk and -23.3 ± 0.8 mV for Core R1-COOH surface). This is due to the small AMPS amount used during the

reaction influencing the particles very slightly. While, for the R1-AMPS 1 Aac, there is an increase in negative charge with a zeta potential value of -25,5±0,8 mV. The repulsive force improved the colloidal stability compared to the previous syntheses. To monitor the swelling behaviour, solutions of both microgels (40 µg/ml) in water at pH 3, pH 7 and pH 10 are prepared and analyzed by dynamic light scattering. Zeta potential and size values are reported in the following chart:

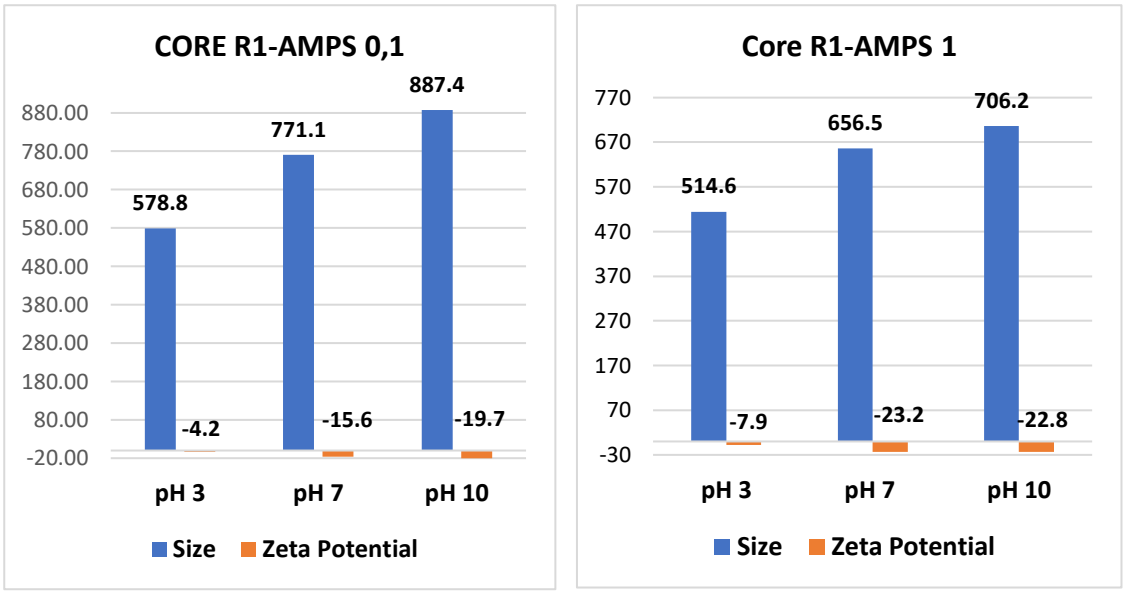


**Figure 29:** Size e Zeta Potential determination at different pH values.

In both cases, the swelling occurs at higher pH values, thanks to the deprotonation of the COOH groups on particle surfaces. For Core R1-AMPS 0.1, the diameter passes from 578.8±8.1 nm to 887.4±21.8 nm and for Core R1-AMPS 1, it passes from 514.6±2.7 nm to 706.2±14.17 nm. The swelling is reduced in the second case due to the higher amount of AMPS that replaces COOH groups. Furthermore, AMPS confers a higher negative charge than those of Core R1-COOH.

The optical characterization was performed by recording the spectra with fluorescence spectrophotometry. For all samples, an integration time of 0.2 s and varying the slit values, input and output, are used to have a value of S1 less than $2x10^6$. The spectra shown in the figure are S1/R1 which is the signal of the sample corrected to a reference reflector. The samples are excited at 548 nm and emission is collected from 568 to 715 nm. Spectra of microgels are recorded at a concentration of 40 µg/mL by varying pH values.

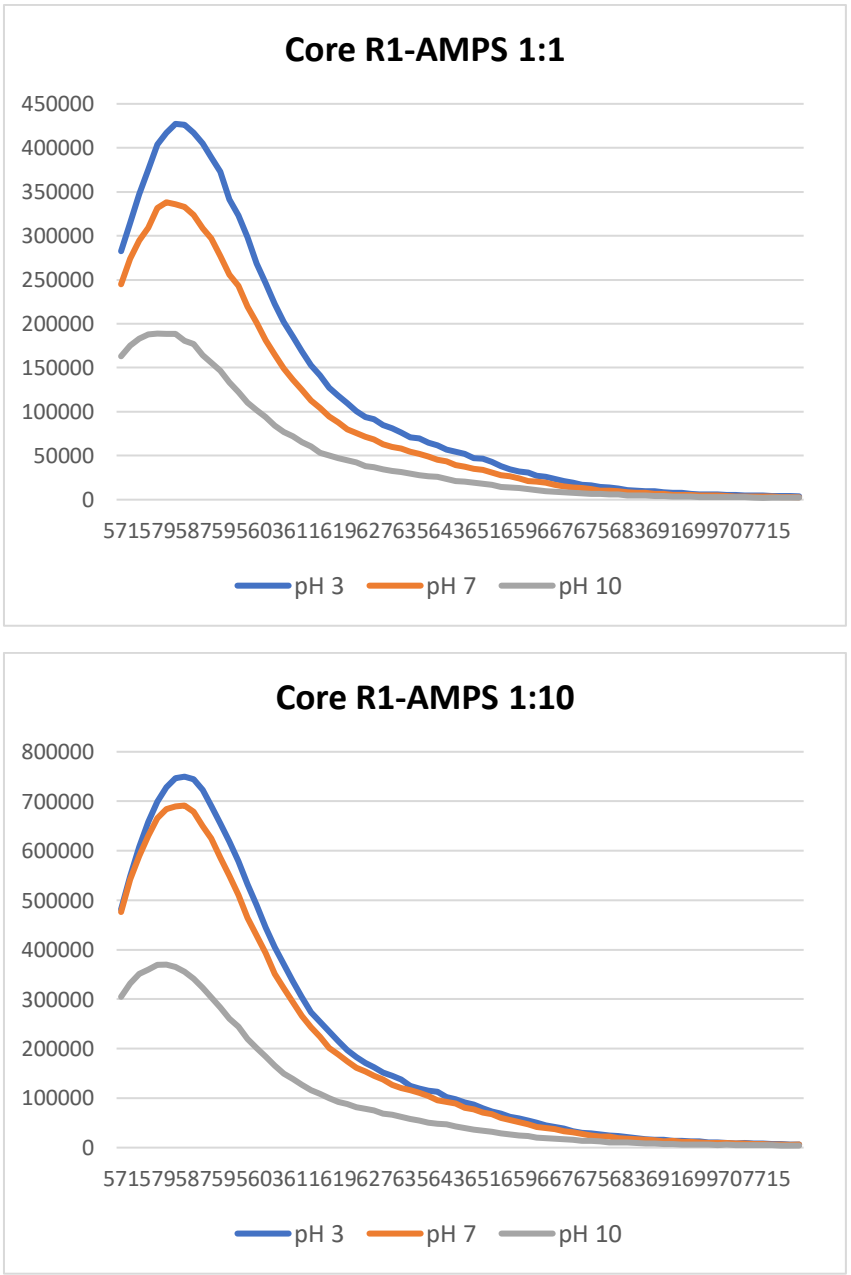


**Figure 30:** emission spectra of microgels Core R1-AMPS 0.1 and Core R1-AMPS 1 at different pH values.

The fluorescence emission for both core microgels follows the same trend. At acidic pH, there is a much higher emission intensity than at basic pH, as for rhodamine in solution.

Microgels with a concentration of 40µg/ml in water are characterized by using the confocal laser scanning microscope. The acquired images are analyzed using the ImageJ software. The following graphs show the size and fluorescence distributions of the core R1-COOH surface obtained by mediating the data of 5 images.

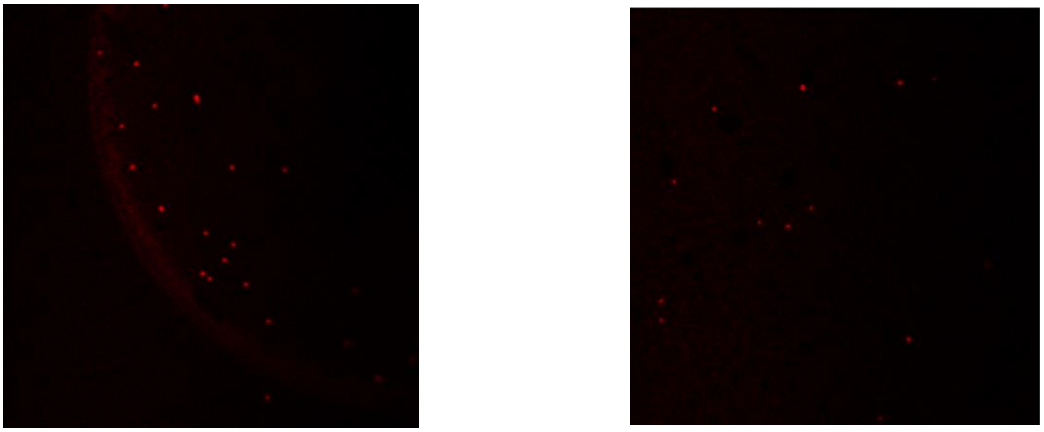

**Figure 31:** Core R1-AMPS 0.1 (left) and Core R1-AMPS 1 (right).

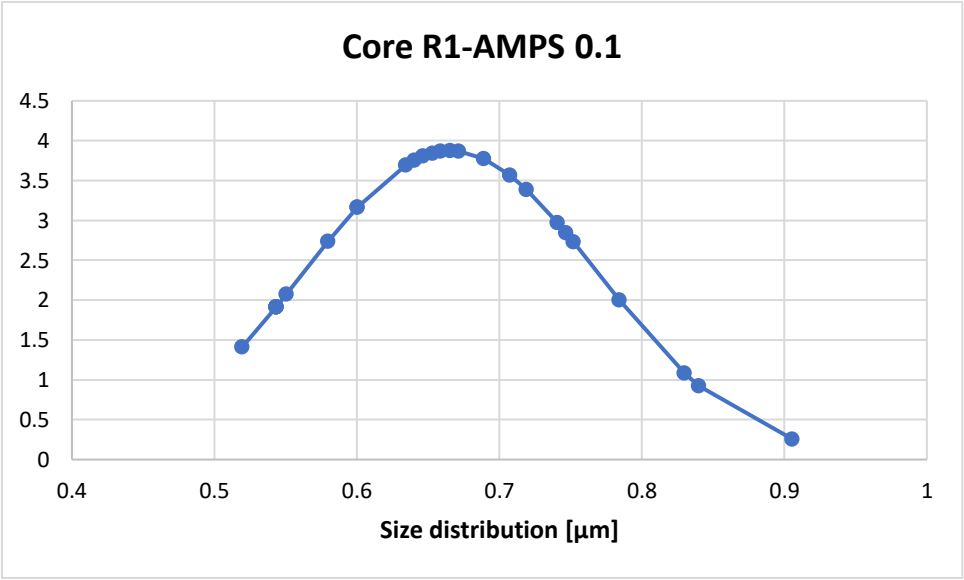

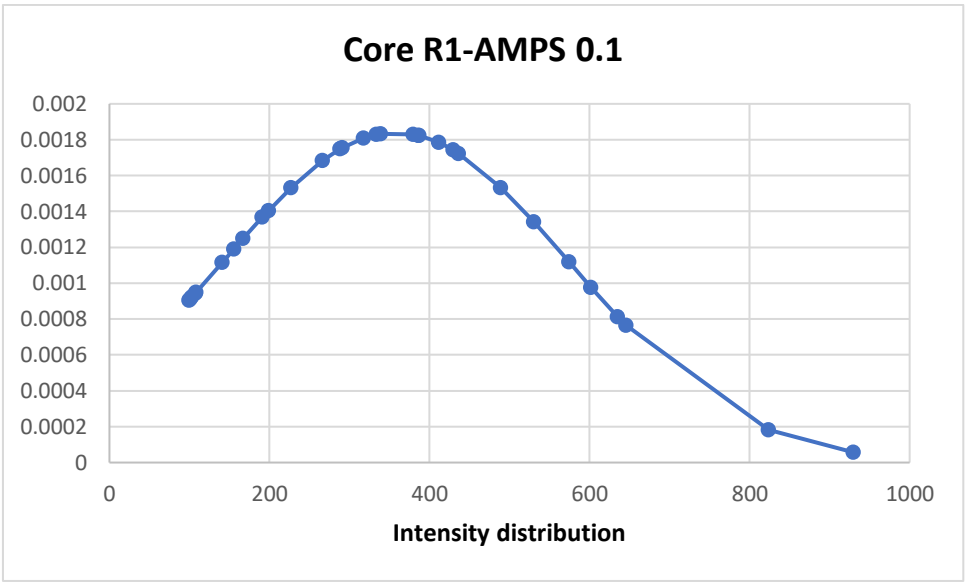


**Figure 32:** Size distribution and fluorescence intensity distribution of core R1-AMPS 0.1.

The size distribution of the Core R1-AMPS 0.1 is uniform at 0.66±0.10 µm and the microgels solution is monodisperse. The distribution of fluorescence emission is uniform at a value of 358.1±216.8.

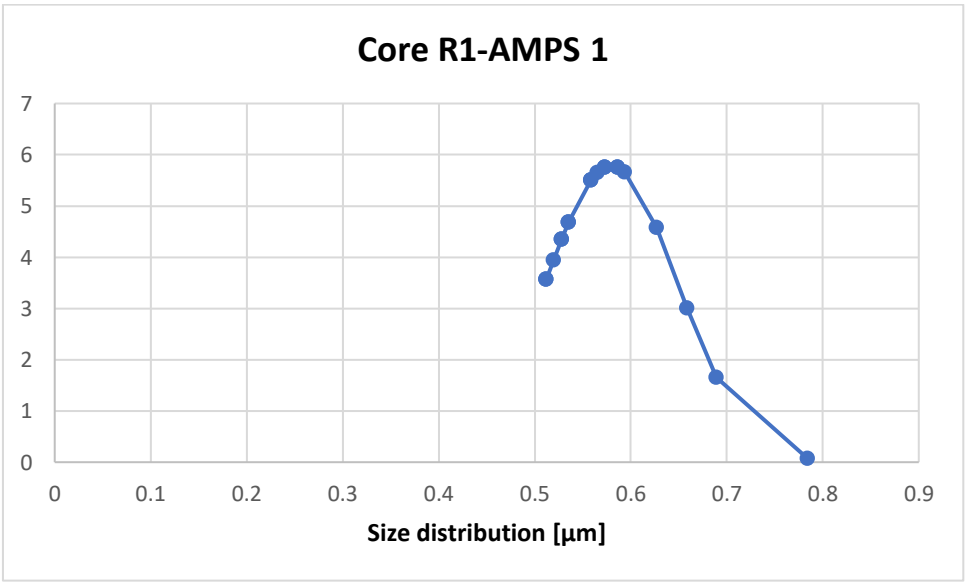

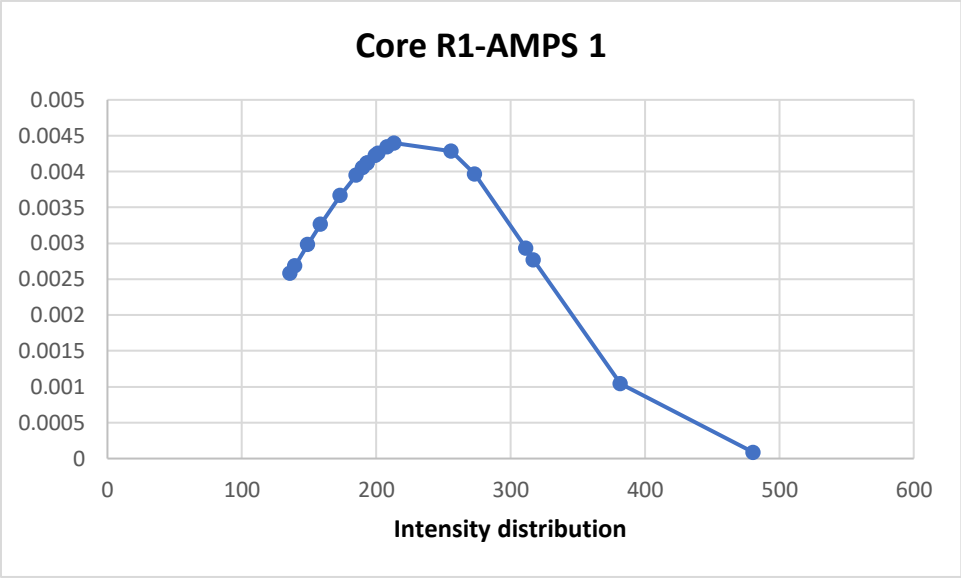


**Figure 33:** Size distribution and fluorescence intensity distribution of core R1-AMPS 0.1.

The size distribution of the Core R1-AMPS 1 is uniform at 0.58±0.07 µm and the microgels solution is monodisperse. The distribution of fluorescence emission is uniform at a value of 229.6±89.2. From the distributions, the optical analysis of the R1-AMPS microgels shows that microgels have a smaller diameter and a lower but still uniform fluorescence intensity.
The mass of the particles and the number of particles per milligram of solution were determined by using the Ubbelohde viscometer.

| Core microgels | Diameter[nm] | k $[cm^3/g]$ | $m_p$ [mg] | $n_p/mg$ |
|---|---|---|---|---|
| R1-AMPS 0,1 | 665,6 | 48,02 | $3{,}22 \cdot 10^{-12}$ | $9{,}6 \cdot 10^{13}$ |
| R1-AMPS 1 | 641,3 | 11,22 | $1{,}23 \cdot 10^{-11}$ | $7{,}73 \cdot 10^{12}$ |

**Table 9:** mass particle determination.

For the chemical characterization, potentiometric titration is carried out to determine the number of -COOH groups in microgels.
The COOH moles per particle are determined for both cores AMPS:

| Core microgels | Mol COOH/mg | N° COOH/mg | N° Particles/mg | N° COOH/particles | Mol COOH/particles |
|---|---|---|---|---|---|
| R1-AMPS 0,1 | $3.25 \cdot 10^{-7}$ | $1.95 \cdot 10^{17}$ | $9.60 \cdot 10^{13}$ | $2.04 \cdot 10^{3}$ | $3.39 \cdot 10^{-21}$ |
| R1-AMPS 1 | $2.50 \cdot 10^{-8}$ | $1.50 \cdot 10^{16}$ | $7.70 \cdot 10^{12}$ | $1.96 \cdot 10^{3}$ | $3.25 \cdot 10^{-21}$ |

**Table 10:** COOH number determination for Cores AMPS.

For Core R1-AMPS 0.1, the mol COOH/mg is $3.25 \cdot 10^{-7}$, higher than the mol COOH/mg for core R1-AMPS 1. This is due to the AMPS amount used for the synthesis. A higher quantity of AMPS produces a reduced number of COOH on microgels.

Microgels are decorated with carboxyl groups on the surface allowing further functionalization with biological probes. It has been chosen the anti-IgG antibody linked to a fluorescent dye, Atto-647N fluorophore. In this way, after the coupling reaction, it is possible to have a direct signal of the trend and yield of the reaction. The immobilization of antibodies started with the activation of carboxylic groups on the microgel surface (250 µg/ml) towards amine groups of antibodies to create a covalent amine bond. This latter has been performed by using Ethyl-N'-(3-(dimethylamino)propyl)carbodiimide hydrochloride (EDC) and N-hydroxy succinimide (NHS) in MES buffer (50 mM, pH=6) for 1 hour. The optimized EDC/NHS concentrations ratio was 0.1 M/0.2 M. After the activation, 10 µg of anti-IgG Atto-647N was added and the reaction was performed overnight. Then, the microgels were purified by centrifugation to remove the unreacted antibodies in the solution. At the end of the reaction, a Dynamic Light Scattering analysis of the 10 µg/mL sample in PBS was carried out both before and after functionalization.

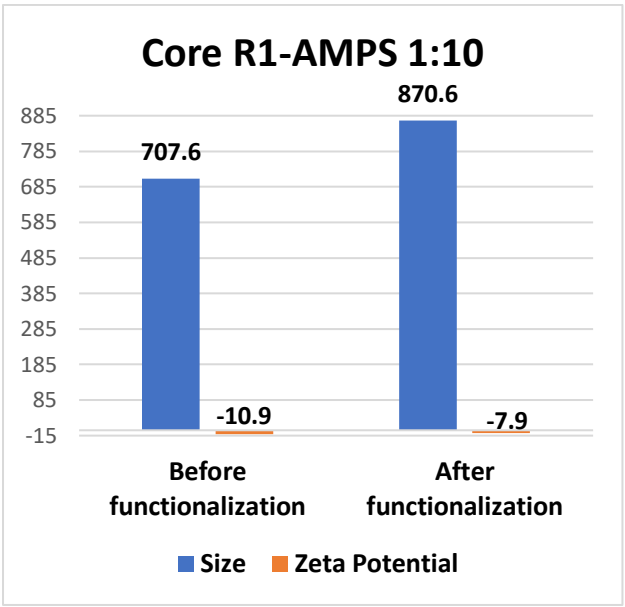


**Figure 34:** Size and zeta potential values before and after functionalization for Core R1-AMPS 0,1

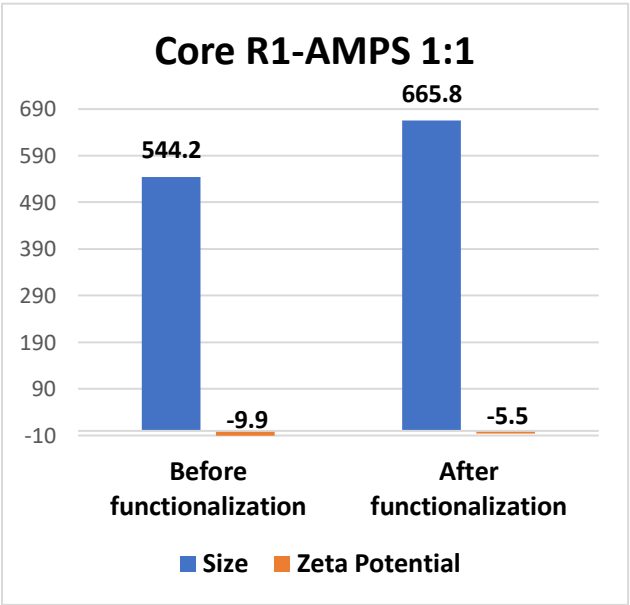


**Figure 35:** Size and zeta potential values before and after functionalization for Core R1-AMPS 1.

After conjugation, the diameter of microgels increases due to the presence of antibodies and the negative charge on the surface decreases. For Core R1-AMPS 0.1, the microgel diameter is 707.6±21.9 nm, before functionalization in PBS. After conjugation, the diameter of microgels increases from 707.6±21.9 nm to 870.6±43.6 nm due to the presence of antibodies. The negative charge on the surface decreases from -10.9±1.2 mV to -7.9±0.1 mV. Fore Core R1-AMPS 1, the diameter of microgels increases from 544.2±8.9 nm to 665.8±9.8 nm and the zeta

potential decreases from -9.9±0.3 mV to -5.5±0.5 mV. These results show that microgels functionalization occurs. In addition, confocal laser scanning microscopy is used to acquire images of the microgel sample (10 µg/ml) showing a fluorescent signal due to the Atto-647N dye of the antibodies.

In addition, confocal laser scanning microscopy is used to acquire images of the microgel sample (10 µg/ml) showing a fluorescent signal due to the Atto-647N dye of the antibodies.

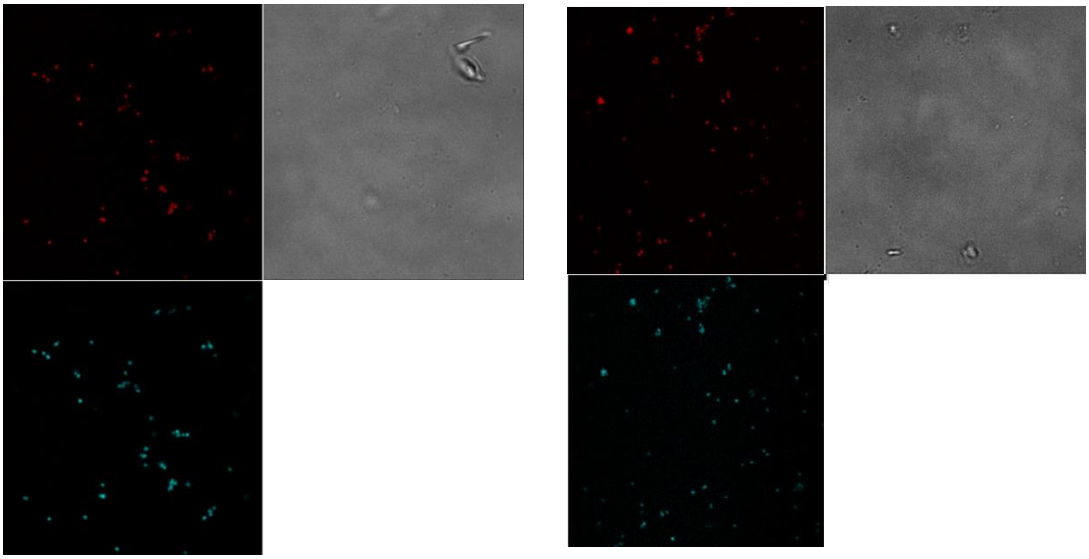

**Figure 36:** images of Core R1-AMPS 0,1 (left) and Core R1-AMPS 1 (right) microgels functionalized with anti-IgG Atto647N.

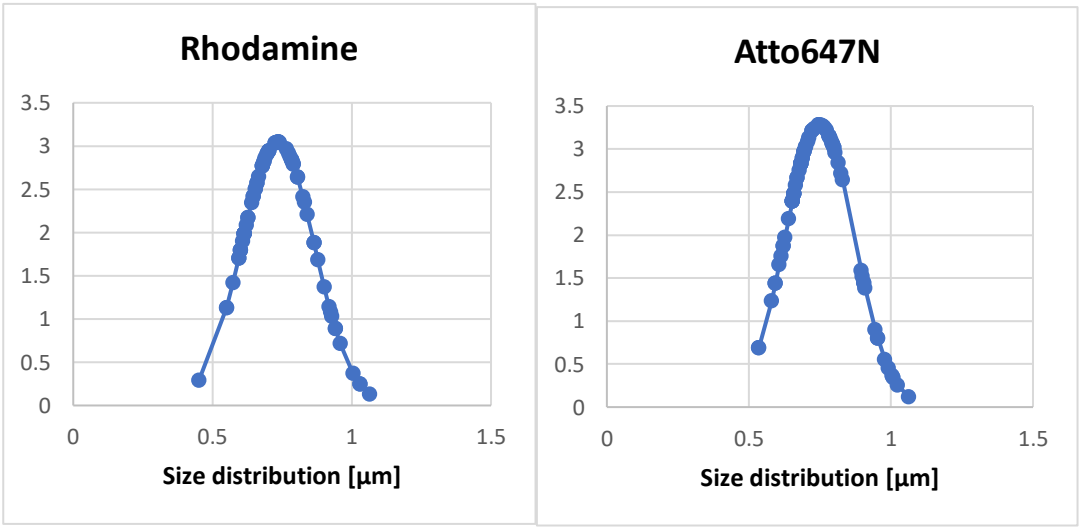


**Figure 37:** size distribution of Core R1-AMPS 0,1

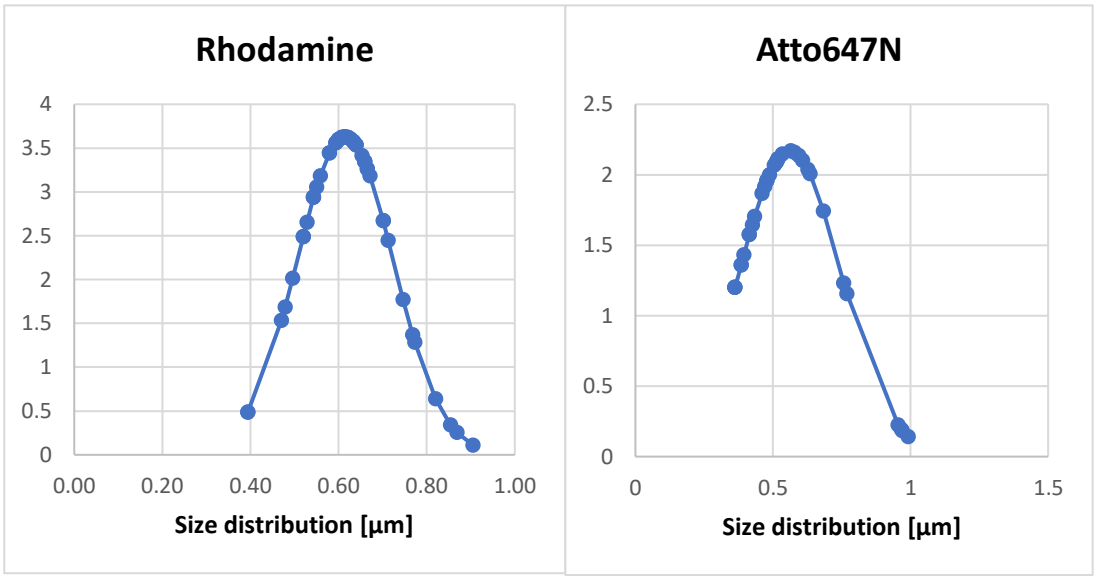


**Figure 38:** Emission intensity distribution of Core R1-AMPS 0,1.

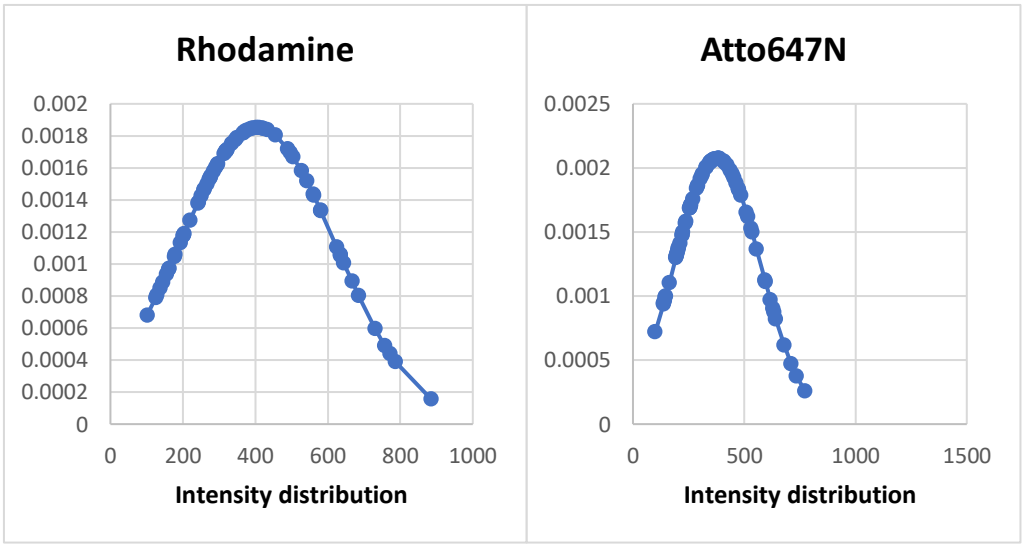


**Figure 39:** Size distribution of Core R1-AMPS 1.

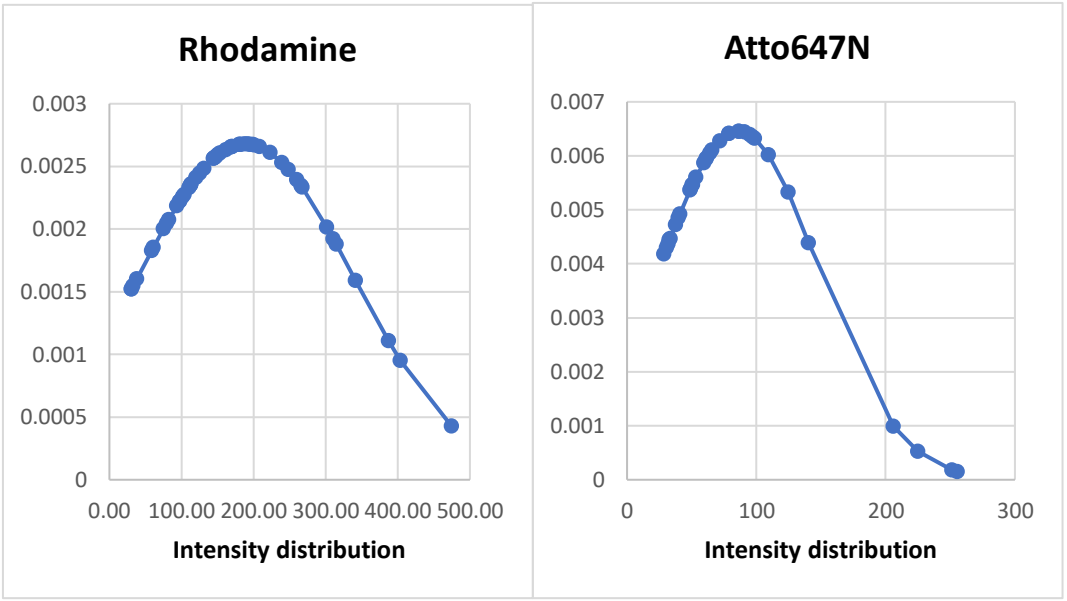


**Figure 40:** Emission intensity distribution of Core R1-AMPS 1.

After conjugation, samples are monodispersed, and the fluorescence intensity is uniform for both rhodamine and Atto647N. For core R1 AMPS, the fluorescence intensity is very low indicating that the number of bound antibodies is lower than the R1-COOH cores. This result proves that cores R1-AMPS have a lower number of COOH groups on the surface.

The emission spectra of functionalized microgels with a concentration of 10 µg / mL in water were evaluated:

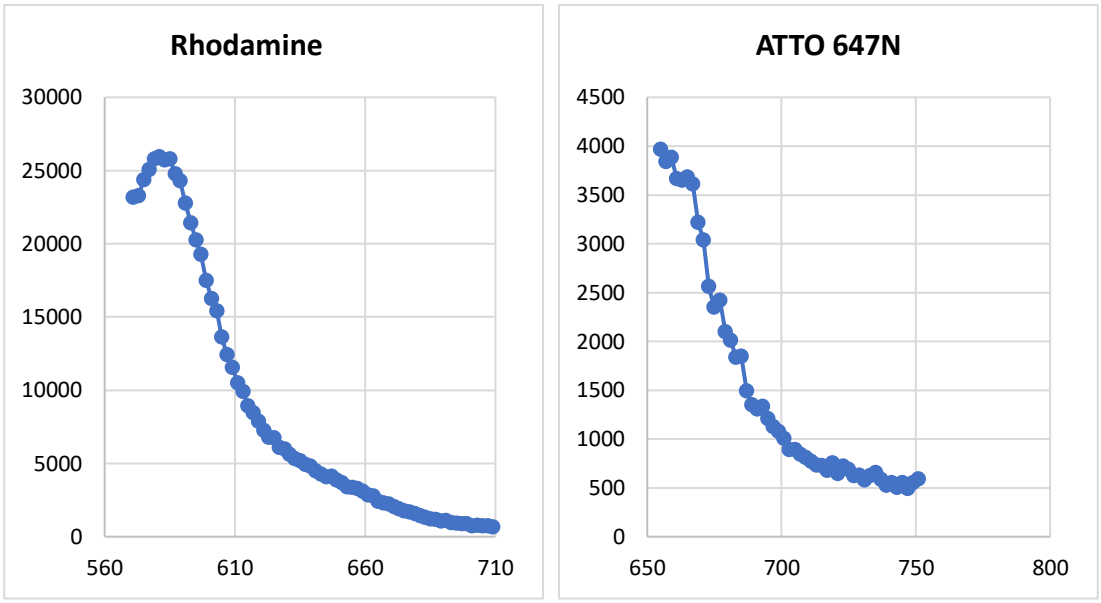


**Figure 41:** Emission spectra of Rhodamine (left) and Atto647N (right) of Core R1-AMPS 0,1 after IgG conjugation.

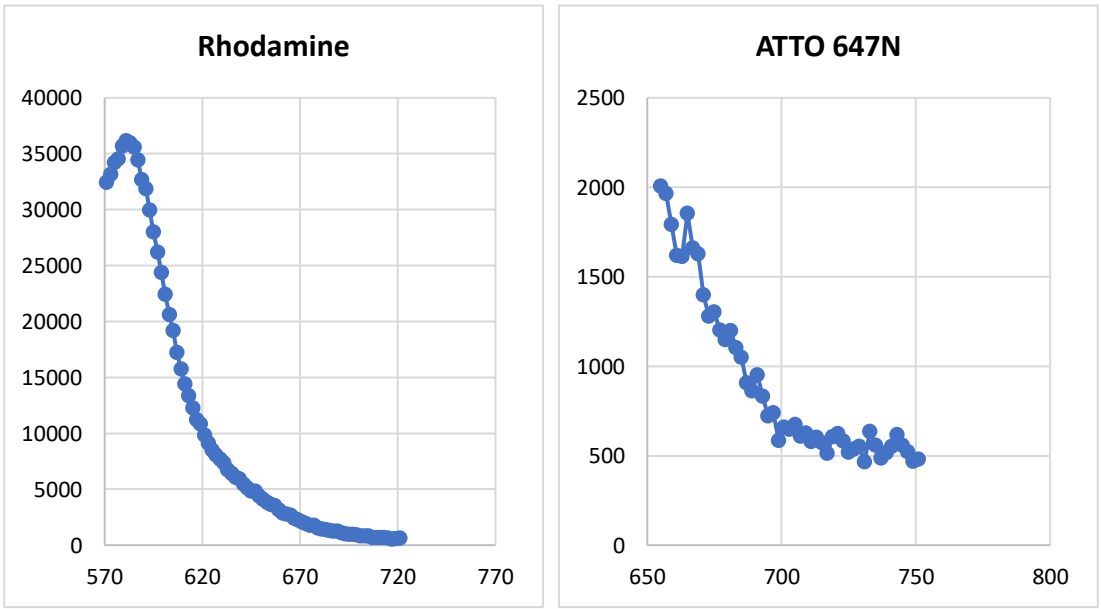


**Figure 42:** Emission spectra of Rhodamine (left) and Atto647N (right) of Core R1-AMPS 1 after IgG conjugation

For R1-AMPS 0,1 and R1-AMPS 1 cores, Rhodamine shows a peak at a wavelength of 580 nm and the Act 647N at 655 nm, but the fluorescence intensity is much higher for the Rhodamine.

In this work, different types of cores microgels are synthesized by varying the nature and amount of monomers introduced during the synthesis. The resultant Core microgels are classified as Core R1-COOH bulk, Core R1-COOH surface, Core R1-AMPS 0,1, and Core R1-AMPS 1. Data regarding the chemical-physical characterization of Core microgels are reported in the following table:

| Core microgels | Diameter [nm] | Zeta Potential [mV] | $n_p/mg$ |
|---|---|---|---|
| R1-COOH bulk | 760.2±16.1 | -20±0.5 | $3{,}26 \cdot 10^{13}$ |
| R1-COOH surface | 749.4±11.9 | -23,3±0.8 | $2{,}28 \cdot 10^{13}$ |
| R1-AMPS 0,1 | 665.6±17.5 | -21.1±0.9 | $9{,}6 \cdot 10^{13}$ |
| R1-AMPS 1 | 641.3±10.3 | -25.5±0.8 | $7{,}73 \cdot 10^{12}$ |

**Table 11:** Chemical and physical characterization of microgels.

Comparing the first two types of particles, the Core R1-COOH bulk presents a diameter of 760±16.1 nm, higher than the Core R1-COOH surface. On the other hand, the surface particles have a slightly more negative charge than bulk microgels, probably due to the confinement of Aac on the outer shell of microgels.

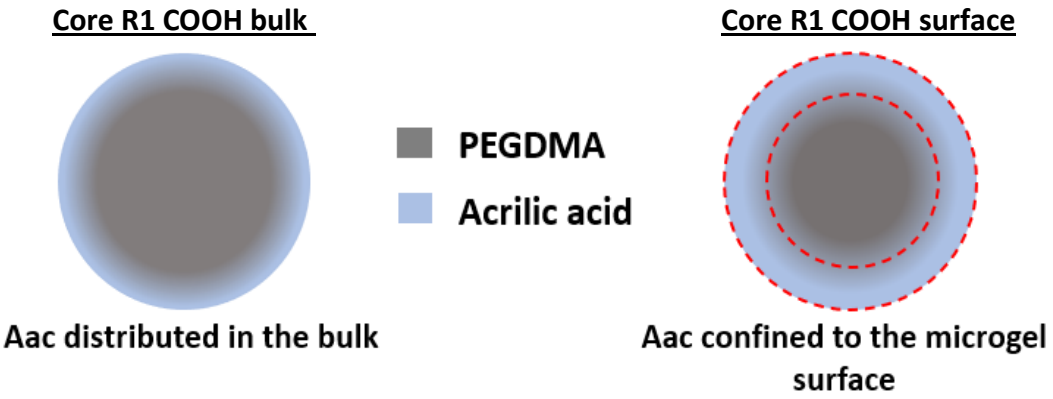


**Figure 43**: Different monomers distribution in core R1-COOH bulk and surface

The core R1-COOH bulk and surface show a higher diameter than microgels containing AMPS. The presence of AMPS produces microgels with a higher surface charge than the previous ones. Increasing the AMPS amount, Core R1-AMPS 1 presents a more negative charge than Core R1-AMPS 0,1 and core R1-COOH. Core R1-AMPS 1 presents a number of particles per milligram an order of magnitude smaller than the other microgels.

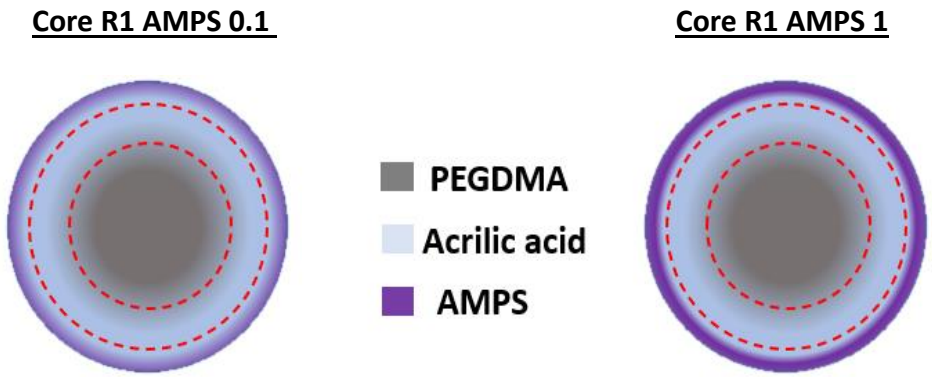


**Figure 44:** Different monomers distribution in core R1-AMPS 0.1 and core-R1 AMPS 1.

The microgels swelling is verified at pH 3, 7 and 10. The swelling was due to the deprotonation of the carboxyl groups, and its effect is present for all core microgels showing an enhancement of the diameter.

| Core microgels | Diameter (nm) at pH 3 | Diameter (nm) at pH 7 | Diameter(nm) at pH 10 |
|---|---|---|---|
| R1-COOH bulk | 544.1±9.3 | 895.1±8.5 | 1029.9±17.1 |
| R1-COOH surface | 557.6±17.1 | 805.5±27.4 | 850.6±19.4 |
| R1-AMPS 0,1 | 578.8±8.1 | 771.1±16.0 | 887.4±21.8 |
| R1-AMPS 1 | 514.6±2.7 | 656.5±9.5 | 706.2±14.2 |

**Table 12:** Size of microgels at different pH values

In particular, the swelling was overwhelming for the core R1-COOH bulk. As reported in the table, the size of core R1-COOH bulk changed from 544.1±9.3 nm at pH 3 to 1029.9±17.1 nm at pH 10. For R1-AMPS microgels, the swelling effect is less evident due to the presence of AMPS and the number of -COOH groups is lower inside the particles.

The fluorescence emission of microgels was evaluated at different pH values. As result, rhodamine in microgels follows the same trend as free rhodamine in solution. For all syntheses, rhodamine emission intensity was higher at acidic pH. Rhodamine B tends to emit a strong fluorescence at acid pH; while at basic pH, the fluorescence intensity is lower.

The synthesized microgels were functionalized with antibodies anti-IgG Atto 647N through the coupling reaction. Functionalized microgels were analyzed by the DLS and the results were compared to microgels before the conjugation. For all four types of functionalized particles, an increase in diameter was observed due to the presence of the antibodies. Furthermore, the zeta potential values decreased due to the binding of antibodies to carboxyl groups onto the surface. Functionalized

microgels were analyzed by CLSM showing the uniform distribution of both the diameter and the fluorescence intensity of rhodamine and Atto 647N, confirming that the samples are monodispersed after the conjugation. In addition, the Atto647N emission intensity of R1-AMPS particles was smaller than that of R1-COOH particles indicating a less amount of antibody bound to the surface. This result was due to the presence of the AMPS whose addition produced a decrease in the COOH groups.

# 4. CONCLUSIONS

In my PhD work, two cores R1-COOH, defined bulk and surface, respectively are produced by using the acrylic acid monomer to create carboxyl groups on their surface. The difference is that the acrylic acid is introduced at different moments during the reaction synthesis and different products are obtained. For the Core-R1-COOH bulk, PEGDMA and acrylic acid are introduced into the reactor at the beginning of the reaction, thus, the -COOH functional groups are distributed both in the bulk and on the surface with the same probability. The Core R1-COOH surface is prepared by introducing the Aac after ten minutes at the beginning of the reaction when nuclei have already formed. The Core R1-COOH bulk presents a diameter of 760±16.1 nm, higher than the Core R1-COOH surface. On the other hand, the surface particles have a more negative charge than bulk microgels, due to the confinement of Aac on the outer shell of microgels. Furthermore, two cores R1-AMPS are produced by introducing an additional monomer (AMPS) resulting in microgels with different properties. Core R1-AMPS 0.1 and core R1-AMPS 1 differ in the number of AMPS: the first one has a molar quantity of AMPS 10 folds smaller than AAc (1:10) and the second one has a molar amount of AMPS equal to AAc (1:1). The obtained microgels solutions are monodisperse and have uniform size and fluorescence distributions. The core R1-AMPS shows a smaller size than the core R1-COOH particles. The surface charge of the R1-AMPS 1 microgels is more negative than the other microgels. The presence of the AMPS allows for maintaining a more negative charge at pH 3 compared to cores R1-COOH, where a charge close to 0 is displayed. At high pH values, the deprotonation of the carboxylic groups results in a repulsive force between them causing the swelling particles. This effect is greater for the core R1-COOH bulk in which Aac polymerizes with PEGDMA as soon as the reaction begins. In this way, COOH groups are present both on the surface and in the bulk of particles. The particles were functionalized with Immunoglobulin G labelled with Atto 647N fluorophore to verify their diverse behaviour. From the optical analysis of the functionalized cores, it is observed that the binding to the IgG

probe occurs for all of the synthesized microgels. The emission intensity of Atto647N is greater for R1-COOH particles than for the other particles. This is because the R1-AMPS particles have a lower amount of carboxylic groups involved in the conjugation reaction and the antibody bound on the surface is less. In conclusion, the presented process can be modified according to the properties of microgels to confer, avoiding more complex structures such as core/shell particles.

# CHAPTER 3


## ABSTRACT

A microgel-based platform is presented here to perform innovative assays. The microgels-based platform is composed of multifunctional particles. Microgels are versatile materials due to their hydrophilic, bio-friendly, and highly tunable nature. Their chemical flexibility allows the embedding of several building blocks into their structure. The high biocompatibility and antifouling properties make possible the employing of the microgels-based platform in biosensing and inspired the development of several sophisticated applications, such as biosensors. The microgels-based platform is applied to design an innovative immunoassay.

The immunoassay set-up consists of a sandwich format combining two diverse particles for human immunoglobulin target detection. Microgels involved in the assay are composed of PEGDMA copolymerized with a fluorescent dye and polyacrylic acid to create pendant groups for post-modifications. Microgels are used as the carrier of both anti-Fab antibodies and horseradish peroxide HRP enzyme. Magnetic particles functionalized with anti-Fc antibodies are involved in acting as capture particles. The immunoglobulin IgG is recognized by antibodies to produce the “sandwich structure” and consequently, particle clusters are formed. Then, a magnet is used to separate clusters of beads and microgels from the rest of the solution. A double detection system is involved. The area of clusters formed among beads and microgels increases proportionally to the target amount. The minimum target amount distinguishable from the background noise has a concentration of 0.28 nM. The supernatants of each sample containing unbound microgels not involved in the cluster’s formation are analyzed by the colourimetric assay due to the presence of the HRP enzyme on microgels. The recovered colourimetric signals are proportional to the enzyme concentration, thus, to the microgels number in the solution. The assay shows a good selectivity toward the target also in presence of an interference protein, BSA. The microgels are capable to detect the target even in presence of crowded protein solutions.


## 1 INTRODUCTION

Biological assays are analytical procedures in which a probe is used as a recognition element for the qualitative identification or quantitative measurement of a target molecule. The probe can bind the target, and after the binding event, an optical, electrical, or fluorescence signal is produced and quantified by a detection method.

Bioassays integrated into biosensors are fundamental in biomedical fields for the diagnosis or the mapping of diseases. Biological assays can be classified on the base of the nature of the probe and the method involved to read the signal.

Nowadays, immunoassays are the most spread analytical procedures used to measure proteins and other biomarkers to predict the development and prognosis of several tumour types and diseases.[118]

In immunoassays, the fundamental elements always are antibodies-antigen pair and a tracer, a biomolecule able to generate a signal to quantify the target.[119] The reaction at the base of the antigen-antibody interaction is Ag + Ab = Ag-Ab, where Ag is the antigen, Ab is the antibody and Ag-Ab is the formed immune complex. Antibodies are very selective biomolecules which only bind to their specific targets, even in the presence of a huge range of other materials in the sample.

Bead-based immunoassays are often considered the most popular type of immunoassays. Microbeads are designed as a carrier for antibodies, antigens or other recognition ligands and also for detection tags. One of the benefits of bead based-assays compared to other solid phase assays is the high surface area of the microparticles, which provides a higher immobilization surface area. The ability to accommodate higher numbers of immobilized molecules helps to improve the sensitivity and detection limit of the assay. Microspheres can be functionalized by a variety of proven chemistries in solution under conditions that are optimum for each probe. When microspheres are used, the panel can easily be changed by adding or subtracting microspheres with different probes. In recent years, many efforts have been made to develop immunodiagnostic methods featured by both sensitive target detection and broad analytical ranges. The non-competitive design usually called sandwich assay is a format used for larger biomolecules possessing more than one recognition site on their structure.[120] The principal characteristic is the use of two antibodies able to bind non-overlapping sites on the same antigen. Usually, the sandwich assay is performed using a microwell plate and in each well, antibodies are immobilized. The first type of antibody is a “capture antibody” able to discriminate from other biomolecules. The secondary antibody of detection binds the free site of the target and forms the “sandwich structure”. This secondary antibody is modified to provide a measurable readout – signal. One of the most spread immunoassays in the sandwich format is called Enzyme-linked immunosorbent assay, ELISA,[121] considered a gold standard technique. Liao et al.[122] designed an ELISA-like detection method combining gold nanoparticles AuNPs and magnetic beads MBs. Gold nanoparticles were functionalized with primary antibody Ab1 and horseperoxidase enzyme HRP, while the detection antibody Ab2

was immobilized onto the magnetic particles' surface. When the target protein was present, the two antibodies Ab1 and Ab2 bound the target leading to a sandwich structure. The presence of the enzymes on AuNPs produced an enhancement in a colourimetric signal. The limit of detection was 5-fold lower than classical ELISA. The standard ELISA and other classical format assays were not sufficient for the detection of an ultralow amount of proteins in the sample. The limited sensitivity of ELISA allows for detecting the target until picomolar (pM) quantity of proteins. Differently, analytes and disease biomarkers are present in fluid and serum at subfemtomolar concentrations. To reach these concentrations, approaches based on single-entity detection and miniaturized structures are increasingly investigated in recent times.[123] The volume of the sample is restricted to a single entity to generate a high local concentration easily to detect thanks to the signal amplification in the confined volume. Single-Molecule Array (SiMoA) is an approach born from the work of Walt et al.[124,125] that makes use of arrays of femtoliter-sized reaction wells that can isolate and detect single molecules. SiMoA allows the detection of single protein molecules in serum simultaneously at subfemtomolar concentrations. Rissin et al.[126] developed the digital ELISA assay employing SiMoA. A classical sandwich structure was formed with free secondary detection antibodies and captured antibodies onto magnetic beads. A fluorescent signal was produced by the enzyme and quantified.[127] By using the array of femtoliter-sized wells, the fluorescent signal generated by the enzymes was confined to a small volume producing a high local concentration of fluorescent molecules. Transportation and confinement of single entities into these small containers have been facilitated through microfluidic techniques. Enzymes are biocatalysts and because of their high selectivity, specificity and activity under mild conditions, enzymes have found a vast variety of applications in different industries. For almost all of the applications, there is a need for enzymes to be immobilized on support before their use. Enzyme immobilization on a heavier entity (e.g. a polymer bead) renders the handling of enzymes easier and enhances their separation from a reaction mixture. The usual supports for enzyme immobilization are synthetic polymers, microgels and hydrogels. In particular, nanoparticles are considered the ideal support due to the minimized diffusional limitations, maximum surface area per unit mass, and high enzyme loading capability. Enzymes can attach to support either through physical bonding (such as hydrophobic interactions), or covalent bonding.[128] Most of the studies on enzyme immobilization focus on the covalent bonding between enzymes and functional carriers.[129] In conventional examples of covalent enzyme immobilization, amino groups in the lysine residue of enzymes and functional

groups on the carriers are activated and coupled via chemical bonding. When enzymes are immobilized on particle support, especially through a multipoint covalent attachment, enzyme stability is increased. This is because the formation of multiple covalent bonds between the enzyme and the carrier reduces conformational flexibility and thermal vibrations thus preventing protein unfolding and denaturation.[130] The widely adopted labelling enzymes for ELISA are horseradish peroxidases (HRP) due to their good stability, high efficiency, and commercial availability. HRP, an enzyme isolated from the roots of horseradish, shows good stability, high efficiency, and commercial availability. HRP is a 44 kDa glycoprotein with 6 lysine residues that are widely studied and often conjugated to a labelled molecule. However, conventional ELISA suffers from unsatisfactory sensitivity. Hence, the development of high-performance ELISA is of great significance for the biosensors field. To overcome this limitation, Yan et al.[131] developed a signal-amplified ELISA strategy for the sensitive detection of metabolites by incorporating gold nanoparticles (AuNPs) into conventional ELISA. A large amount of the reporter antibody and horseradish peroxidase molecules loaded onto AuNPs allowed to amplify the colourimetric signals. This enhancement strategy resulted in higher sensitivity than traditional ELISA.

Hydrogel microparticles and microgels are applied to develop sensitive beads-based assay and detect circulating biomarkers in human serum.[132] The high biocompatibility and antifouling properties[133] of hydrogel make possible their employment in biosensing and inspired the development of bioassay and biosensors.[134,135] Pelton et al.[136] introduced a novel type of microgel-based biosensors for the detection of different pathogens. In their work, PNIPAM microgels were initially functionalized with either an antibody (IgG) and then, used as an ink that can be applied to filter paper through ink-jet printing to produce inexpensive test paper. Recently, an electrochemiluminescence biosensor based on $Ru(bpy)^{3}]^{2+}$-functionalized microgels was developed for interleukin IL-8 detection by Han and coworkers.[137] Polystyrene beads were decorated with modified microgels and anti-IL-8 for the detection of the target. The ECL signal produced by this method was 9-fold higher than molecularly functionalized beads due to the presence of microgels. Yang et al. realized a non-competitive immunoassay on encoded silica–hydrogel hybrid beads for the detection of tumour markers.[138] The fluorescence of encoded beads with labelled antibodies was measured before and after, compared to the levels in solution, and reported to a calibration curve for each marker.

In this work, a novel bioassay based on magnetic beads and PEG microgels for antibody detection is presented. Microgels are adopted as the carrier of anti-Fab antibody and HRP enzyme, while, magnetic particles are functionalized with anti-Fc antibodies acting as capture particles. The assay starts when microgels and beads are mixed in the test sample. Anti-Fab and anti-Fc antibodies are used for recognition of the target antigen human IgG forming a sandwich structure. Particle clusters are formed and visible by a confocal laser scanning microscope (CLSM). The cluster area increases as the target concentration increase too. After the interaction, unbound microgels are separated from the solution and used to produce a colourimetric signal for target detection. Increasing the target concentration in samples, the number of free microgels in the solution decreases. The colourimetric signal produced by HRP-microgels free in solution decreases too.

# 2 MATERIALS AND METHODS

## 2.1 MATERIALS

Poly (ethylene glycol) Dimethacrylate Mn 550 (PEGDMA), Alcohol Polyvinyl 40-88 (PVA), Rhodamine B Methacryloxy-Tricarbonyl, Dimethyl sulfoxide (DMSO), Acrylic Acid (Aac), Potassium Persulfate (KPS), 2-Acrylamide-2-Methyl-1-Acid Propanesulfonate (AMPS), 1-Ethyl-3-(3-dimethyl aminopropyl) carbodiimide (EDC), N Hydroxyisuccinimide (NHS), Acid 2-(N-Morpholino) Ethane sulfonic (MES), Tris (Hydroxymethyl) Aminomethane (TRIS), Phosphate Buffer Saline (PBS), human Immunoglobulin G, Anti-Human IgG (Fab specific), Anti-Human IgG (Fc specific) were purchased from Sigma-Aldrich.

## 2.2 CORE SYNTHESIS

PEG microgels were prepared according to a previously reported work.[139]
Microgels are obtained by free-radical precipitation polymerization carried out in a three-neck, 100 mL round-bottom flask to which a filtered, aqueous solution of 1% (w/v) PVA, 1% (w/v) PEGDMA and Acrylic acid 0.25% (w/v) were added and heated to 65 °C. The reaction was initiated by adding KPS aqueous solution (to make a final KPS concentration of 2mM). The solution turned turbid, indicating successful initiation. After 10 minutes, Rhodamine B dye (0.1 mM) was added to the stirred mixture. The solution was allowed to heat and stir for an additional 5 h while being purged with $N_2$ gas. After 5 hours, the reaction was stopped by cooling to 0°C in an ice bath. The microgels were dialyzed for 15 days against distilled water, purified

several times by centrifuging for 15 minutes at 12000 rpm and resuspending in deionized water to remove unreacted monomers, oligomers and surfactants and stored at 4 °C until further use. The microgels size and electrophoretic mobility were characterized by Dynamic light scattering (Malvern Zetasizer Nano ZS instrument, 633 nm laser, 173° scattering angle). Carboxyl group content was quantified by titration before further conjugation of biomolecules. Ubbelohde viscometer was used for determining the intrinsic viscosity of different microgel preparation as already described by Romeo et al.[140]

## 2.3 HORSERADISH PEROXIDE ENZYME HRP ACTIVITY

HRP solutions are prepared in 100 µL of PBS buffer (pH 8, Tween 0.05%) to reach final concentrations of 0.1, 5, 10, and 20 ng/mL. 50 µL of each sample is mixed with 50 µL of TMB solution in a 96-well plate (Greiner UV-Star®). The absorbance values are measured by PerkinElmer EnSight Multimode Microplate Reader at 562 nm every 20 seconds.

## 2.4 MICROGELS FUNCTIONALIZATION

The microgels surface is functionalized with anti-Fab antibodies and HRP enzyme through a coupling reaction. The activation of the carboxy groups is performed by using 1-Ethyl-3-(3-dimethyl aminopropyl) carbodiimide (EDC) and N-Hydroxy succinimide (NHS).[141] 250 µg of microgels are suspended in 2-(N-Morpholino) Ethane Sulfonic acid (MES) buffer solution (50 mM, pH 6) and 19 mg of EDC and 23 mg of NHS (0.1 M and 0.2 M, 1:2) are added dropwise.

After 3 hours, 10 µg of anti-Fab antibodies and 1 mg of HRP enzyme are added. The reaction is allowed to run overnight at room temperature. Then, the reaction solution is centrifuged for 10 minutes (10.000 rpm, 4°C) and, after removing the supernatant, a solution of 450 µL of MES and 50 µL of TRIS (pH 8) is added.

After removing the supernatant, PBS (1x, pH 8, 0,05% Tween) is added to the functionalized microgels to a final concentration of 250 µg/ml. The solution is stored at 4°C until further use.

## 2.5 MAGNETIC BEADS FUNCTIONALIZATION

Dynabeads™ M-270 Epoxy (500 µg, Thermo Fisher Scientific) are suspended in MES buffer (25 nM, pH 6) and anti-Fc antibodies (5 µg) are added. The reaction is allowed to proceed overnight at room temperature. Magnetic beads are separated from the solution magnetically and the supernatant is discarded. Finally, 500 µl of PBS pH 8

(0.05% Tween, BSA 0.1%) is added to a final concentration of 1 mg/ml and stored at 4°C for further use.

## 2.6 ASSAY SET-UP

Anti-Fc beads (15 µL, 10^6 beads) in PBS buffer (pH 8, 0,1% BSA, 0.05% Tween) and anti-Fab-HRP-microgels (11 µL, 2.2x10^9 microgels) are mixed to 24 µL of human IgG antibody solution from $13 \cdot 10^{-9}$ to $2.7 \cdot 10^{-6}$ M. The sample with no target was used as the control sample. Particles are allowed to react overnight. Then, beads are separated from the solution magnetically and the supernatants are recovered. The pellet is resuspended in 50 µL of PBS buffer.

## 2.7 COLOURIMETRIC ASSAY

Both supernatants and solutions containing the pellet are analyzed by colourimetric assay. 20 µL of each sample are spiked with 50 µL of TMB substrate and incubated for 20 minutes. Then, 50 µL of HCl 1M was added to stop the enzymatic reaction. Samples are transferred in a 96-well plate (Greiner UV-Star®) and absorption measurements are conducted by PerkinElmer EnSight Multimode Microplate Reader at 452 nm.

## 2.8 CLSM ANALYSIS

The confocal laser scanning microscope STED-SP5 was used to collect images of samples containing the pellet. 20 µl of each sample were loaded onto µ-slide channels (Ibidi, Martinsried, DE). The objective used was HC PL FLUOTAR 20x0.5 dry, section thickness 3.99 µm, scan speed 8000 Hz, image size 387.5x387.5 $\mu m^2$ (resolution 512x512). All captured images were analysed with Image J (version 1,43i, NIH, Bethesda, MD) to calculate the area of clusters.

## 2.9 SPECIFICITY ASSAY

To examine the specificity of the MB/microgels system, the assay is performed as reported previously by using bovine albumin serum protein BSA. Sample*1 is prepared by mixing anti-Fc beads (15 µL, 10^6 beads) in PBS buffer (pH 8, 0,1% BSA, 0.05% Tween) and anti-Fab-HRP-microgels (11 µL, 2.2x10^9 microgels) to 24 µL of BSA solution $6 \cdot 10^{-4}$ M. Sample*2 is prepared by mixing anti-Fc beads (15 µL, 10^6 beads) in PBS buffer (pH 8, 0,1% BSA, 0.05% Tween) and anti-Fab-HRP-microgels (11 µL, 2.2x10^9 microgels) to 24 µL of BSA:IgG solution 1:1. Particles are allowed

to react overnight. The sample with no target was used as the control sample. Then, beads are separated from the solution magnetically and the supernatants are recovered. The pellet is resuspended in 50 µL of PBS buffer.

### 2.10 STATISTICAL ANALYSIS

All experiments were performed at least three times, reported as mean ± standard deviation. The significant difference was determined at P values smaller than 0.05. To estimate the Limit of detection and the Limit of quantification, the values subtracted from the background and reported as mean ± standard deviation are fitted by applying linear regression. The LOD value is calculated as three standard errors (SE) above the slope.

## 3 RESULTS AND DISCUSSION

A new bioassay is developed including particles with different roles. Microgels are involved as the carrier of both anti-Fab antibodies and the HRP enzyme. Antibodies are used for human IgG detection and the HRP enzyme to produce an optical signal, respectively. Magnetic particles functionalized with anti-Fc antibodies behave as capture particles. The anti-Fab antibodies bind the Fab region and the anti-Fc antibodies recognize the Fc tail. The first step of the assay involves the interaction among anti-Fab-microgels and anti-Fc-beads in presence of the target in the sample producing a sandwich structure. Clusters containing microgels and beads are formed due to the presence of the IgG target. Then, a magnet is used to separate clusters of beads and microgels from the rest of the solution. A double detection system is involved: the supernatant containing unbound microgels is analyzed by a colourimetric assay and the pellet containing clusters is analyzed by a confocal laser scanning microscope (CLSM).

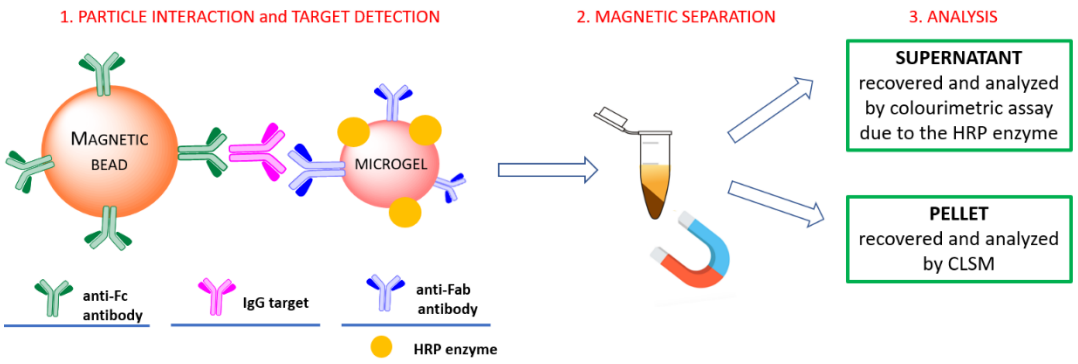


**Figure 1:** Immunoassay format for the human IgG antibodies detection.

## 3.1 MICROGEL SYNTHESIS AND CHARACTERIZATION

Microgels composed only of a polymeric core have been chosen as a starting point, obtained by free-radical precipitation polymerization. The core is composed of PEGDMA co-polymerized with a fluorescent dye, Rhodamine, and acrylic acid to decorate the particles with carboxylic groups useful for successive conjugation. After the synthesis, microgels were characterized to determine their physical, chemical, and optical properties. Core microgels result in uniform size with a hydrodynamic diameter of 760.2±16.1 nm. The polydispersity index (PDI) recorded is very low 0.076 highlighting that the microgel solution was monodisperse. The microgels show a negative zeta potential of around -20.1±0.5 mV due to the presence of acrylic acid on the surface. This negative charge confers colloidal stability allowing them to stay suspended and not aggregated. These functional groups are fundamental for the subsequent functionalization of microgel surfaces with antibodies or other biomolecules.

Microgels with a concentration of 40 μg/ml in water are characterized using the confocal laser scanning microscope. The images were thresholded by Otsu algorithm and then processed with the Image J Analyze Particles function to computationally determine the number of single fluorescent particles.

The following graphs show the size and fluorescence distributions of the core R1-COOH bulk obtained by mediating the data of 5 images.

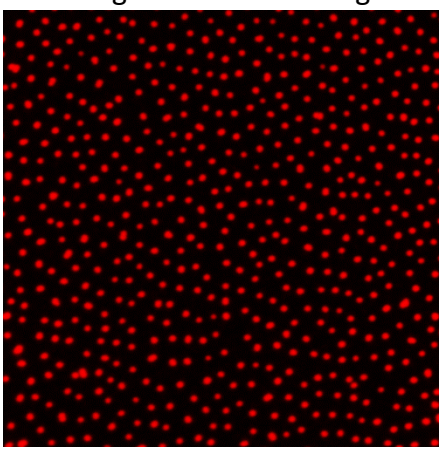

**Figure 2**: Images of Core R1 COOH

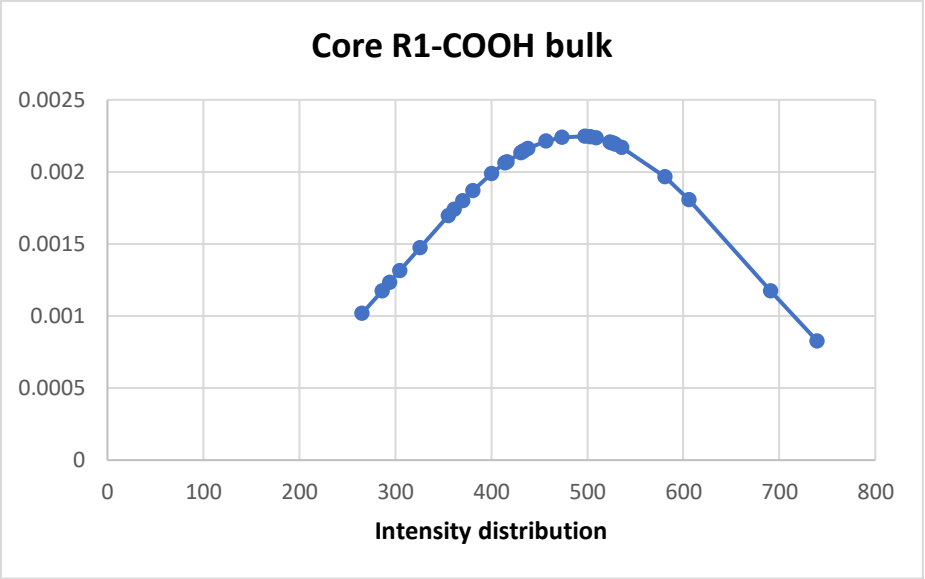


**Figure 3:** Fluorescence intensity distribution of core R1-COOH bulk.

The distribution of fluorescence emission is uniform at a value of 463.5±14.18.

The mass of the particles and the number of particles per mg of solution are determined by using the Ubbelohde viscometer. The particle mass is 1,3·10^(-11) mg and the number of particles/mg is 3,26·10^13.

Potentiometric titrations were performed using Compact Titrator G20 (Mettler Toledo AG, Analytical Schwerzenbach, CH) to determine the COOH content of microgels. Samples were prepared by suspending 0.050g of the microgel in 50 mL of $10^{-3}$ M KCl solution. During the titration, pH was measured as the function of the volume of the delivered standard NaOH solution. The carboxyl content of microgels was $1{,}73 \cdot 10^{-6}$ mol/mg particles.

## 3.2 HRP ACTIVITY STUDY

HRP samples of 0.1, 5, 10, and 20 ng/mL are prepared to determine enzyme activity in presence of TMB-specific substrate. 50 µL of each sample is mixed with 50 µL of TMB solution in a 96-well plate (Greiner UV-Star®) and the absorbance values are measured by PerkinElmer EnSight Multimode Microplate Reader at 562 nm every 20 seconds. Data are reported in the following chart:

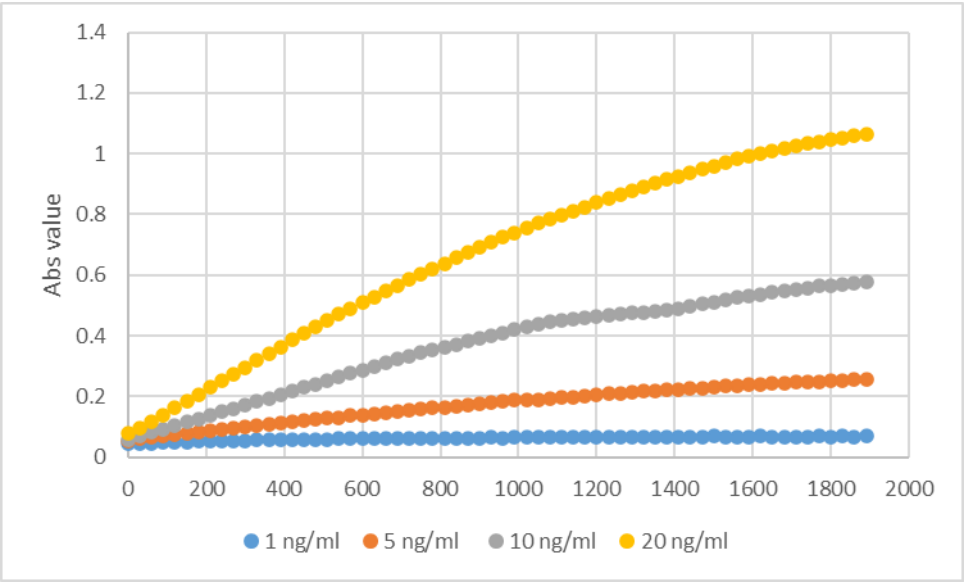


**Figure 4:** Kinetic curves of HPR solutions at different concentrations in presence of a fixed amount of TMB solution.

As shown in the chart, for each sample the absorbance value increases from 0 s to 1800 s. Values increases from 1 ng/mL to 20 ng/mL HRP solutions. At 20 minutes (1200 s), the curve for 20 ng/mL reaches the plateau. Thus, it is chosen as the time to stop the colourimetric reaction between HRP and TMB during the assay.

## 3.3 HRP AND ANTI-FAB CONJUGATION ON MICROGELS

Carboxyl groups onto microgels are exploited for decoration with antibodies and HRP enzyme. The immobilization of biomolecules starts with the activation of carboxylic groups on the microgel surface (250 µg/ml) towards amine groups of antibodies to create a covalent amine bond. This latter has been performed by using Ethyl-N'-(3-(dimethylamino)propyl)carbodiimide hydrochloride (EDC) and N-hydroxy succinimide (NHS) in MES buffer (50 mM, pH=6) for 3 hours. The optimized EDC/NHS concentrations ratio was 0.1 M/0.2 M. After the activation, 10 µg of anti-Fab antibody and 1 mg of HRP enzyme are added and the reaction is performed overnight. Then, the microgels are purified by centrifugation to remove the unreacted antibodies in the solution.

## 3.4 MAGNETIC BEADS FUNCTIONALIZATION

Dynabeads™ M-270 Epoxy (Thermo Fisher Scientific) are chosen as the capture particle in the developing immunoassay. Beads have a size of 2.8 um and are decorated with epoxy groups on the surface. Anti-Fc antibody is specific for the Fc

region of the target antigen IgG generating a sandwich structure that can be separated from the solution magnetically. Magnetic beads are put in contact with 5 µg of anti-Fc antibodies overnight. Then, beads are separated magnetically from the solution and suspended in the PBS buffer.

## 3.5 ASSAY SET-UP AND CONFOCAL LASER SCANNING MICROSCOPE (CLSM) ANALYSIS

The sandwich assay is performed with microgels and beads in the presence of the target. Functionalized microgels and beads are mixed with 24 µL of human IgG antibody solution from $0.28 \cdot 10^{-9}$ to $2.8 \cdot 10^{-6}$ M. The sample with no target is used as the control sample. Microgels and beads are allowed to interact overnight under mild shaking at room temperature. The IgG target is bound by anti-Fc and anti-Fab antibodies at the Fc and Fab moieties resulting in the formation of sandwich structures. As result, microgels surround beads forming clusters of different dimensions as a function of the target amount.

A magnet is used to precipitate clusters of beads and microgels and separate them from the solution. Microgels unbound to beads are not precipitated but free in the supernatants. The magnetic separation allows the recovery of clusters formed by magnetic beads and microgels. Assay buffer is added into samples containing the clusters and the resulting samples are analyzed by CLS microscope. In this case, a wide working range of human IgG targets is explored from 0.28 nM to 2.8 µM. Ten images for each sample are acquired showing the formation of clusters among microgels and beads in presence of the IgG target. In particular, clusters of different dimensions are visible: the higher the IgG amount is present, the higher the cluster area is.

Images acquired by CLSM for different samples are shown:

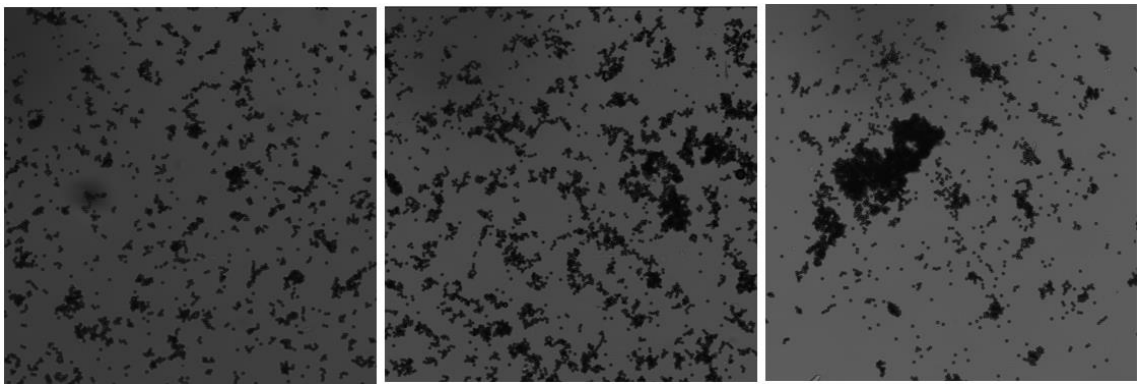

**Figure 5**: control sample (on the left), sample of 0.13 µM human IgG target (in the centre), sample of 1.38 µM human IgG target (on the right).

In the case of the control sample, the formation of cluster area is not very considerable due to the absence of the target. Thus, the small clusters present in the sample are due to the non-specific interaction among particles functionalized with antibodies. Introducing the target, anti-Fab and anti-Fc antibodies on beads and microgels bind the IgG, producing clusters of particles. Their area increases as the target concentration increase too. Images are analyzed by using the Image J software to determine the cluster's area formed by microgels and beads. The mean area for each sample is reported in the following chart:

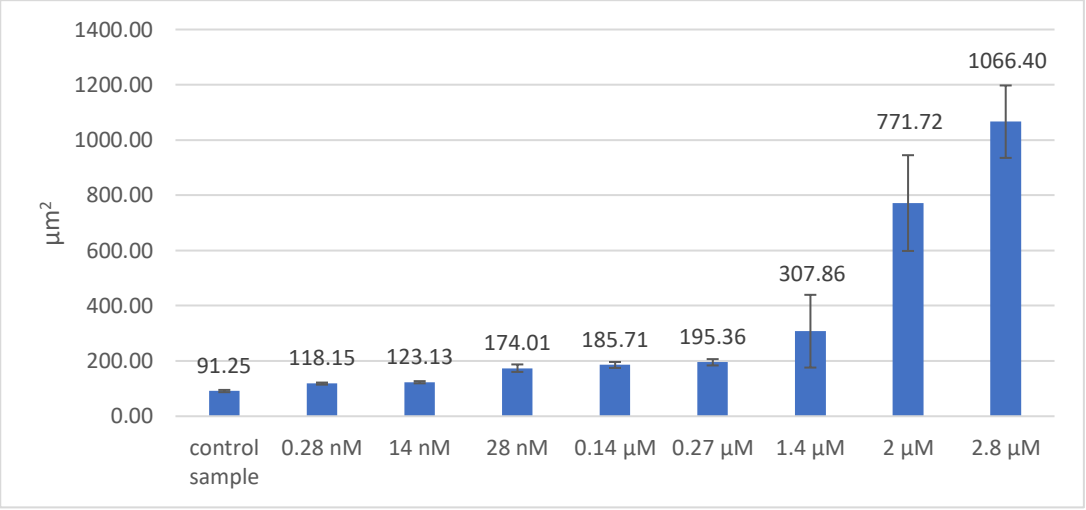


**Figure 6**: Clusters area for each assay sample.

The area of clusters formed among beads and microgels increases from 91.25±4.03 $\mu m^2$ for the control sample in absence of the target to 1066.4±131.1 $\mu m^2$ for 2.8 µM of the target. The minimum target amount distinguishable from the background noise has a concentration of 0.28 nM.

A calibration curve is obtained by plotting the cluster's area values over a dynamic range concentration of $28 \cdot 10^{-9}$ – $2.8 \cdot 10^{-6}$ M:

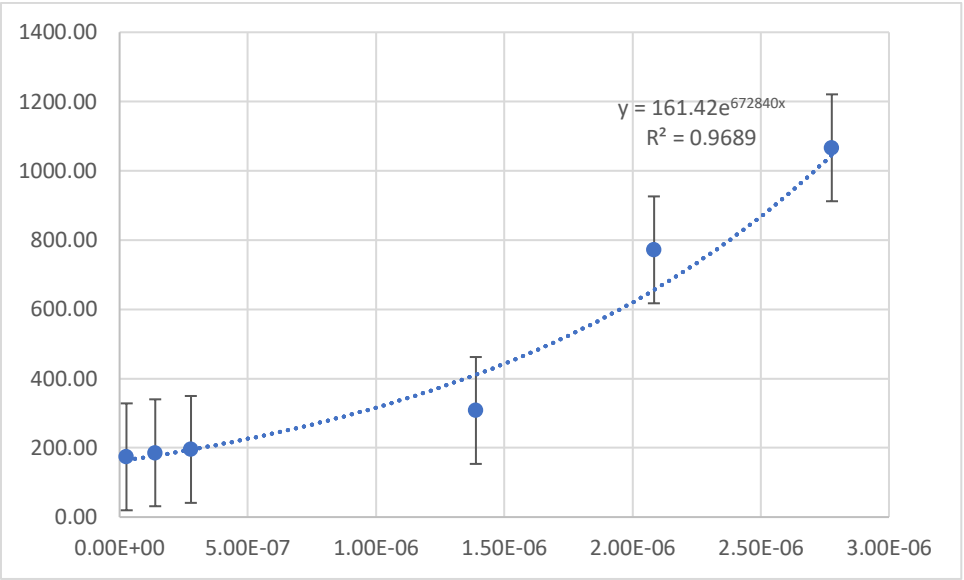


**Figure 7**: Plot of cluster's area values.

The calibration curve is used to determine the IgG target concentration in unknown samples by comparing the cluster's area values to the curve.

## 3.6 COLOURIMETRIC ASSAY

The supernatant of each sample contains unbound microgels not involved in the cluster's formation. To determine the number of free microgels, supernatants are analyzed by the colourimetric assay. Microgels are functionalized with the HRP enzyme which produces a blue-coloured solution in presence of its specific substrate. A fixed amount of TMB (50 µL) solution is added to 20 µL of each supernatant allowing the enzyme reacts in the dark. After 20 minutes, the reaction is stopped by adding 50 µL HCl 1M producing a change in colour from blue to yellow. The colour intensity produced by the enzymatic reaction is proportional to the enzyme concentration, thus, to the microgels number in the solution.

The colour formation of supernatants is stronger for the control sample and decreases from $28 \cdot 10^{-9}$ to $2.8 \cdot 10^{-6}$ M.

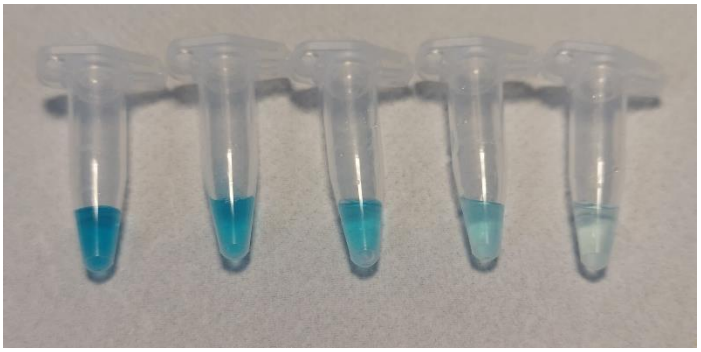

**Figure 8**: Colourimetric assay with TMB solution. The blue colour decreases from the control sample with no target (left) to the solution $2.8 \cdot 10^{-6}$ M (right).

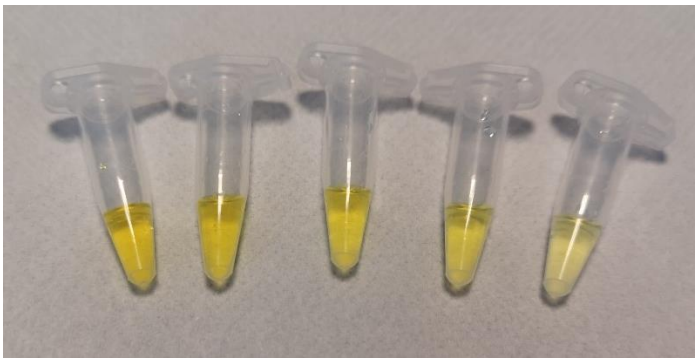

**Figure 9**: Colourimetric assay after the addition of HCl 1M. The solution colour changes from blue to yellow.

The colourimetric signal is recorded by the PerkinEklmer spectrofluorometer at 450 nm and absorbance values are reported in the following chart:

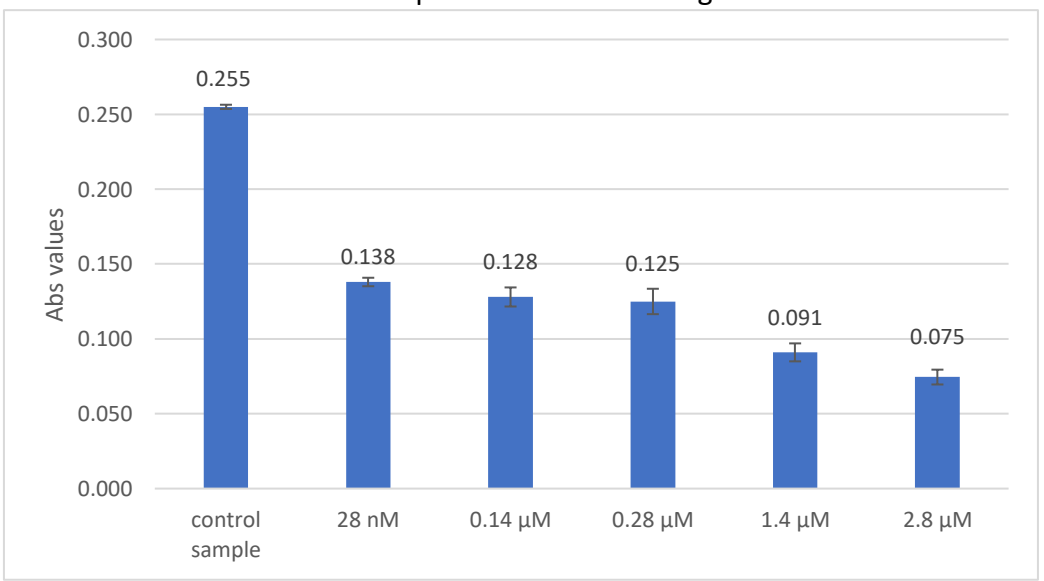


**Figure 10**: Abs values for each supernatant of assay samples.

The colourimetric signal decreases from 28 nM to 2.8 µM of the IgG target. The presence of the IgG target allows the formation of clusters among beads and microgels due to anti-Fc and anti-Fab antibodies binding to the IgG target. An increasing amount of the target results in bigger clusters including more microgels. When the magnetic separation occurs, the number of free microgels in the solution decreases at a higher amount of IgG. Consequently, the higher the target concentration is, the fewer microgels in the supernatants are. Thus, the colourimetric signal produced by HRP-microgels free in solution decreases too. The control sample with no target has a value of 0.2550±0.01. Observing the Abs values, it appears that they are lower than the Abs value of the control sample. The Abs value decreases as the IgG concentration increases too, from 0.138±0.003 to 0.075±0.005.

Furthermore, the pellet recovered during the precipitation contains clusters formed by beads and microgels due to the presence of IgG antibodies. Pellets are suspended in PBS sample buffer and 50 µL of TMB substrate is added to each of them. The reaction is performed as in the previous case and then, the absorbance values are recorded and shown:

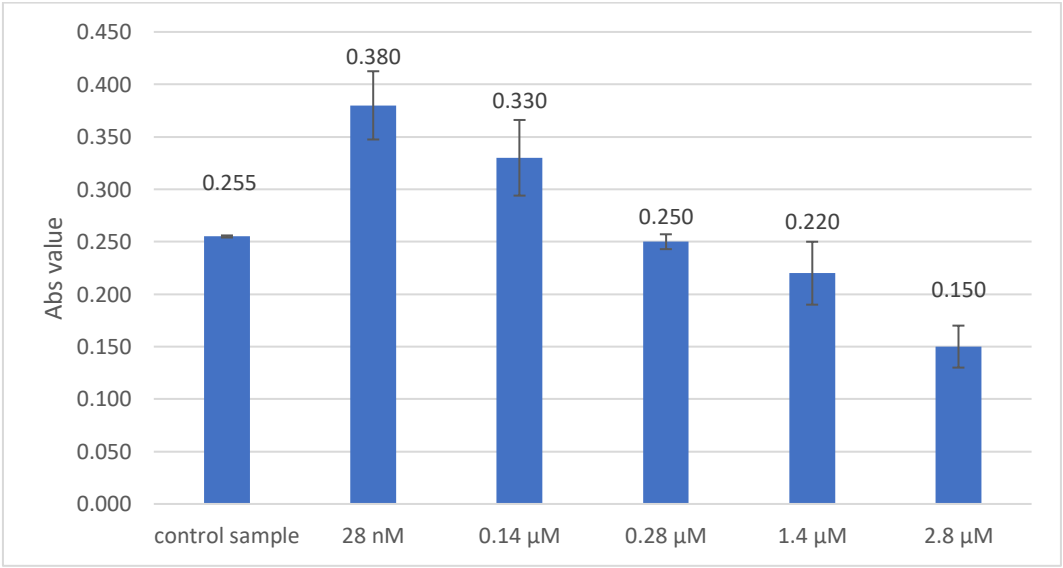


**Figure 11**: Abs values for each pellet sample of the assay.

Also, in this case, the absorbance values decrease as the target concentration increases too. When clusters are formed, microgels and beads bind to each other and their size increases at high target concentrations including more microgels. The HRP on microgels is shielded preventing the TMB substrate reach the enzyme to give the reaction.

The assay is repeated for the control sample and 2.8 µM of IgG. After magnetic separation, the pellet samples are shaken for about 30 minutes to allow the break of clusters. The obtained absorbance values are reported in the following chart:

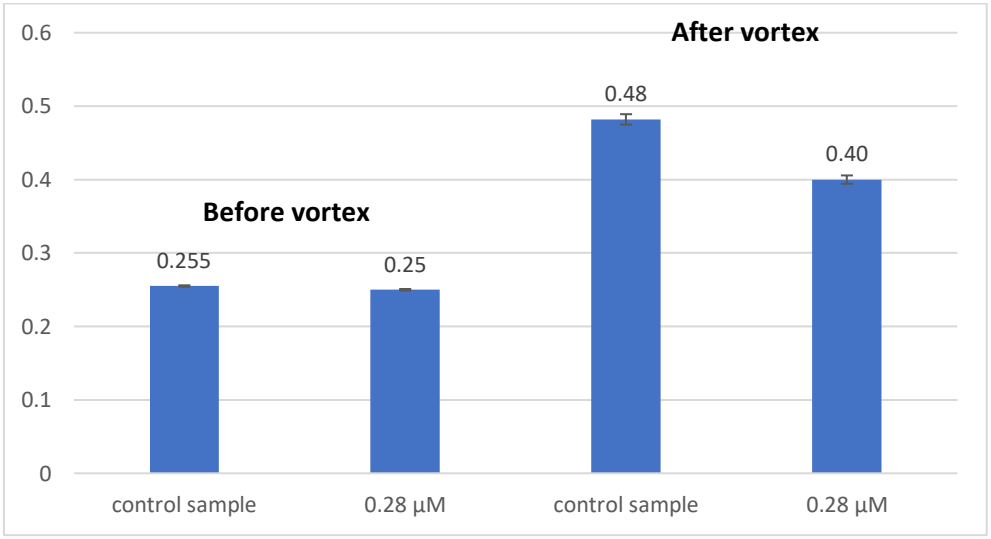


**Figure 12**: Abs values for the control sample and 0.28 µM IgG after shaking for 30 minutes.

The absorbance value increases from 0.255±0.03 to 0.48±0.01 for the control sample and from 0.25±0.01 to 0.40±0.01 in the case of 0.28 µM of the target. When clusters are broken, the HRP enzyme is less shielded and the absorbance values increases compared to the previous results. Since it cannot be defined with certainty that all clusters have been broken, we decide to perform the colourimetric assay considering only the supernatants.

Finally, the colourimetric assay presents a working range from 28 nM to 2.8 µM. The minimum target amount distinguishable from the background noise has a concentration of 28 nM.

## 3.7 SPECIFICITY ASSAY

To evaluate the specificity, the assay is performed in the same conditions by using the bovine serum protein BSA as an interferent protein. Sample*1 and sample*2 contain 1 µg of BSA and IgG/BSA in a 1:1 ratio. The cluster's area and absorbance values are determined for all samples.

Solutions containing clusters of microgels and beads are analyzed by CLSM to determine the cluster's area:

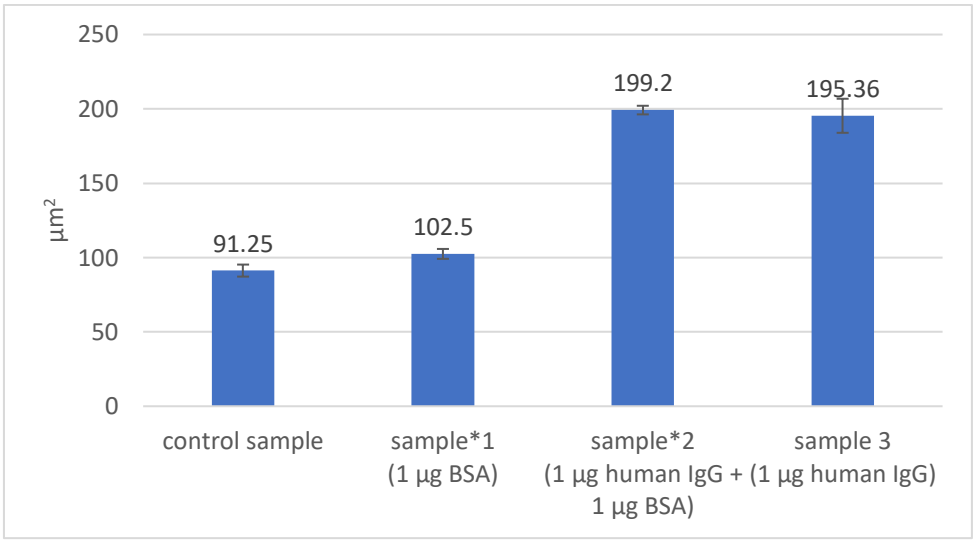


**Figure 13**: Clusters area values for specificity assays.

The chart shows there aren't significant differences among the area of the clusters for sample*1 with 1 ug of BSA and that of the control sample. Furthermore, for sample*2 in which human IgG and BSA are present in a 1:1 ratio, the cluster's area value is 199.2±2.9, very similar to the value of sample 3 with 1 µg of human IgG. This result indicates that the cluster's formation occurs in the presence of the IgG target, only.

The absorbance values of supernatants are reported in the following chart:

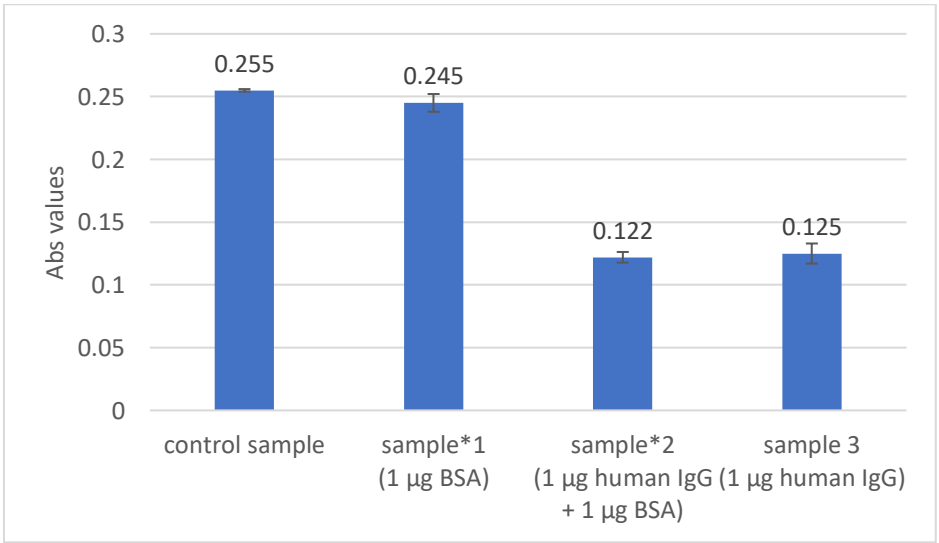


**Figure 14**: Abs values for each supernatant of samples*.

Sample*1 shows an absorbance value similar to the control sample indicating the absence of non-specific binding and that anti-Fab and anti-Fc antibodies used for

the assay don't bind the BSA protein used. When the human IgG antibody is present, the absorbance value is 0.122 for sample*2, very similar to that of sample 3 in which only human IgG antibody is present. This is due to the specific binding of the target by the anti-Fab and anti-Fc on particles. The assay shows a good selectivity toward the target and the microgels are capable to detect the target even in presence of crowded protein solutions.

## 4 CONCLUSIONS

A novel bioassay based on magnetic beads and PEG microgels for human IgG antibodies is presented. The assay starts when microgels and beads are mixed in the test sample. Microgels are functionalized with anti-Fab antibodies and HRP enzyme while magnetic beads are modified with anti-Fc antibodies. Antibodies are used for recognition of the target antigen human IgG forming a sandwich structure and consequently, particle clusters are formed. Then, a magnet is used to separate clusters of beads and microgels from the rest of the solution. A double detection system is involved: the supernatant containing unbound microgels is analyzed by a colourimetric assay and the pellet containing clusters is analyzed by a confocal laser scanning microscope (CLSM). A wide working range of human IgG targets is explored from 0.28 nM to 2.8 μM. The area of clusters formed among beads and microgels increases from 91.25±4.03 $\mu m^2$ for the control sample in absence of the target to 1066.4±131.1 $\mu m^2$ for 2.8 μM of the target. The minimum target amount distinguishable from the background noise has a concentration of 0.28 nM. The supernatants of each sample containing unbound microgels not involved in the cluster's formation are analyzed by the colourimetric assay. The TMB substrate is added to samples reacting with HRP enzyme on microgels producing a colour solution. The colourimetric signal is recorded by the PerkinEklmer spectrofluorometer at 450 nm showing that the absorbance values are proportional to the enzyme concentration, thus, to the microgels number in the solution. The assay is carried on in the presence of an interference protein, BSA, showing a good selectivity toward the target and the microgels are capable to detect the target even in presence of crowded protein solutions.

# 5 APPENDIX

## CONJUGATION OF ANTIBODIES ON MICROGEL SURFACE

To determine the possibility of the conjugation of antibodies onto the microgels surface, an anti-IgG antibody linked to a fluorescent dye, Atto-647N fluorophore, is chosen. In this way, after the coupling reaction, it is possible to have a direct signal

of the trend and yield of the reaction. The first attempts involved the optimization of coupling reaction conditions. The immobilization of antibodies starts with the activation of carboxylic groups on the microgel's surface towards amine groups of antibodies to create a covalent amine bond. This latter is performed by using Ethyl-N'-(3-(dimethylamino)propyl)carbodiimide hydrochloride (EDC) and N-hydroxy succinimide (NHS) in MES buffer (50 mM, pH=6) for 1 hour. EDC and NHS reagents are used in different concentration ratios to determine the optimal one for the reaction. The optimized EDC/NHS concentrations ratio is 0.1 M/0.2 M. After the activation, 1 µg of anti-IgG Atto-647N is added and the reaction is performed for two hours. Then, the microgels are purified by centrifugation to remove the unreacted antibodies in the solution.

Different amounts of microgels (50 µg, 500 µg and 1 mg) are tested with the same quantity of antibodies using the reaction conditions mentioned above. Confocal laser scanning microscopy is used to acquire images of the microgel sample showing a fluorescent signal due to the Atto-647N dye of the antibodies. These results highlight that covalent immobilization occurs and thus, the microgels are functionalized. The antibodies immobilization yield is determined by an indirect method of quantification. Probes number immobilized is given by the difference between the initial number of antibodies and the number of unreacted antibodies after the reaction. The quantification is performed relative to a calibration curve in which fluorescence emission is reported against the mole number of antibodies. Known concentrations solutions of Atto-647N-linked antibodies in the range from 0.1 µg/ml to 1 µg/ml are prepared and their fluorescence emission was recovered by the spectrofluorometer (Horiba Jobin Yvon Inc. FluoroMax®-4). The emission signals are reported against the respective mole numbers in the calibration curve.

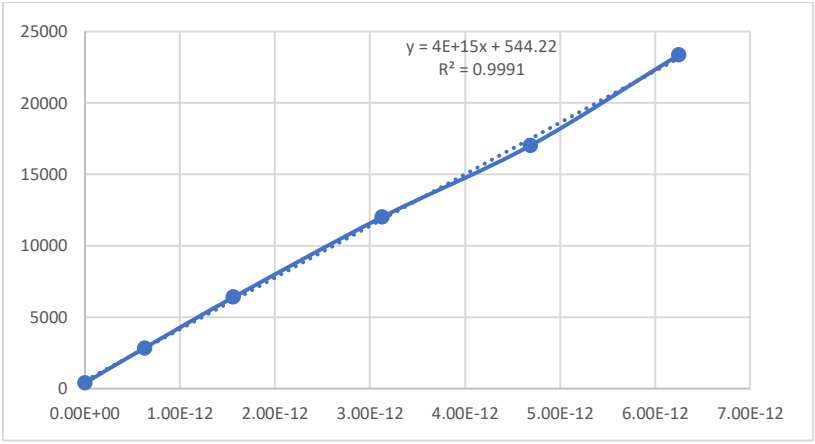


**Figure 1**: calibration curve of fluorescence emission as a function of mole numbers.

After the conjugation reactions, the recovered supernatants containing the unreacted antibodies are read by the spectrofluorometer. The obtained fluorescent signals are compared to the calibration curve and the mole number of unreacted antibodies is determined. The difference between the initial amount and the final one is the number of antibodies coated onto the microgel surface.

| Microgels amount | µg of antibodies bound to microgels | µg of antibodies/microgel | Binding yields % |
|---|---|---|---|
| 50 µg | 0.21 | 1.53E-11 | 21.18% |
| 250 µg | 0.32 | 2.27E-12 | 31.52% |
| 500 µg | 0.39 | 1.41E-12 | 39.06% |

**Table 1:** Quantification of antibodies bound to microgels and binding yields.

As shown in table 1, increasing the microgels concentration involved in the reaction, the total amount of antibodies conjugated increased and thus, the binding yields too. At the same time, the number of antibodies per single microgel decreases obtaining a less functionalization degree.

## CONJUGATION OF HPR ENZYME ON MICROGEL SURFACE

The next step is about proofs of horseradish peroxide HRP conjugation on the microgels surface. HRP, an enzyme isolated from the roots of horseradish, is the most widely used catalyst in enzymatic reactions. HRP is characterized by good stability, high efficiency, and commercial availability.

The coupling reaction is performed on 250 µg and 500 µg of core R1 COOH microgels with a two steps method by using EDC and NHS as activation reagents. Starting from the procedure optimized for the antibodies coupling, some modifications are made. The first step of carboxylic group activation is performed with EDC and NHS (0.1 M/ 0.2 M) increasing the reaction time to 3 hours. After the centrifugation and washing step, 10 µg of HRP enzyme is introduced into the reaction mixture and left to react for 24 hours. Microgels are centrifugated to recover the supernatants necessary for the quantification.

QuantiPro™ BCA Assay Kit (Sigma-Aldrich) is used to determine the unreacted protein-free in the supernatant. The bicinchoninic acid (BCA) assay relies on the formation of a $Cu^{2+}$-protein complex under alkaline conditions. The quantification is performed relative to a calibration curve using BSA protein as the standard. For the Lamber-Beer law, the absorbance value is linearly proportional to the concentration only for very dilute solutions and for absorbance values ranging from

0 to 1. Thus, known concentrations of BSA in MES buffer (50 mM, pH=6) are prepared to range from 0.5 µg/ml to 30 µg/ml and positioned in a 96-well plate (Greiner UV-Star®). Reagent components in the BCA kit are mixed according to the manufacturer's protocol and added to each well. The reaction is allowed to carry out for 1 hour at 60°C. The absorbance at 562 nm is measured for each well by using the plate reader EnSight Multimode Microplate Reader and the blank value is subtracted. Absorbance values are reported as a function of the BSA protein concentration used to build the standard curve. The supernatants of coupling reactions containing the unknown concentration of unreacted HRP are treated following the same procedure. In this case, the absorbance response is very high over the linear range of the curve. This problem is due to the NHS that interferes strongly with the BCA protein assay by causing the reduction of $Cu^{2+}$ in the BCA working reagent. NHS and BSA have similar absorbance values and identical absorbance peaks at 562 nm. In presence of NHS, it is not possible to quantify the residue protein, thus a purification step is necessary. Residue protein in supernatants is purified by inducing precipitation by adding an organic solvent. Equal aliquots of supernatant in different tubes are treated with acetone at -20°C and incubated for 30 minutes at the same temperature. Then, the samples are centrifugated at 14000 rpm for 10 minutes and supernatants are discarded. The procedure is repeated three times for each sample and the BCA assay is carried on. The absorbance values decrease laying in the standard curve attesting that NHS residue is eliminated. The recovery of the assay is determined as $\% \, Recovery = \frac{measured \; concentration}{theoretical \; cancentration} * 100$, with an acceptance range from 80–120%. The HRP sample at a known concentration is precipitated and treated with BCA assay and the absorbance is compared with that of the untreated sample at the same concentration. The recovery percentage is determined for six pairs of samples and is from 97 to 107%.

Thus, supernatants of the two coupling reactions are purified by NHS and quantified, comparing absorbance with the BSA standard curve.

| Microgels amount | µg of HRP bound to microgels | µg of HRP/microgel | Binding yields % |
|---|---|---|---|
| 250 µg | 8.3 µg | 5.99E-11 | 83% |
| 500 µg | 8.6 µg | 3.11E-11 | 86% |

**Table 2:** quantification of HRP bound to microgels and binding yields.

The difference between the initial amount and the final one gives the number of enzymes conjugated onto the microgel surface. As shown in the table, the binding yields increase from 83% to 86% increasing the microgels concentration involved in the reaction. At the same time, the number of antibodies per single microgel decreases obtaining a less functionalization degree.

## ACTIVITY EVALUATION OF FREE AND BOUND ENZYME

After the quantification, the activity of the enzyme bound to microgels is evaluated. The substrate used is the 3,3',5,5'-tetramethylbenzidine (TMB, Sigma-Aldrich) that HRP converts from its colourless form to its oxidized green product. The absorbance of the solution presented two peaks at 370 nm and 652 nm. The TMB colour development process is stopped by the addition of an acidic stopping solution to quench the redox activity. The blue-green reaction product is converted into a yellow species producing a shift of the absorbance maximum to 450 nm. For the previous two coupling reactions, aliquots of 2.5 µg and 5 µg are tested by TMB assay. A 96-well microplate is used to perform activity measurements for each aliquot. The wells are filled up to 200 µL with MES buffer containing microgels functionalized with HRP and 50 µL of TMB is added. After incubation for 20 minutes, reactions are stopped with 50 µL of HCl 1M and the solution colour changes from blue to yellow. The absorbance values are measured by the plate reader at 450 nm. As result, for each coupling, absorbance values increase passing from 2.5 µg to 5 µg of microgels due to the increasing amount of HRP present in the well. On the other hand, microgels from the coupling with 250 µg have a higher functionalization than the other coupling resulting in a much higher absorbance value in the first case rather than the second one.

The catalytic activity of free HRP is determined and compared to that of bound enzyme on microgels following the experimental protocol published by Yan et al.[142] The HRP activity is evaluated by studying its ability to oxidize peroxidase colourimetric substrate TMB and determining kinetics parameters. The activity unit (U) is defined as the amount of enzyme that catalyzes 1 µmol of product per minute. The specific activity (SA, U $mg^{-1}$) is defined as activity units per milligram of the enzyme. First, solutions of known HRP concentration (5 ng/ml, 10 ng/ml, 20 ng/ml, 30 ng/ml) are prepared in MES buffer. A 96-well plate is used for the absorbance reading filling the wells with up to 200 µL of HRP solutions. 50 µL of TMB working reagents are introduced in each well and absorbance values are measured at the

plate reader at 652 nm every 20 seconds. So, for each solution, a kinetics curve of Abs against time is obtained and reported below (Figure 2). In the first part of the curve, absorbance variations are approximately linear to the reaction times. The value of the slope in the initial rate period (ΔA/Δt) of the enzyme reaction is constant and represents the substrate µmol processed per minute (U).

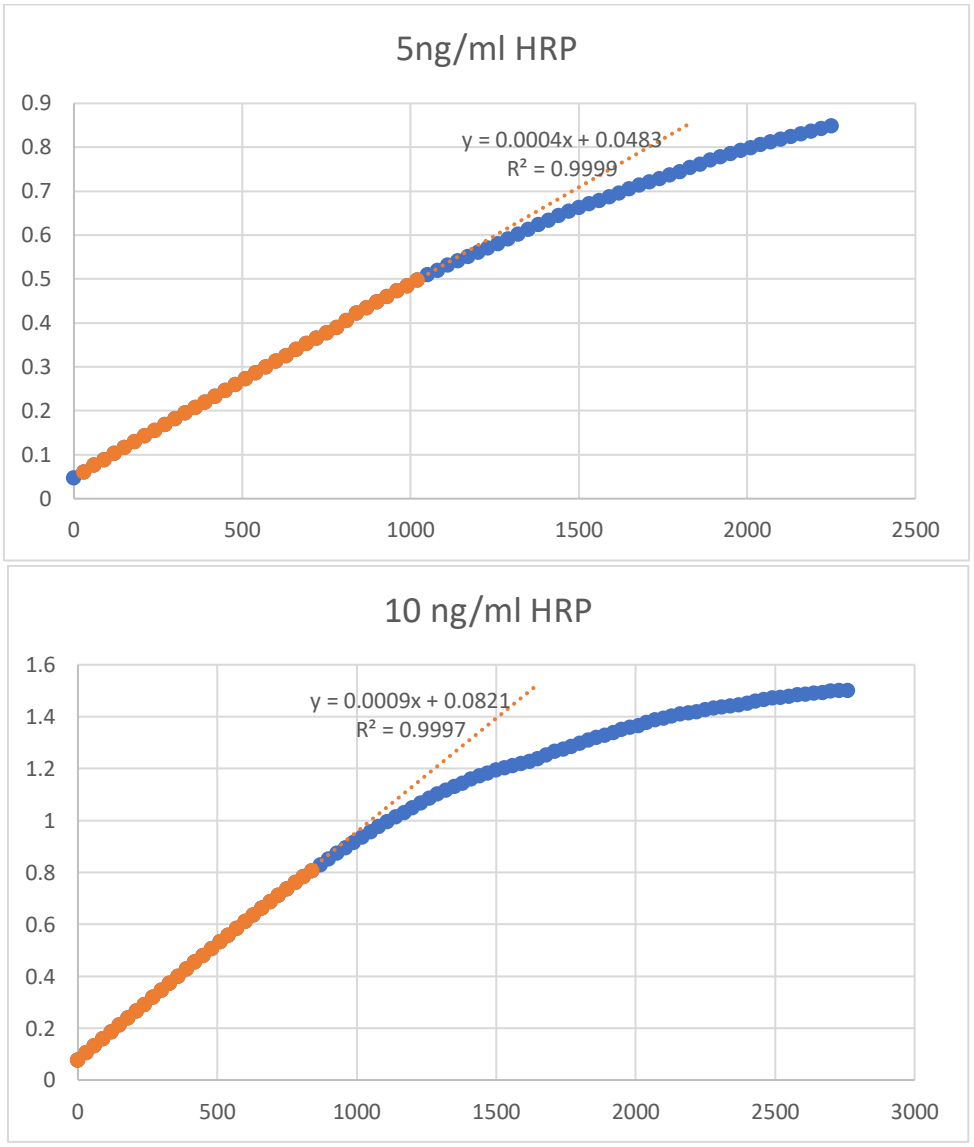

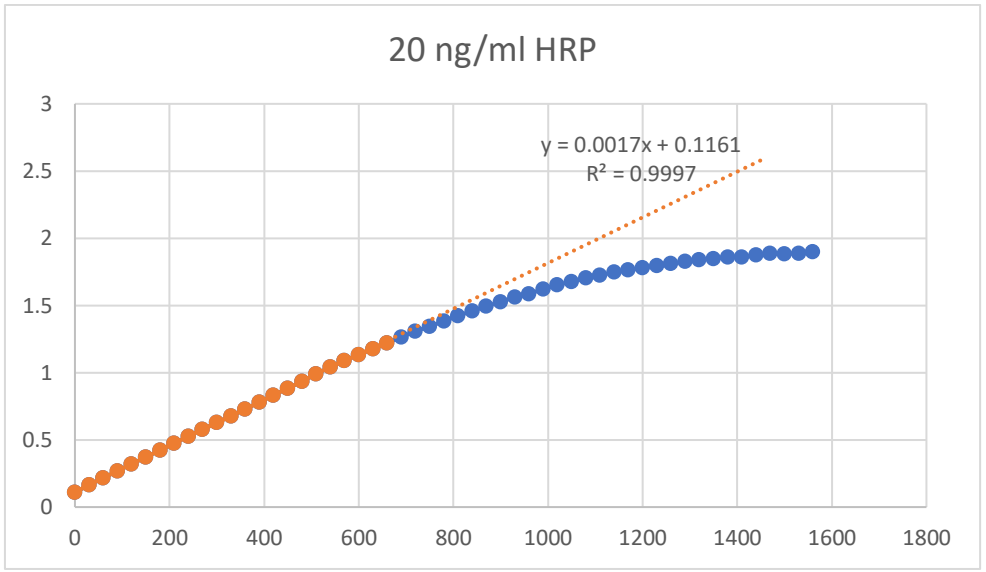


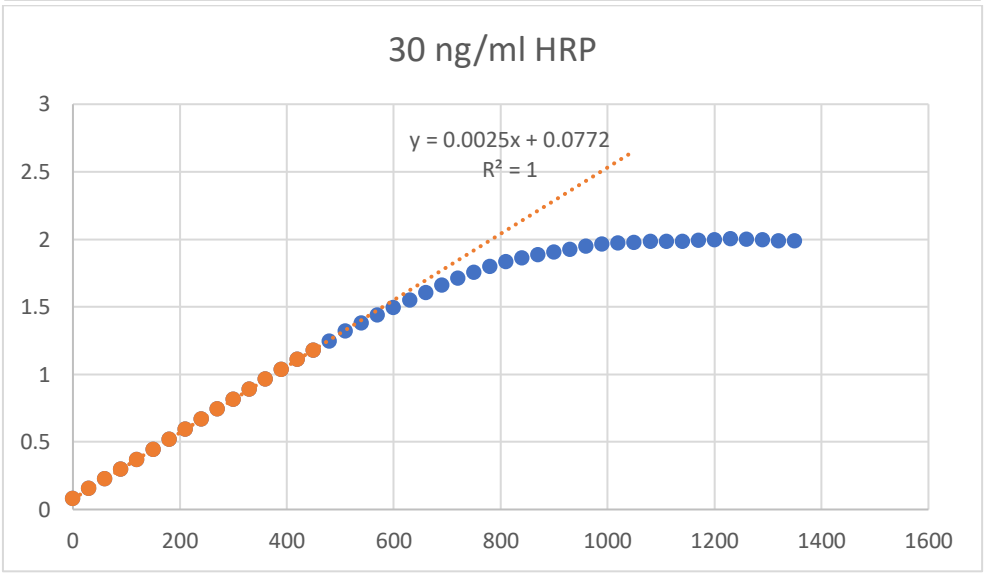


**Figure 2**: Kinetics curve of Abs against time for each HRP concentration. Absorbance variations are approximately linear to the reaction times in the first part of the curve (in orange). The value of the slope in the initial rate period (ΔA/Δt) of the enzyme reaction represents the substrate µmol processed per minute (U).

The slope values ΔA/Δt of each kinetic curve are used to calculate the enzyme activity U by using the following equation:

$$U = \left[\frac{V}{\varepsilon/l}\right] * \left(\frac{\Delta A}{\Delta t}\right)$$

In which V is the total volume of reaction solution (µL); ε is the molar absorption coefficient of the colourimetric substrate (39,000 $M^{-1}$ $cm^{-1}$ at 652 nm for TMB), l is the path length of light travelling in the cuvette (about 0.37 cm in this case) and ΔA/Δt is the initial rate of change in absorbance at 652 nm $min^{-1}$. The obtained U values are reported in table 3:

| HRP solutions concentration | Enzyme activity (U) |
|---|---|
| 5 ng/ml | 6.88E-06 |
| 10 ng/ml | 1.55E-05 |
| 20 ng/ml | 2.92E-05 |
| 30 ng/ml | 4.30E-05 |

**Table 3**: enzyme activity (U) for free HRP solutions.

The enzyme activity U increases as the HRP amount increases due to the higher amount of substrate processed by the enzyme.

After activity U determination, the specific activity (U/mg) is evaluated by plotting U values against milligrams of HRP assayed (Figure 3) and measuring the slope of the resultant straight line. As shown below, the specific activity was 7.19 U/mg.

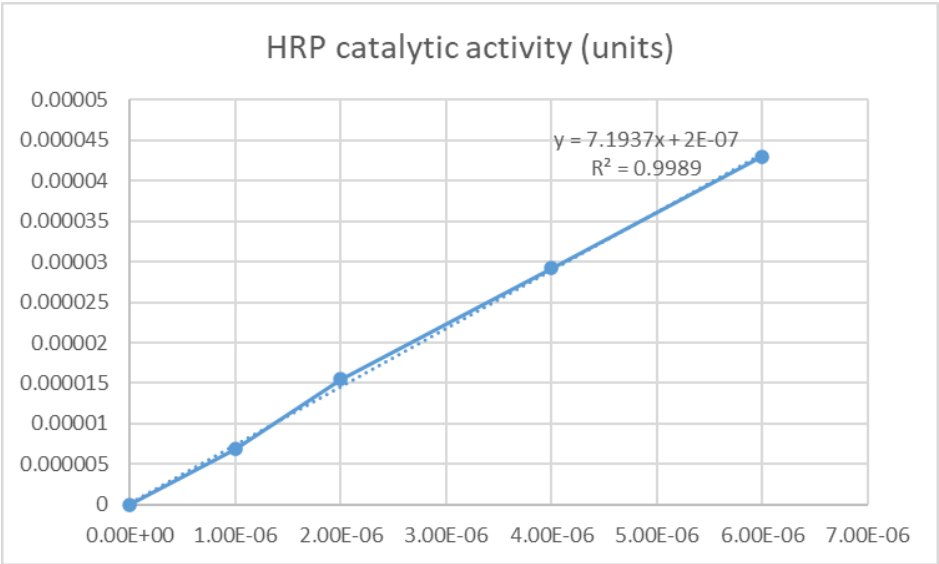


**Figure 3**: Plot of U values against the free HRP amount.

The same procedure is applied for the determination of HRP bound on microgels. Solutions of HRP-coated microgels are prepared in 0.2 mL of MES buffer by taking microgels aliquots of 0.5 µg, 1 µg, 2.5 µg, and 5 µg reaching final concentrations of 2.5 µg/ml, 5 µg/ml, 12.5 µg/ml and 25 µg/ml, respectively (Table 4). 50 µL of TMB working reagents are introduced in each well of the 96-well plate and absorbance values are measured at the plate reader at 562 nm every 20 seconds. The kinetics curves of Abs against time for each sample are reported below (Figure 4):

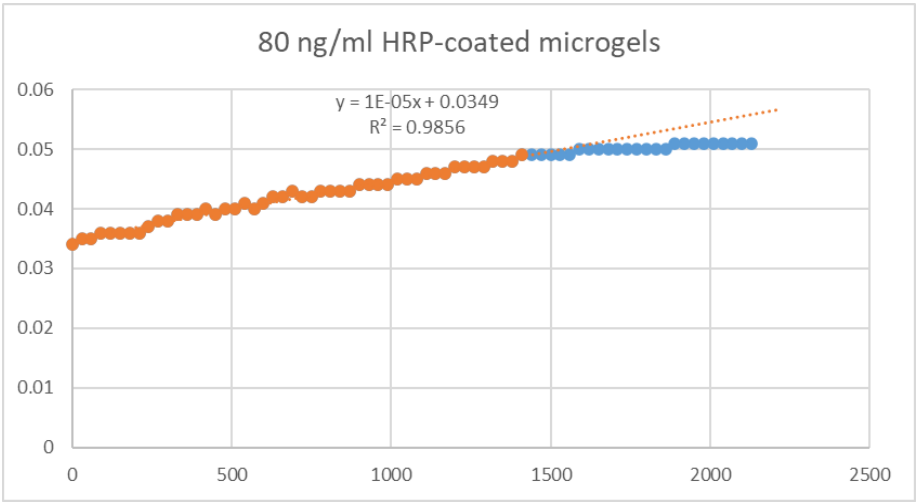


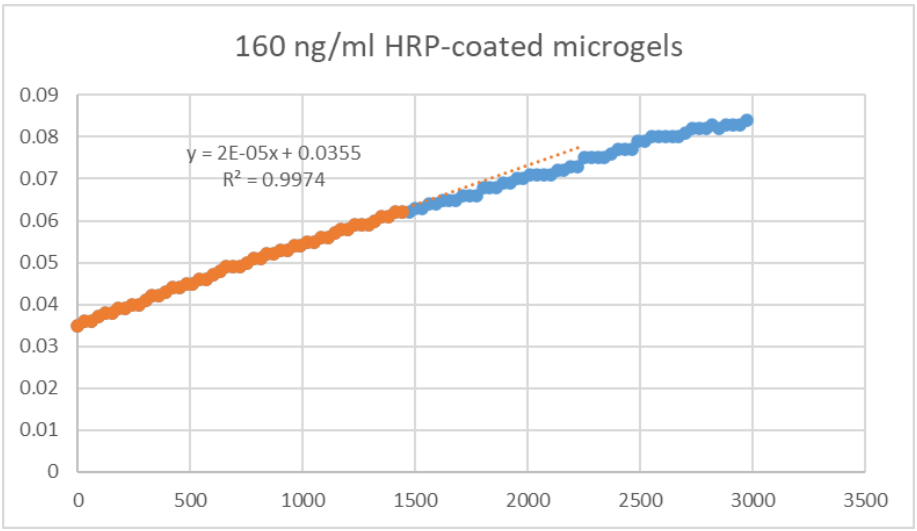

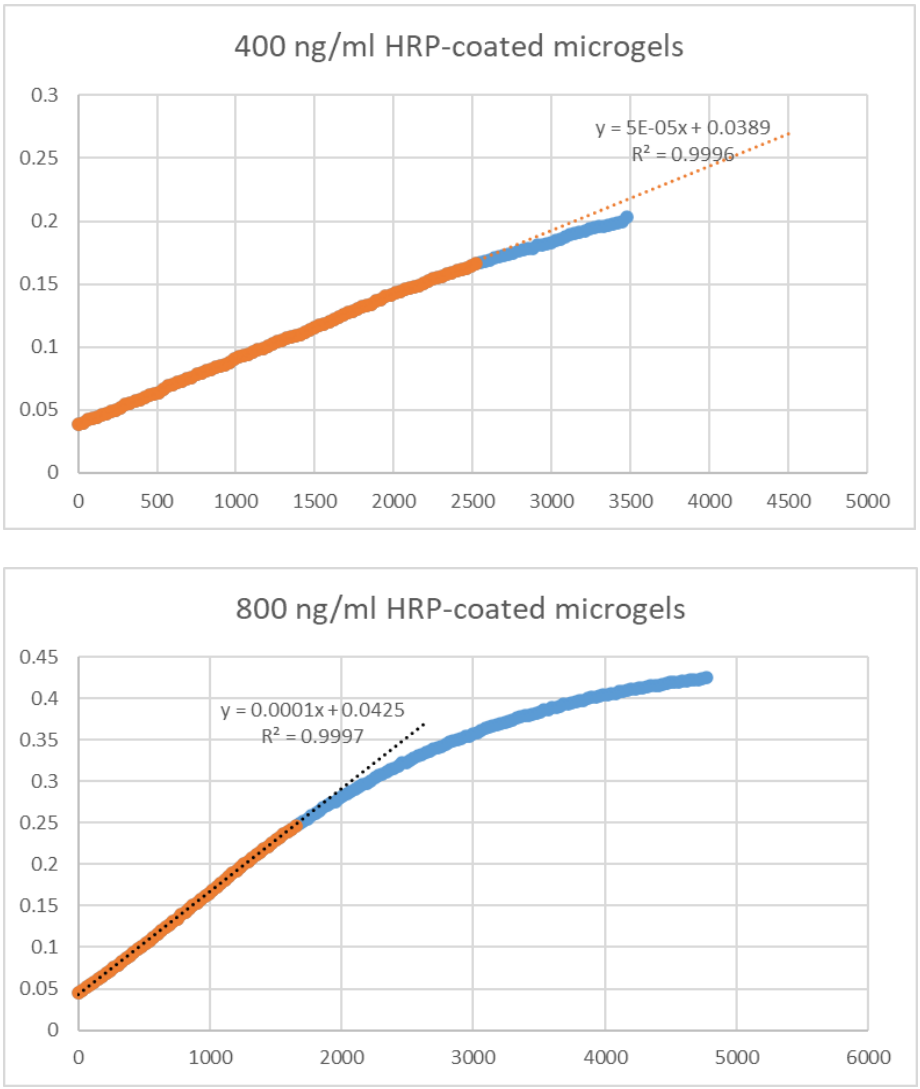


**Figure 4**: Kinetics curve of Abs against time for each HRP concentration. Absorbance variations are approximately linear to the reaction times in the first part of the curve (in orange). The value of the slope in the initial rate period (ΔA/Δt) of the enzyme reaction represents the substrate µmol processed per minute (U).

The slope values ΔA/Δt are used to calculate the enzyme activity U as in the previous case and reported in the following table:

| Microgels concentration | HRP solutions concentration | Enzyme activity (U) |
|---|---|---|
| 2.5 µg/mL | 80 ng/mL | 1.72E-07 |

| | | |
|---|---|---|
| 5 µg/mL | 160 ng/mL | 3.44E-07 |
| 12.5 µg/mL | 400 ng/mL | 8.60E-07 |
| 25 µg/mL | 800 ng/mL | 1.72E-06 |

**Table 4:** determination of enzyme activity (U) of bound HRP.

The specific activity (U/mg) is evaluated by plotting U values against milligrams of HRP assayed (Figure 5) and measuring the slope of the resultant straight line:

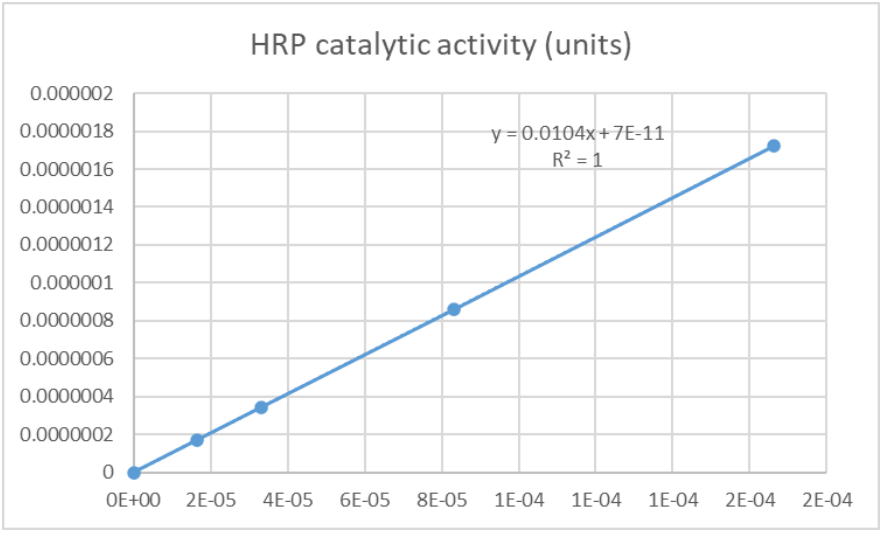


**Figure 5:** Plot of U values against HRP amount.

The SA value for bound HRP is 0.0104 U/mg, 10-fold smaller than the SA of free HRP. Based on these preliminary results, HRP activity decreases after the covalent bonding on microgels. This could be due to either a crowding effect on the microgels surface or a conformational modification of the enzyme during the coupling.

## MAGNETIC BEADS CHARACTERIZATION

Magnetic beads are characterized by spectroscopically acquiring the emission spectrum by confocal laser scanning microscopy. The spectrum shows an emission peak at 580 nm and doesn't overlap with emission peaks of rhodamine of microgels and Atto647N dye of antibodies.

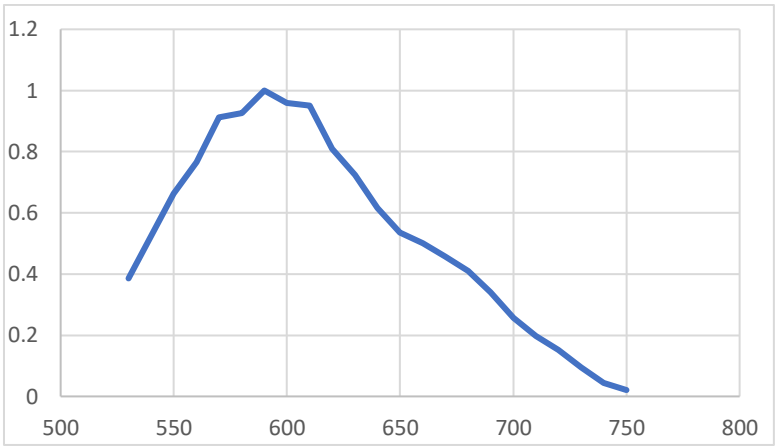


**Figure 6**: emission spectra of magnetic beads.

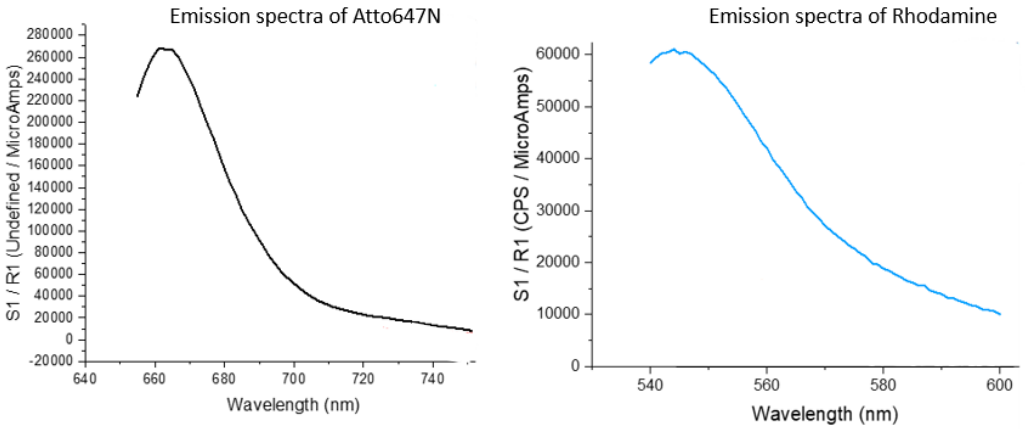


**Figure 7**: emission spectra of Atto647N dye and Rhodamine in microgels.

## FUNCTIONALIZATION OF MAGNETIC BEADS

The IgG/anti-IgG couple is chosen as a preliminary system to determine the feasibility of interaction between functionalized particles and magnetic beads.

The compatibility of antibodies with magnetic beads is evaluated by performing a coupling reaction with antibodies anti-IgG linked to a fluorescent dye Atto647N. Magnetic beads don't need a preliminary activation step of epoxy groups for the conjugation but only the mixing of biomolecules and beads. As reported in the datasheet of Dynabeads (Thermo Fisher Scientific), 500 µg of magnetic beads are suspended in MES buffer (25 nM, pH 6) and anti-IgG-Atto647N antibodies (5 µg) are added. The reaction is allowed to proceed overnight at room temperature. Magnetic beads are separated from the solution magnetically and the supernatant is discarded. Finally, 500 µl of PBS pH 8 (0.05% Tween, BSA 0.1%) is added to a final

concentration of 1 mg/ml and stored at 4°C for further use. The functionalization of beads is imaged by confocal laser scanning microscopy showing a fluorescent signal due to the Atto-647N dye of the antibodies. The images showed a 647N fluorescent signal on beads due to the positive results of the coupling.

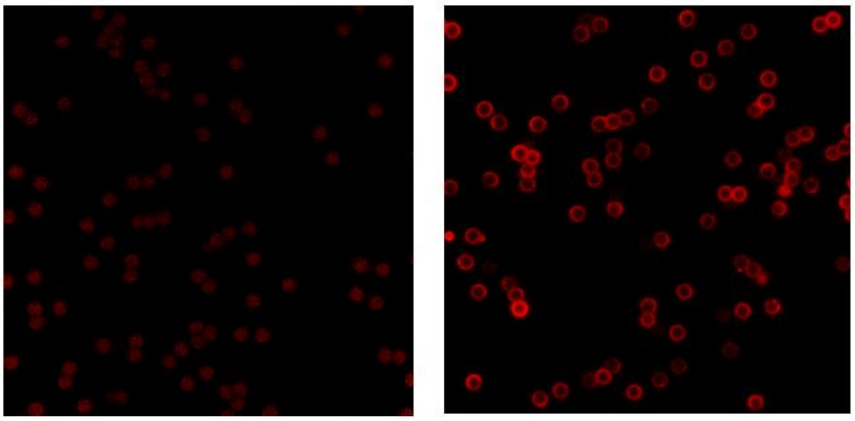

**Figure 8**: CLSM images of magnetic beads before functionalization (left) and magnetic beads after functionalization with anti-IgG-Atto647N (right).

## MICROGELS/BEADS INTERACTIONS

To determine the possibility of interaction between microgels and magnetic beads, I have functionalized microgels (250 µg) with 10 µg of anti-IgG-Atto647N antibodies and magnetic beads (500 µg) with 5 µg of IgG antibodies. Then, the resulting magnetic beads and microgels are put in contact with different concentration ratios to perform interactions. The ratios of microgels and beads are:

| Microgels | Magnetic beads |
|---|---|
| 10^7 | 10^6 |
| 10^8 | 10^6 |
| 10^9 | 10^6 |

**Table 5**: beads/microgels ratio used for interaction attempts.

Beads and microgels in 50 µL of PBS buffer (pH 8, 0,1% BSA, 0.05% Tween) are allowed to interact overnight at room temperature. Then, the magnetic separation is performed and pellets containing clusters are recovered. Confocal laser scanning images are acquired for each sample showing that interaction occurs due to the binding of IgG and anti-IgG. Microgels have a size smaller than magnetic beads, so they surrounded the bead surface and, in some cases, form clusters among more beads.

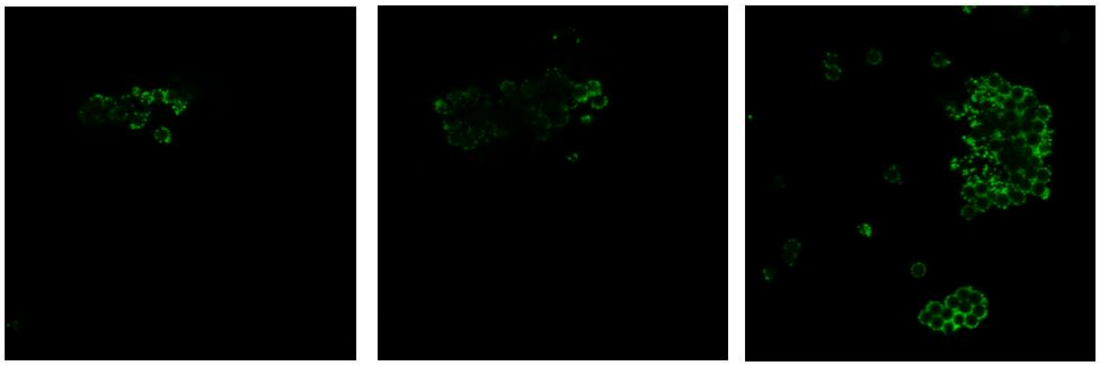

**Figure 9**: Images of interaction between magnetic particles and microgels. The green colour corresponds to the Atto647N channel. 10^7:10^6 ratio of microgels/beads (on the left), 10^8:10^6 ratio of microgels/beads (in the centre) and 10^9:10^6 ratio of microgels/beads (on the right).

As shown, an increasing amount of microgels results in clusters of higher area, thus, the 10^9:10^6 microgels/beads ratio is chosen to perform further experiments.

## ASSAY SET-UP OPTIMIZATION

Microgels (250 µg) are functionalized with 10 µg of anti-Fab antibodies and 1 mg of HRP enzyme. Magnetic beads (500 µg) are functionalized with 5 µg of anti-Fc antibodies. Human IgG linked to the Atto647N dye is used to prove the specific binding with anti-Fab and anti-Fc antibodies.

Anti-Fc beads (15 µL, 10^6 beads) in PBS buffer (pH 8, 0,1% BSA, 0.05% Tween) are mixed with 2 µg of human IgG-Atto647N. Anti-Fab-HRP-microgels (11 µL, 2.2x10^9 microgels) in PBS buffer (pH 8, 0,1% BSA, 0.05% Tween) are mixed with 2 µg of human IgG-Atto647N. Particles are allowed to react with the antibodies overnight. Images of both samples are acquired by CLSM and compared to images of the control samples.

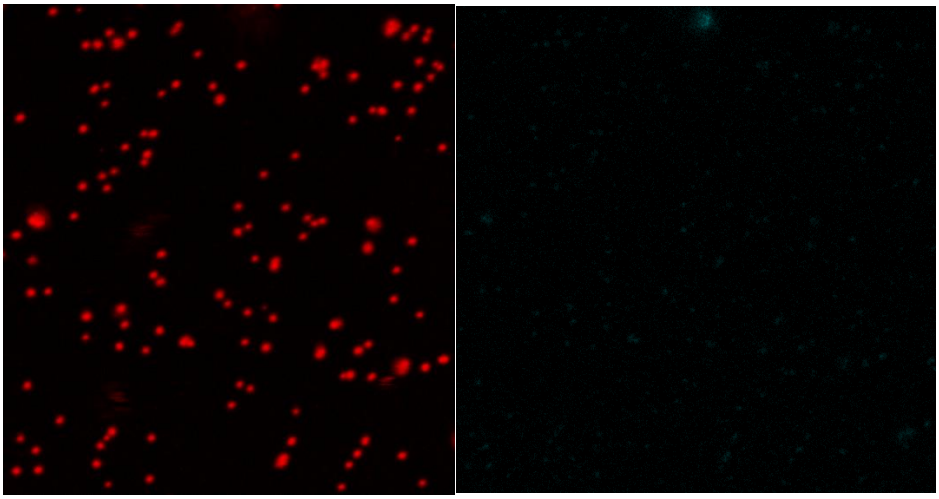

**Figure 10**: control sample of microgels without target (on the left, rhodamine channel, on the right, Atto647N channel)

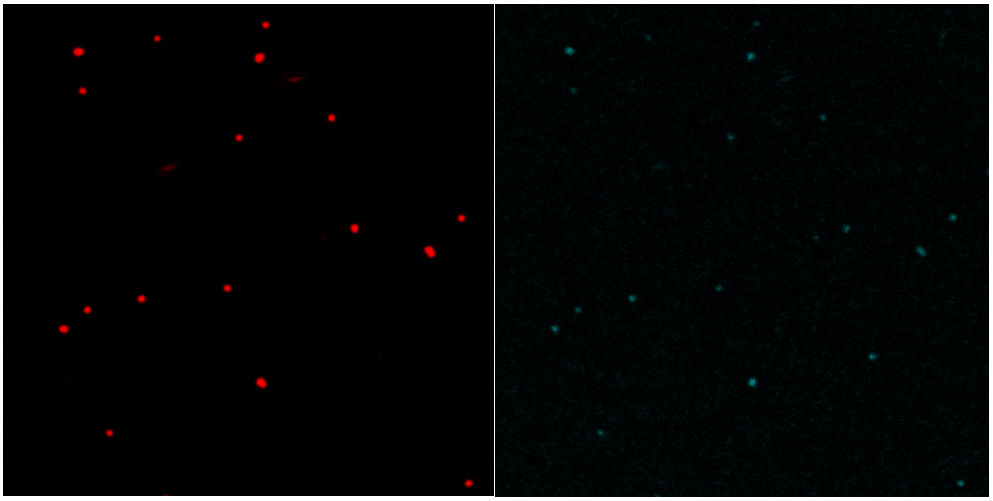

**Figure 11**: interaction of microgels with the target (on the left, rhodamine channel, on the right, Atto647N channel)

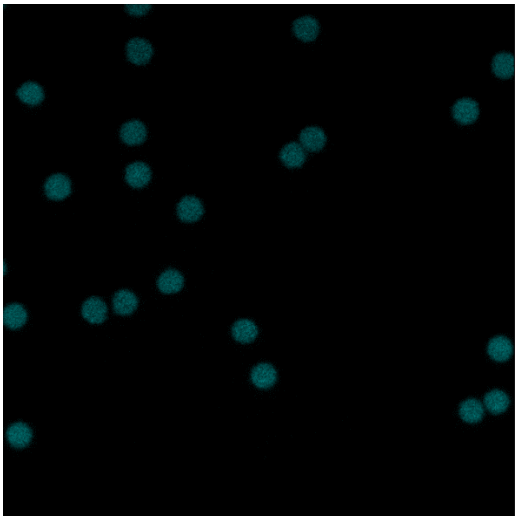

**Figure 12**: control sample of beads without target (Atto647N channel)

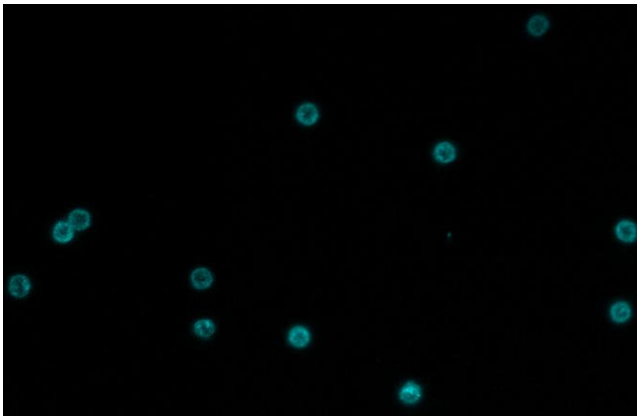

**Figure 13**: Interaction of beads with the target (Atto647N channel)

Both for microgels and beads, the interaction with human IgG-atto647N antibodies has a positive response. Comparing the Atto647N channel of the control sample to the interaction sample images, it's visible that the emission signal is higher in presence of the target. Thus, the specific binding of anti-Fab and anti-Fc antibodies with human IgG occurs.

# CHAPTER 4

## CONCLUSIONS

Throughout this thesis, we have tested the microgel-based platform, which has proved to be attractive for biosensing applications. The microgels-based platform is composed of multifunctional particles which possess multiple properties. The chemical flexibility of hydrogel microparticles and microgels allows the embedding of several building blocks into their structure during the synthesis. The high biocompatibility and antifouling properties of hydrogel make possible the employing of the microgels-based platform in biosensing and inspired the development of several sophisticated applications, such as biosensors. Core R1-COOH, bulk and surface, and two Core-R1 AMPS are produced. They are synthesized by keeping the synthesis process constant, adding chemicals at different moments and varying their nature. The obtained microgels solutions are monodisperse and have uniform size and fluorescence distributions. The acrylic acid monomer is introduced into the reactor at different moments during the reaction synthesis and different products are obtained. Comparing the first two types of particles, the Core R1-COOH bulk presents a diameter of 760±16.1 nm, higher than the Core R1-COOH surface. On the other hand, the surface particles have a slightly more negative charge than bulk microgels, probably due to the confinement of Aac on the outer shell of microgels. Furthermore, the cores R1-AMPS are produced by introducing an additional monomer (AMPS) resulting in microgels with different properties. Core R1-AMPS 0.1 and core R1-AMPS 1 differ in the amount of AMPS. The presence of AMPS produces microgels with a higher surface charge than the previous ones. Increasing the AMPS amount, Core R1-AMPS 1 presents a more negative charge than Core R1-AMPS 0,1 and core R1-COOH. Core R1-AMPS 1 presents particles number per milligram an order of magnitude smaller than the other microgels. The core R1-AMPS shows a smaller size than the core R1-COOH particles. The surface charge of the R1-AMPS 1 microgels is more negative than the other microgels. The presence of the AMPS allows for maintaining a more negative charge at pH 3 compared to cores R1-COOH, where a charge close to 0 is displayed. At high pH values, the deprotonation of the carboxylic groups results in a repulsive force between them causing the swelling particles. This effect is greater for the core R1-COOH bulk in which Aac polymerizes with PEGDMA as soon as the

reaction begins. In this way, COOH groups are present both on the surface and in the bulk of particles. In conclusion, the presented process can be modified according to the properties of microgels to confer, avoiding more complex structures such as core/shell particles.

Microgels are used to develop an innovative immunoassay for the detection of new biomarkers such as antibodies. Core microgels with Rhodamine dye as an optical barcode are adopted as the carrier of both anti-Fab antibodies and the HRP enzyme. Magnetic particles functionalized with anti-Fc antibodies are involved as capture particles. When the target antigen IgG is present, the two antibodies used can form a sandwich structure capturing the target. A double detection system is involved: the supernatant containing unbound microgels is analyzed by a colourimetric assay and the pellet containing clusters is analyzed by a confocal laser scanning microscope (CLSM). A wide working range of human IgG targets is explored from 0.28 nM to 2.8 µM. The area of clusters formed among beads and microgels increases from 91.25±4.03 $\mu m^2$ for the control sample in absence of the target to 1066.4±131.1 $\mu m^2$ for 2.8 µM of the target. The minimum target amount distinguishable from the background noise has a concentration of 0.28 nM. The assay is carried on in the presence of an interference protein, BSA, showing a good selectivity toward the target and the microgels are capable to detect the target even in presence of crowded protein solutions.

Single-entity detection approaches and miniaturized structures are increasingly spreading to overcome the limits linked to sensitivity. The flexibility of the microgels-based platform allows for decreasing the number of particles involved in the assay. The application of the single-entity method and the use of microfluidic devices can lead to the development of bioassays characterized by ultrahigh sensitivity.

# REFERENCES


[1]Peppas, N.A.; Bures, P.; Leobandung, W.; Ichikawa, H. *Eur. J. Pharm. Biopharm.* **2000**, *50*, 27–46.

[2]Hoare, T.; Pelton, R. *J. Phys. Chem. B* **2007**, *111*, 11895–11906.

[3]Le Goff, G. C.; Srinivas, R. L.; Hill, W. A.; Doyle, P. S. *Eur. Polym. J.* **2015**, *72*, 386–412.

[4]Peppas, N. A., Hilt, J. Z., Khademhosseini, A. & Langer, R. *Adv. Mater*. **2006**, *18*, 1345–1360.

[5]Caló, E. & Khutoryanskiy, V. V. *Eur. Polym. J.* **2015**, *65*, 252–267.

[6]Li, J. & Mooney, D. J. *Nat. Rev. Mater.* **2016**, *1*, 16071.

[7]Van Vlierberghe, S., Dubruel, P. & Schacht, E. *Biomacromolecules* **2011**, *12*, 1387–1408.

[8]Jagur-Grodzinski, J. *Polym. Adv. Technol*. **2010**, *21*, 27–47.

[9]Zalipsky, S., Harris, J. M. *ACS Symposium Series*, **1997**, *680*, 1-13.

[10]Peppas, N. A., Hilt, J. Z., Khademhosseini, A.; Langer, R. *Adv. Mater.*, **2006**, *18*, 1345–1360.

[11]Caló, E.; Khutoryanskiy, V. V. *Eur. Polym. J.* **2015**, *65*, 252–267.

[12]Battista, E.; Mazzarotta, A.; Causa, F.; Cusano, A., M.; Netti, P., A. *Polym. Int.* **2016**, *65*, 747–755.

[13]Causa, F.; Aliberti, A.; Cusano, A., M.; Battista, E.; Netti, P., A. *J. Am. Chem. Soc.* **2015**, *137*, 1758–1761.

[14]Aliberti, A.; Cusano, A., M.; Battista, E.; Causa, F.; Netti, P., A. *Analyst*. **2016**, *141*, 1250–1256.

[15]Xia, F.; Jiang, L. *Adv. Mater.* **2008**, *20*, 2842–2858.

[16]Heida, T.; Neubauer, J. W.; Seuss, M.; Hauck, N.; Thiele, J.; Fery, A., *Macromolecular Chemistry and Physics* **2017**, 218 (2)

[17]Zhu, P.; Wang, L.. *Lab on a Chip* **2017**, 17 (1), 34-75.

[18]Pregibon, D. C.; Toner, M.; Doyle, P. S., Science **2007**, *315* (5817), 1393-1396.

[19]Appleyard, D. C.; Chapin, S. C.; Srinivas, R. L.; Doyle, P. S., *Nature protocols* **2011**, 6 (11), 1761.

[20]Pregibon, D. C.; Toner, M.; Doyle, P. S. *Science*. **2007**, *315*, 1393-1395.

[21]Amalvy, J.; Wanless, E.; Li, Y.; Michailidou, V.; Armes, S.; Duccini, Y. *Langmuir* **2004**, 20 (21), 8992-8999.

[22]Wild, D. *The Immunoassay Handbook*. **2013**.

[23]Goldsby, R., A.; Kindt, T., J.; Osborne, B., A. *Kuby's Immunology*. **2000**.

[24]Koivunen, M., E.; Krogsrud, R., L. *Laboratory Medicine*. **2006,** *8*, 490-497.

[25]Zhang, H.; Williams, P., S.; Zborowski, M.; Chalmers, J., J. *Biotechnol Bioeng.* **2006**, *95*(5), 812-29.

[26]Ekins, R.; Edwards, P. *Clin Chem*. **1997**, *43*, 1824–1837.
[27]Findlay, J., W.; Smith, W., C.; Lee, J., W.; Nordblom, G., D.; Das, I.; DeSilva, B., S.; Khan, M., N.; Bowsher, R., R. *J Pharm Biomed Anal.* **2000**, *21*(6), 1249-1273.
[28]Li, J.; Li, L.; Bian, Y.; Yu. Y.; Qiang, Z.; Zhang, Y.; Li, H. *J Clin Lab Anal.* **2020,** *34,* 23014
[29]Darwish, I., A.; Blake, D., A. *Anal. Chem*. **2001**, *73*, 1889-1895.
[30]Darwish, I., A. *Int J Biomed Sci*. **2006**, *2*, 217-235.
[31]Wang, X.; Cohen, L.; Wang, J.; Walt, D., R. *J. Am. Chem. Soc.* **2018**, *140*, 18132-18139.
[32]Yagisawa, S.; Tanimori, H.; Kitagawa, T. *J. Biochem.* **1986**, *99*, 793-802.
[33]Li, J.; Li, L.; Bian, Y.; Yu, Y.; Qiang, Z.; Zhang, Y.; Li, H. *Journal of Clinical Laboratory Analysis*. **2020**, *34*(1), 23014.
[34]Ngo, T. *Analytical Letters.* **2005**, *38*, 1057-1069.3
[35]Tabatabaei, M., S.; Islam, R.; Ahmed, M. *Analytica Chimica Acta*, **2020**.
[36]Elshal, M., F.; Mccoy, J. P. *Methods*. **2006**, *38*, 317–323.
[37]Gan, S., D.; Patel, K., R. *J. Invest. Dermatol.* **2013**, *133*.
[38]Appleyard, D., C.; Chapin, S., C.; Srinivas, R., T.; Doyle, P., S. *Nature Protocols*. **2011**, *6*, 1761-1774.
[39]Lee, W.; Choi, D.; Kim, J.; Koh, W. *Biomed Microdevices.* **2008**, *10*, 813-822.
[40]Wilson, R.; Cossins, A., R.; Spiller, D., G. *Angew. Chem. Int. Ed. Engl.* **2006**, *45*, 6104-6117.
[41]Pang, S.; Smith, J.; Onley, D.; Reeve, J.; Walker, M.; Foy, C. *J. Immunol. Methods.* **2005**, *302*, 253.
[42]Liao, T.; Yuan, F.; Yub, H.; Li, Z. *Anal. Methods*. **2016**, *8*, 1577.
[43]Daniel Geibler, D.; Charbonniere, L., J.; Ziessel, R., F.; Butlin, N., G.; Lohmannsroben, H.; Hildebrandt, N. *Angew. Chem. Int. Ed.* **2010**, *49*, 1396-1401.
[44]Birtwell, S.; Morgan, H. *Integr. Biol*. **2009**, *1*, 345-362.
[45]Ven, K.; Vanspauwen, B.; Perez-Ruiz,́ E.; Leirs, K.; Decrop, D.; Gerstmans, H.; Spasic, D.; Lammertyn, J. *ACS Sens*. **2018**, *3*, 264−284.
[46]Rissin, D., M.; Walt, D., R. *Nano Lett.* **2006**, *6*, 520–523.
[47]Rissin, D., M.; Walt, D., R. *J. Am. Chem. Soc.* **2006**, *128*, 6286–6287.
[48]Rissin, D., M.; Gorris, H., H.; Walt, D., R. *J. Am. Chem. Soc.* **2008**, *130*, 5349–5353.
[49]Rissin, D., M.; Kan, C., W.; Campbell, T., G.; Howes, S., C.; Fournier, D., R.; Song, L.; Piech, T.; Pate, P., P.; Chang, L.; Rivnak, A., J.; Ferrell, E., P.; Randall, J., D.; Provuncher, G., K.; Walt, D., R.; Duffy, D., C. *Nat Biotechnol.* **2010**, *28*(6), 595-599.
[50]Rissin, D., M.; Fournier, D., R.; Piech, T.; Kan, C., W.; Campbell, T., G.; Song, L.; Chang, L.; Rivnak, A., J.; Patel, P., P.; Provuncher, G., K.; Ferrell, E., P., Howes, S., C.; Pink, B., A.; Minnehan, K., A.; Wilson, D., H.; Duffy, D., C. *Anal Chem.* **2011**, *83*(6), 2279-85.
[51]Yagisawa, S.; Tanimori, H.; Kitagawa, T. *J. Biochem.* **1986**, *99*, 793-802.

[52]Li, J.; Li, L.; Bian, Y.; Yu, Y.; Qiang, Z.; Zhang, Y.; Li, H. *Journal of Clinical Laboratory Analysis*. **2020**, *34*(1), 23014.
[53]Ngo, T. *Analytical Letters.* **2005**, *38*, 1057-1069.
[54]Geibler, D.; Charbonniere, L., J.; Ziessel, R., F.; Butlin, N., G.; Lohmannsroben, H.; Hildebrandt, N. *Angew. Chem. Int. Ed.* **2010**, *49*, 1396-1401.
[55]Birtwell, S.; Morgan, H. *Integr. Biol*. **2009**, *1*, 345-362.
[56]http://www.luminexcorp.com/technology/index.html.
[57]Hu, L.; Zhang, C.; Zeng, G.; Chen, G.; Wan, J.; Guo, Z.; Wu, H.; Yu, Z.; Zhou, Y.; Liu, J. *RSC Adv.* **2016**, *6*, 78595.
[58]Zhao, Y.; Shum, H., C.; Chen, H.; Adams, L., A.; Gu, Z.; Weitz, D., A. *J. Am. Chem. Soc.* **2011**, *133*, 8790-8793.
[59]Han, M.; Gao, X.; Su, J., Z.; Nie, S. *Nat Biotechnol.* **2001**, *19*, 631-635.
[60]Peppas, N., A.; Bures, P.; Leobandung, W.; Ichikawa, H. *Eur. J. Pharm. Biopharm.* **2000**, *50*, 27–46.
[61]Le Goff, G., C.; Srinivas, R., L.; Hill, W., A.; Doyle, P., S. *Eur. Polym. J.* **2015**, *72*, 386–412.
[62]Langer, R.; Tirrell, D., A. *Nature*. **2004**; *428*(6982), 487-492.
[63]Koeller, K.; Wong, C., H. *Nature*. **2001**, *409*, 232–240.
[64]A.A. Desa. *Angew Chem* **2011**, *50*, 1974-1976.
[65] Meghwanshi, G. K.; Kaur, N.; Verma, S.; Dabi, N. K.; Vashishtha, A.; Charan, P. D.; Purohit, P.; Bhandari, H. S.; Bhojak, N.; Kumar, R. *Biotechnol Appl Biochem.* **2020**, 67, 586-601.
[66]Choi, J.; Han, S.; Kim, H. *Biotechnology Advances.* **2015**, *33*, 1443-1454.
[67]Kucherlapati, M.; Yang, K.; Kuraguchi, M.; Zhao, J.; Lia, M.; Heyer, J.; Kane, M. F.; Fan, K.; Russell, R.; Brown, A. M.; Kneitz, B.; Edelmann, W.; Kolodner, R. D.; Lipkin, M.; Kucherlapati, R. *Proc Natl Acad Sci* USA. **2002**, *99*, 9924-9.
[68] Steiner, M.; Duerkopa. A.; Wolfbeis, O., S. *Chem. Soc. Rev.* **2011**, *40*, 4805-4839.
[69]Soldà, A.; Valenti, G.; Marcaccio, M.; Giorgio, M.; Pelicci, P.; Paolucci, F.; Rapino. S. *ACS Sensors* **2017**, *2* (9), 1310-1318
[70]Deng, Y., Miyake, T., Keene, S. et al. *Sci Rep* **2016**, *6*, 24080.
[71]Chen, L.; Lyubimov, A. Y.; Brammer, L.; Vrielink, A.; Sampson, N. S. *Biochemistry*. **2008**, 47,5368-77.
[72]Takeda, K.; Kusuoka, R.; Inukai, M.; Igarashi, K.; Ohno, H.; Nakamura, N. *Biosensors and Bioelectronics*. **2021**, *174*, 112831.
[73] Abdolrahim, M.: Rabiee, M.; Alhosseini, S. N.; Tahriri, M.; Yazdanpanah, S.; Tayebi, L. *Analytical biochemistry*. **2015**, *485*, 1-10.
[74]Rena, C.; Wena, X.; Menciusa, J.; Quan, S. PNAS, **2021**, *118*.
[75]Quintanilla-Villanueva, G. E. et al. *Biosensors* **2021**, *11*(2), 43.
[76]Kulkarni, S. J.; Karve, M. S. *SN Appl. Sci.* **2020**, *2*, 1118.

[77]Zhang, J.; Mai, X.; Hong, X.; Chen, Y.; Li, X. *Sensors and Actuators B: Chemical* **2022**, *366*, 131984,
[78]Ma, L., Abugalyon, Y.; Li, X. *Anal Bioanal Chem* **2021**, *413*, 4655–4663.
[79]Homaei, A., A.; Sariri, R.; Vianello, F.; Stevanato, R. *J Chem Biol.* **2013**, *6*, 185-205.
[80]Mateo, C.; Palomo, J. M.; Fernandez-Lorente, G.; Guisan, J. M.; Fernandez-Lafuente, R. *Enzyme Microb. Technol.* **2007**, *40*, 1451–1463.
[81]Hanefeld, U.; Gardossib, L.; Magnerc, E. *Chem. Soc. Rev*. **2009**, *38*, 453–468.
[82]Kazenwadel, F.; Wagner, H.; Rapp, B. E.; Franzreb, M. *Anal. Methods.* **2015**, *7*, 10291.
[83]Phiri, M. M.; Mulder, D. W.; Mason, S.; Vorster, B. C. *R. Soc. open sci.* **2019**, *6,* 190205.
[84]Li, D.; He, Q.; Cui, Y.; Duan, L.; Li, J. *Biochem. Biophys. Res. Commun.* **2007**, *355*, 488– 493.
[85]Cao, J.; Xu, J.; Liu, X.; Wang, S.; Peng, L. *Journal of Chromatography A*. **2016**, *1468*, 86-94.
[86]Jiang, B.; Duan, D.; Gao, L. et al. *Nat Protoc*. **2018**, *13*, 1506–1520.
[87]Le Goff, G. C.; Srinivas, R. L.; Hill, W. A.; Doyle, P. S. *Eur. Polym. J.* **2015**, *72*, 386–412.
[88]Zalipsky, S., Harris, J. M. *ACS Symposium Series*, **1997**, *680*, 1-13.
[89]Peppas, N. A., Hilt, J. Z., Khademhosseini, A.; Langer, R. *Adv. Mater.*, **2006**, *18*, 1345–1360.
[90]Caló, E.; Khutoryanskiy, V. V. *Eur. Polym. J.* **2015**, *65*, 252–267.
[91]Su, S.; Ali, M. M.; Filipe, C. D. M.; Li, Y.; Pelton, R. *Biomacromolecules*. **2008**, *9*, 935–94.
[92]Dios, A., S.; Díaz-García, M. E. *Analytica Chimica Acta*, **2010**, *666*, 1–22.
[93]Seleci, M.; Seleci, D., Joncyzk, R.; Stahl, F.; Blume, C.; Scheper, T. *BioNanoMaterials*, **2016**, *17*, 33-41.
[94]Battista, E.; Mazzarotta, A.; Causa, F.; Cusano, A., M.; Netti, P., A. *Polym. Int.* **2016**, *65*, 747–755.
[95]Pregibon, D. C.; Toner, M.; Doyle, P. S. *Science*. **2007**, *315*, 1393-1395.
[96]Battista, E., Causa, F.; Netti, P. *Gels,* **2017**, *3*, 20.
[97]Sabadasch, V.; Dirksen, M.; Fandrich, P.; Hellweg, T. *Front Chem.* **2022**, 10, 889521.
[98]Appleyard, D. C., Chapin, S. C., Srinivas, R. L.; Doyle, P. S. *Nat. Protoc.* **2011**, *6*, 1761–1774.
[99]Reinicke, S.; Fischer, T.; Bramski, J.; Pietruszka, J.; Boker, A. *RSC Adv.* **2019**, *9*, 28377.
[100]Tehrani, S. M.; Lu, Y.; Winnik, M. A. *Macromolecules* **2016**, *49*, 8711–8721.
[101]Choi, N. W.; Kim, J.; Chapin, S.; Duong, T.; Donohue, E.; Pandey, P.; Broom, W.; Hill, W. A.; Doyle, P. S. *Anal. Chem.* **2012**, *84*, 9370–9378.

[102]Srinivas, R. L., Chapin, S. C.; Doyle, P. S. *Anal. Chem.* **2011**, *83*, 9138–9145.
[103]Causa, F.; Aliberti, A.; Cusano, A., M.; Battista, E.; Netti, P., A. *J. Am. Chem. Soc.* **2015**, *137*, 1758–1761.
[104]Aliberti, A.; Cusano, A., M.; Battista, E.; Causa, F.; Netti, P., A. *Analyst*. **2016**, *141*, 1250–1256.
[105]Roh, Y.; Lee, H.; Kim, J.; Kim, H.; Kim, S.; Bong, K. *Lab Chip*, **2020**, *20*, 2841.
[106]Roh, Y.; Lee, H.; Kim, J.; Kim, H.; Kim, S.; Bong, K. *Lab Chip*, **2019**, *19*, 111.
[107]A. B. Lowe, *Polym. Chem*., **2010**, *1*, 17.
[108]Le Goff, G., C.; Srinivas, R., L.; Hill, W., A.; Doyle, P., S. *Eur. Polym. J.* **2015**, *72*, 386–412.
[109]Langer, R.; Tirrell, D., A. *Nature*. **2004**; *428*(6982), 487-492.
[110]Caputo, T., M.; Cummaro, T.; Lettera, V.; Mazzarotta, A.; Battista, E.; Netti, P., A.; Causa, F. *Analyst*. **2019**, ***144***, 1369-1378.
[111]Cohen, L.; Cui, N.; Cai, Y.; Garden, P. M.; Li, X.; Weitz, D. A.; Walt, D. R. *ACS Nano* **2020**, *14*, 9491−9501.
[112]Rissin, D., M.; Fournier, D., R.; Piech, T.; Kan, C., W.; Campbell, T., G.; Song, L.; Chang, L.; Rivnak, A., J.; Patel, P., P.; Provuncher, G., K.; Ferrell, E., P., Howes, S., C.; Pink, B., A.; Minnehan, K., A.; Wilson, D., H.; Duffy, D., C. Anal Chem. **2011**, *83*(6), 2279-85.
[113]Cohen, L.; Walt, D. R. *Bioconjugate Chem*. **2018**, *29*, 3452−3458.
[114]He, R.; Niu, Y.; Li, Z.; Li, A.; Yang, H.; Xu, F.; Li, F. *Adv Healthc Mater.* **2020**, 9, 1901201.
[115]Romeo, G.; Imperiali, L.; Kim, J.W.; Fernandez-Nieves, A.; Weitz, D.A. *J. Chem. Phys.* **2012**. 136(12), 124905.
[116]Sam, S.; Touahir, L.; Andresa, J. S.; Allongue, P.; Chazalviel, J. N.; Gouget-Laemmel, C.; Henry de Villeneuve, C.; Moraillon, A.; Ozanam, F.; Gabouze, N.; Djebbar, S. Lagmiur, **2010**, *26*(2), 809–814.
[117]Battista, E.; Mazzarotta, A.; Causa, F.; Cusano, A., M.; Netti, P., A. Polym. Int. 2016, 65, 747–755.
[118]Appleyard, D., C.; Chapin, S., C.; Srinivas, R., T.; Doyle, P., S. *Nature Protocols*. **2011**, *6*, 1761-1774.
[119]Wild, D. *The Immunoassay Handbook*. **2013**.
[120]Tabatabaei, M., S.; Islam, R.; Ahmed, M. *Analytica Chimica Acta,* **2020**.
[121]Smolsky, J.; Kaur, S.; Hayashi, C.; Batra, S. K.; Krasnoslobodtsev, A. *Biosensors*, *7*, **2017**.
[122]Liao, T.; Yuan, F.; Yub, H.; Li, Z. *Anal. Methods*. **2016**, *8*, 1577.
[123]Ven, K.; Vanspauwen, B.; Perez-Ruiz, E.; Leirs, K.; Decrop, D.; Gerstmans, H.; Spasic, D.; Lammertyn, J. *ACS Sens*. **2018**, *3*, 264−284.
[124]Rissin, D., M.; Walt, D., R. *J. Am. Chem. Soc.* **2006**, *128*, 6286–6287.
[125]Rissin, D., M.; Gorris, H., H.; Walt, D., R. *J. Am. Chem. Soc.* **2008**, *130*, 5349–5353.

[126]Rissin, D., M.; Kan, C., W.; Campbell, T., G.; Howes, S., C.; Fournier, D., R.; Song, L.; Piech, T.; Pate, P., P.; Chang, L.; Rivnak, A., J.; Ferrell, E., P.; Randall, J., D.; Provuncher, G., K.; Walt, D., R.; Duffy, D., C. *Nat Biotechnol.* **2010**, *28*(6), 595-599.
[127]Rissin, D., M.; Fournier, D., R.; Piech, T.; Kan, C., W.; Campbell, T., G.; Song, L.; Chang, L.; Rivnak, A., J.; Patel, P., P.; Provuncher, G., K.; Ferrell, E., P., Howes, S., C.; Pink, B., A.; Minnehan, K., A.; Wilson, D., H.; Duffy, D., C. *Anal Chem.* **2011**, *83*(6), 2279-85.
[128]Hanefeld, U.; Gardossi, L.; Magner, E. *Chem. Soc. Rev.* **2009**, *38*, 453–468.
[129]Kazenwadel, F.; Wagner, H.; Rapp, B., E.; Franzreb, M. *Anal. Methods*, **2015**, *7*, 10291.
[130]Hanefeld, U.; Gardossib, L.; Magnerc, E. *Chem. Soc. Rev.*, **2009**, *38*, 453–468.
[131]Yan, C.; Teng, J.; Liu, F.; Yao, B.; Xu, Z.; Yao, L.; Chen, W. *Microchemical Journal*. **2020**, *159*, 105414.
[132]Le Goff, G. C.; Srinivas, R. L.; Hill, W. A.; Doyle, P. S. *Eur. Polym. J.* **2015**, *72*, 386–412.
[133]Zalipsky, S., Harris, J. M. *ACS Symposium Series*, **1997**, *680*, 1-13.
[134]Peppas, N. A., Hilt, J. Z., Khademhosseini, A.; Langer, R. *Adv. Mater.*, **2006**, *18*, 1345–1360.
[135]Caló, E.; Khutoryanskiy, V. V. *Eur. Polym. J.* **2015**, *65*, 252–267.
[136]Su, S.; Ali, M. M.; Filipe, C. D. M.; Li, Y.; Pelton, R. *Biomacromolecules*. **2008**, *9*, 935–94.
[137]Han, D.; Goudeau, B.; Lapeyre, V.; Ravaine, V.; Jiang, D.; Fang, D.; Sojic, N. *Biosens. Bioelectron*, **2022**, 114640.
[138]Yang, Z.X.; Chen, B.A.; Wang, H.; Xia, G.H.; Cheng, J.; Pei, X.P.; Wang, F.; Bao, W. Handy, *Biosens. Bioelectron*. **2013**, 48, 153–157.
[139]Causa, F.; Aliberti, A.; Cusano, A., M.; Battista, E.; Netti, P., A. *J. Am. Chem. Soc.* **2015**, *137*, 1758–1761.
[140]Romeo, G.; Imperiali, L.; Kim, J.W.; Fernandez-Nieves, A.; Weitz, D.A. *J. Chem. Phys.* **2012**, *136*(12), 124905.
[141]Sam, S.; Touahir, L.; Andresa, J. S.; Allongue, P.; Chazalviel, J. N.; Gouget-Laemmel, C.; Henry de Villeneuve, C.; Moraillon, A.; Ozanam, F.; Gabouze, N.; Djebbar, S. Lagmiur, **2010**, *26*(2), 809–814.
[142]Jiang, B.; Duan, D.; Gao, L. et al. *Nat Protoc*. **2018**, *13*, 1506–1520.